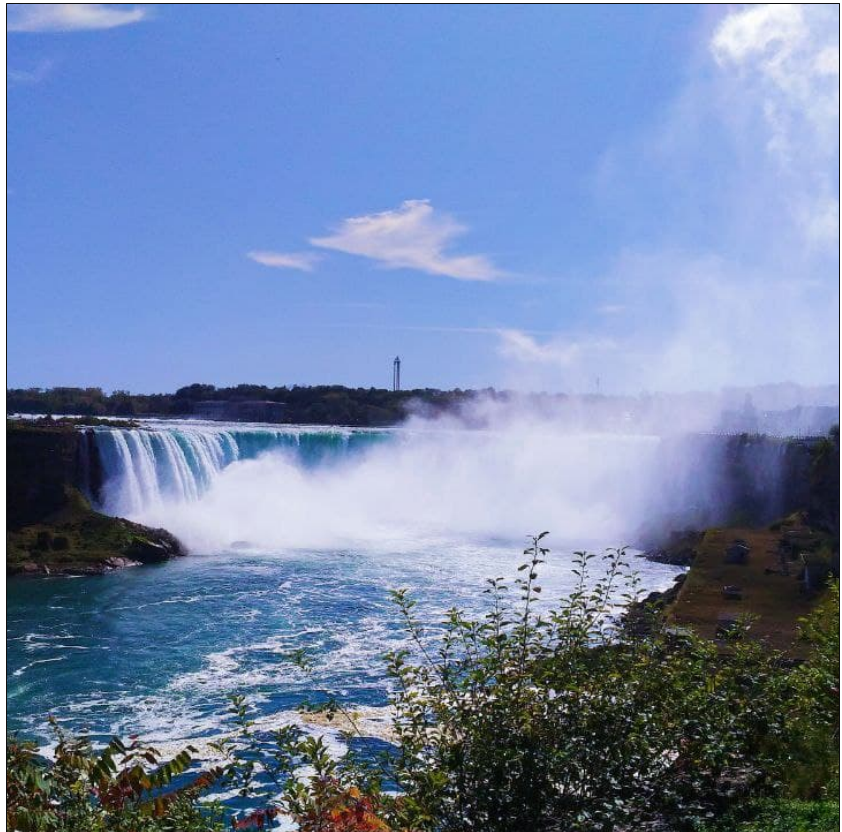




Niccolò Tubini

Theoretical and numerical tools for studying the Critical Zone from plot to catchments



Credits of the cover image: Niagara Falls, Niagara Falls, ON, Canada.



Except where otherwise noted, contents on this book are licensed under a Creative
Common Attribution - Non Commercial - No Derivatives
4.0 International License.

University of Trento
Doctoral School in Civil, Environmental and Mechanical Engineering
<http://web.unitn.it/en/dricam>
Via Mesiano 77, I-38123 Trento Tel. +39 0461 282670 / 2611 - dicamphd@unitn.it

UNIVERSITY OF TRENTO



Doctoral School in Civil, Environmental and Mechanical
Engineering
Topic 1. Civil and Environmental Engineering
Doctoral Thesis

NICCOLÒ TUBINI

THEORETICAL AND
NUMERICAL TOOLS FOR
STUDYING THE CRITICAL
ZONE FROM PLOT TO
CATCHMENTS

Supervisors

Riccardo RIGON (University of Trento, Italy)
Stephan GRUBER (Carleton University, Ottawa,
Canada)

ACKNOWLEDGEMENTS

*As you set out for Ithaka
hope your road is a long one,
full of adventure, full of discovery.*
– C. P. Cavafy

I wish first of all to acknowledge my supervisors for their precious guidance throughout this journey. Prof. Riccardo Rigon, I remember when I was a student attending your Hydrology class during my Bachelor studies and now I am completing my Ph.D. studies. Thank you for all the opportunities, for your support, and for letting me part of your research.

Prof. Stephan Gruber, thank you for your guidance, comments and suggestions. The period I spent at Carleton University has highly contributed to my personal growth and professional development.

Thanks to Prof. Vincenzo Casulli and Prof. Michael Dumbser for your stimulating thinking and discussion about numerical aspects of my reasearch.

I am also thankful to the reviewers of the Thesis, Prof. Stefano Ferraris and Prof. Antonio Coppola, for their review and their precious advice to improve my work.

I like to thank very much the Department of Civil and Environmental Engineering in Trento University: all the professors, the administrative and technical staff. I would also like to thank the Carleton University: all the professors, the colleagues and the administrative staff who welcomed me.

I would like to thank all the GEOframe group, and in particular Concetta and Giuseppe. The lunches together and their friendship helped me in the everyday work. Concetta, thank you for being such a positive and genuine person and helped me in key moments of my work.

I would like to dedicate this thesis to my family: to my parents Graziella and Corrado, to my darling sister Annachiara, and to my fiancée Giorgia and my new family Zenia, Antonio and Elena. I thank each of them for their encouragement without which this milestone would not be possible. Special thanks to Giorgia for always being at my side and for helping me keep things in perspective. Thanks also to whom I know would be happy with this achievement.

CONTENTS

1	INTRODUCTION	7	
1.1	Setting up the water budget	8	
1.2	The three or four worlds	10	
1.3	The necessary coupling with the energy budget	12	
1.4	Heat transport	14	
1.5	Solutes transport	15	
1.6	Organisation and scope	16	
2	WHETGEO-1D	17	
2.1	General issues of the R^2 equation	18	
2.1.1	The discretization of the R^2 equation	20	
2.1.2	Surface boundary condition	21	
2.2	Heat transport and numerics issues	24	
2.2.1	The discretization of the heat equation	25	
2.2.2	Driving the heat equation with the surface energy budget	27	
2.3	Algorithms	29	
2.3.1	The NCZ algorithm	30	
2.3.2	The scalar case	34	
2.4	Informatics	36	
2.4.1	Design requirements	36	
2.4.2	The software organisation	40	
2.4.3	Generic Programming at work	47	
2.5	Information for Users and Developers	52	
2.5.1	Workflow for Users	54	
2.5.2	Inputs and outputs	55	
2.5.3	Workflow for Developers	58	
2.6	R^2 test cases	61	
2.6.1	Analytical solution of Srivastava and Yeh (1991)	61	

2.6.2	Analytical solution of Vanderborght et al. (2005)	66
2.6.3	Surface boundary condition	66
2.6.4	Energy budget	79
2.7	Code availability	80
2.8	Conclusion remarks	80
3	HEAT CONDUCTION IN FROZEN SOIL 1D	85
3.1	Introduction	85
3.2	The governing equations and their numerical issues	89
3.3	Discretization of the enthalpy equation	93
3.4	Analytical benchmarks	95
3.4.1	Neumann analytical solution	95
3.4.2	Lunardini analytical solution	102
3.5	Numerical test	106
3.6	FreeThaw-1D and WHETGEO-1D	115
3.7	Commonly used simulation software	123
3.8	Code availability	132
3.9	Conclusion remarks	133
4	RICHARDS 2D	135
4.1	Grid	136
4.2	Algorithms	141
4.2.1	Conjugate gradient method	141
4.2.2	Matrix-free algorithm	143
4.3	Code design	143
4.3.1	The matrix-vector product, Matop	144
4.3.2	The Conjugate gradient method, ConjugateGradient	144
4.3.3	The NCZ algorithm, NestedNewtonCG	146
4.4	Test cases	146
4.4.1	Analytical solution of Srivastava and Yeh (1991)	146
4.4.2	Test problem 1	150
4.4.3	Test problem 2	153
4.4.4	Test problem 3	159
4.5	Conclusion remarks	160

5	SYNOPSIS	163
5.1	Concluding remarks	163
5.2	Contribution	165
5.3	Future research	166
5.3.1	Frozen ground	166
5.3.2	Lysimeter GEO	170
5.3.3	WHETGEO-2D	171
A	OBJECT MODELLING SYSTEM V. 3	173
B	GEOFRAME	175
C	ENTHALPY AND INTERNAL ENERGY	179
D	NEUMANN ANALYTICAL SOLUTION	181
E	LUNARDINI ANALYTICAL SOLUTION	185
	BIBLIOGRAPHY	189

ABSTRACT

After the seminal works by Freeze and Harlan (1969), the scientific community realized that groundwater and vadose zone equation were breaking up. Hydrologists split into three communities following the motto “you are my boundary condition”: groundwater people, vadose zone scientists and surface water hydrologists. This compartmentalization of the scientific community fostered a deepening of knowledge in single branches, allowing to break things down into simple parts. However, this division represented an obstacle to the comprehension of the complexity that characterises the interactions between them. Eventually, this separation of the communities continued into software code. As a matter of fact, the boundary conditions were hard-wired, but they offered a poor representation of the physics in the interaction between different domains.

Recently, there has been a renewed interest in studying the big picture, the interactions between different domains. This it is evident in the development of a new research field named the Earth’s Critical Zone (CZ). It is defined as the “ heterogeneous, near surface environment in which complex interactions involving rock, soil, water, air, and living organism regulate the natural habitat and determine the availability of life-sustaining resources” (National Research Council, 2001). Further interest in the studying the CZ is given by the ever-increasing pressure due to the growth in human population, wealth, and climatic changes.

This thesis focuses on the CZ while recognising the central role of having a solid set of tools for modeling the water movements in all conditions. Recently, Prentice et al. (2015) identified Reliable,

Robust, and Realistic, the three R's, as the three characteristics that numerical models should have.

Soil moisture is one of the key components to simulate the processes in the critical zone. The governing equation to describe the water flow in a porous material is known as the Richards equation and it dates back to 1931.

The numerical solution of the Richards equation is far from trivial because of its mildly nonlinearity and it is often discarded in favour of more empirical models. After the pioneering work by Celia et al. (1990), a lot of work has been done in this direction and several models, for instance Hydrus, GEOtop, Cathy, Parflow adopted variants of the Newton algorithm to allow global convergence.

Since Casulli and Zanolli (2010), anticipated by Brugnano and Casulli (2008), a new method called nested Newton has been found to guarantee convergence in any situation, even under the use of large time steps and grid sizes. The research presented in this thesis used this integration algorithm.

Besides the numerical aspect, another issue was the correct definition of the boundary condition at the soil surface. As a matter of fact, the definition of the surface boundary condition is necessary to capture the generation of surface run-off. In the literature several approaches were proposed to couple surface and subsurface flow, and in this work the approach presented by Gugole (2016) has been used. The novelty regarded the discretization of the shallow water equation and the Richards equation in a unique algebraic system that was solved in a conservative manner.

Richards equation was criticized from many points of view, but it is difficult to criticize its core mass conservation. The definition of the hydraulic properties of the soil, including both the soil water retention function (SWRC) and the hydraulic conductivity models, often uses simplified representation of the pore system

describing it as bundle of cylindrical capillaries where the largest ones drain first and are filled last. As pointed out by Bachmann et al. (2002), “physical effects, like surface water film adsorption, capillary condensation and surface flow in liquid films, as well as volumetric changes of the pore space are often ignored”. Thus, the capillary bundle concept is a rough, even if still useful approximation of soil reality.

From these observations, during the research the code has been designed to offer the opportunity to easily implement new soil water hydraulic models that might be proposed in the future.

The Richards’ equation alone is not anymore sufficient to model the water flow in soils. In fact, soil temperature affects the water flow in soils. This is evident in cold regions where soil water is subject to freezing and thawing processes, but also in unfrozen soil, where temperature modifies water properties such as viscosity, the surface tension, and the contact angle.

These microscopic variations of the water physical properties have significant impacts in the mass and energy budget within the CZ. For instance, it has been observed that the infiltration rates between the stream and the vadose zone show a clear diurnal pattern: infiltration rates are highest in late afternoon, when stream temperature is greatest, and they are lowest in early morning when stream temperature is least. In cold regions the run-off production is strongly affected by the presence of ice with the soil. Nonetheless, soil moisture modifies the thermal properties of the soil: water is characterised by a high thermal inertia and the thermal conductivity of ice is almost four times larger than that of liquid water, and water flow carries a significant amount of sensible heat. These aspects come under one the R of realistic.

Hence, the Richards’ equation has been coupled with the energy equation for the unfrozen case. Moreover, the research developed

a model to study the heat transfer considering the phase change of water. In both cases robust numerical schemes have been used.

There are few models that already coupled the equations. One of these models is GEOtop that was conceived and built in the research group where this work was carried out. Such models have some limitations. One of the main limitations regards their implementations. In fact, these models were built as a monolithic code and this turns in difficulties in maintaining and developing existing codes.

In this work the codes have been developed by using Design Patterns. As a result, the codes are easy to maintain, to extend, and to reuse. Considering the CZ, these aspects are of crucial importance. Researchers should have a model that can be extended to include more processes, i.e. increase its complexity and avoiding the code to become too complicated.

The models were integrated in the Object Modelling System v3 (OMS3) framework. The system provides various components for precipitation treatment, radiation estimation in complex terrain, evaporation and transpiration that can be connected to each other's for generating inputs and outputs. Due to the modularity of the system, whilst the components were developed and can be enhanced independently, they can be seamlessly used at run time by connecting them with the OMS3 DSL language based on Groovy. OMS3 provides the basic services and, among them, tools for calibration and implicit parallelization of component runs.

In sum, the thesis analyses the relevant literature to date. It presents a detailed description of the physical processes related to the water flow and the energy budget within the soil. Then, it describes the numerical method used to solve and coupled the equations. It also provides the informatics behind WHETGEO 1D (Water HEat Tracers in GEOframe). Finally, the work focuses on

the WHETGEO extension for the bidimensional case by showing how the code can be designed to store grid information.

1

INTRODUCTION

Contents

1.1	Setting up the water budget	8
1.2	The three or four worlds	10
1.3	The necessary coupling with the energy budget	12
1.4	Heat transport	14
1.5	Solutes transport	15
1.6	Organisation and scope	16

The Earth's Critical Zone (CZ) is defined as the heterogeneous, near surface environment in which complex interactions involving rock, soil, water, air, and living organism regulate the natural habitat and determine the availability of life-sustaining resources (National Research Council, 2001). Clear interest in studying the CZ is spurred on by ever-increasing pressure due to the growth in human population and wealth, and climatic changes. Central to simulating the processes in the CZ is the study of soil moisture dynamics (Clark et al., 2015a). In the following we suggest that studying the CZ requires tools that are not yet readily available to researchers; then I propose one of my own. These tools should be flexible enough to allow the quick embedding of advancements in science.

1.1 SETTING UP THE WATER BUDGET

It is understood that the motion of water in soil is regulated by a Darcian-Stokesian flow, meaning that any force is immediately dissipated and water under a gradient of generalised forces acquires a velocity which is linearly proportional to the gradient of the generalised force. This law is known as the Darcy-Buckingham law and reads

$$\vec{J} = K(\theta)\vec{\nabla}(\psi + z) \quad (1)$$

where the forces acting are gravity (z L) and the matric potential ψ L, and where: J LT^{-1} is the Darcian flux; K LT^{-1} is the hydraulic conductivity; θ – is the dimensionless volumetric water content; $\vec{\nabla}$ L^{-1} is the gradient operator; and z L is the vertical coordinate, positive upward. The assumptions under which such a law is derived from Newton's law are presented in (Di Nucci, 2014; Whitaker, 1986). The hydraulic conductivity depends on soil type (texture and structure) and water content, while the thermodynamic forces must be understood as gradients of the water potential, which, in turn, can be split as matric potential, osmotic potential and other potentials (Lu and Godt, 2013; Nobel, 1999). However, in Eq. (1) we consider only the action of the matric potential and of the gravity. On the basis of the law of motion in Eq. (1), the mass conservation reads:

$$\frac{\partial\theta}{\partial t} = \nabla \cdot \left(K(\theta)\vec{\nabla}(\psi + z) \right) \quad (2)$$

where $\nabla \cdot [L^{-1}]$ is the divergence operator. Equation (2) is usually known as the Richards equation (Richards, 1931), but was previously formulated by Richardson (1922). Therefore, in the following we call it the R^2 equation to remind of this double origin. There are very informative reviews that cover its general, historical and numerical aspects, such as: (Farthing and Ogden, 2017;

Paniconi and Putti, 2015; Zha et al., 2019). Therefore, it is not deemed necessary to further summarize the matter here. The R^2 equation is a function of two variables, θ and ψ , and its resolution requires another relation between these two quantities. This relation is known as soil-water retention curves (SWRC), written in the plural because we have many SWRC depending on soil characteristics. A simple analytic model was proposed by Mualem, 1976 that assumed that soil is a bundle of capillaries and that the largest capillaries drain first and fill last. In this case a relation can be obtained between the radius of the capillaries and the suction, which was fully derived (Kosugi, 1999). However, there are various reasons to take the capillary bundle concept as a rough approximation of natural soil. To enumerate some of the issues:

1. Firstly, pores in soils are not bundles of well defined capillaries of a single diameter; in fact, they can have quite random structures, as revealed, for instance, by tomography (Yang et al., 2018).
2. Secondly, logic and pore scale simulations, as in Tomin and Lunati, 2016 for example, indicate that fluids fill the cavities where they fall, and only eventually are they redistributed according to the microstructure of the soil; that is to say, fluids do not move instantaneously from the largest pores to the smallest ones.
3. A set of relatively large pores can, in certain conditions, preferentially drive the flow of water in a short time scale according to laminar viscous flow driven by gravity, before any redistribution happens (Germann and Beven, 1981).
4. The role of living matter, such as bacteria, animals, fungi, vegetation, and roots, is usually eliminated from the hydrological picture but it should have a relevant place (Benard et al., 2019).

Besides,

5. Capillary forces are not the only ones acting at the microscale (Lu, 2016). In fact, measured suction values are far below pressures that can be sustained by capillarity alone.
6. Temperature affects water viscosity; infiltration is faster at warm temperatures and slower at cold ones (Constantz and Murphy, 1991).
7. In high-latitude and high-elevation environments, soils may be subject to freezing and thawing processes which affect pore volume and water dynamics (Dall'Amico et al., 2011).

These facts certainly do not threaten the nature of mass conservation in (2). However, they can certainly alter the statistics which generate the closure equations, i.e. the SWRC we currently use.

- Requirement I - Without entering into further details, we can observe that the aforementioned issues have consequences that would require a new software to include the possibility of adopting new parameterizations of SWRC and hydraulic conductivity quickly, easily and neatly.

1.2 THE THREE OR FOUR WORLDS

The flow of water obeys the general laws of physics for conservation of mass and momentum but, since the seminal works of Freeze and Harlan in 1969, the scientific community has split up (Furman, 2008) into three groups: groundwater people, vadose zone scientists, and surface water hydrologists. This compartmentalisation of the scientific community was fostered to deepen the knowledge within single branches, with the interactions between

the different parts have been governed in models by assigning boundary conditions (Furman, 2008). However, these boundary conditions are intrinsically inadequate and inappropriate in representing the physics of interactions between different domains whose interactions depend strictly on the state of the system. When these conditions are prescribed *a priori* (Furman, 2008), the proper dynamics of the CZ fluxes cannot be obtained. There is the need to overcome this situation and, therefore:

- Requirement II - the boundary conditions hard-wired into algorithm implementation should be removed in favour of a simultaneous treatment of the three compartments (surface waters, vadose zone and groundwater).

Fortunately, Šimůnek et al. (2012) found the way to smoothly extend Richards equation into the groundwater equation. This and other similar approaches are now used in various codes, such as Hydrus, ParFlow (Ashby and Falgout, 1996; Jones and Woodward, 2001; Kollet and Maxwell, 2006), CATHY (Paniconi and Putti, 1994; Paniconi and Wood, 1993), and GEOtop 2.0 (Endrizzi et al., 2014; Rigon et al., 2006a). To extend the R^2 equation into the saturated domain it is necessary to include the contribution of groundwater storativity due matrix and fluid compressibility. The common approach is to write the R^2 equation as:

$$\frac{\partial \theta}{\partial t} + S_s \frac{\theta}{\theta_s} \frac{\partial \psi}{\partial t} = \nabla \cdot \left(K(\psi) \vec{\nabla}(\psi + z) \right) \quad (3)$$

where $S_s \text{ L}^{-1}$ is the specific storage coefficient, defined as

$$S_s = \rho g(n\beta + \alpha), \quad (4)$$

with $\rho \text{ ML}^{-3}$ being the water density, $g \text{ LT}^{-2}$ gravitational acceleration, n – the soil porosity, $\beta \text{ LT}^2\text{M}^{-1}$ the liquid compressibility, and $\alpha \text{ LT}^2\text{M}^{-1}$ the matrix compressibility. In the left-hand-side of

Eq. (3), the first term accounts for changes in liquid saturation, while the second term accounts for the compression or expansion of the porous medium and the water. The left-hand-side term in Eq. (3) can be rewritten as

$$\left(c + S_s \frac{\theta}{\theta_s} \right) \frac{\partial \psi}{\partial t} \quad (5)$$

where $c \text{ L}^{-1}$ is the water retention capacity. Comparing the two terms in brackets, we can see that for $\psi < 0$, then $c \gg S_s \frac{\theta}{\theta_s}$; this means that under unsaturated conditions, the contribution of the specific storage is negligible. Whereas when the soil is saturated and $\psi > 0$, then $c = 0$ and therefore what counts is the specific storage. Because of this, it is possible to account for groundwater specific storage simply by modifying the SWRC as:

$$\theta(\psi) = \begin{cases} \theta(\psi) & \text{if } \psi < 0 \\ \theta_s + S_s \psi & \text{if } \psi > 0 \end{cases} \quad (6)$$

Furthermore, switching from Richards to shallow water was made possible in the equation writing thanks to, for example, (Casulli, 2017b; Gugole et al., 2018). Therefore, switching to a fully integrated, simultaneous treatment of the three domains is now possible.

1.3 THE NECESSARY COUPLING WITH THE ENERGY BUDGET

As remarked in point 6 above, temperature affects water viscosity, which effectively doubles in passing from 5 to 20 °C (Eisenberg et al., 2005), with a positive feedback on the infiltration process. This has been clearly observed in natural systems (Eisenberg et

al., 2005; Engeler et al., 2011; Ronan et al., 1998) where infiltration rates follow diurnal and seasonal temperature-cycles. In fact, according to Muskat and Meres (1936), the unsaturated hydraulic conductivity can be expressed as

$$K(\theta) = \kappa_r(\theta) \kappa \frac{\rho g}{\nu} \quad (7)$$

where $\kappa_r(\theta)$ – is the relative permeability, $\kappa \text{ L}^2$ is the intrinsic permeability, $\rho \text{ L}^3\text{M}^{-1}$ is the liquid density, g is the acceleration of gravity, and $\nu \text{ L}^2\text{T}^{-1}$ is the kinematic viscosity of the liquid. Thus, for constant θ , variations in $K(\theta)$ due to temperature can be accounted as (Constantz and Murphy, 1991):

$$K(\theta, T_2) = K(\theta, T_1) \frac{\nu(T_1)}{\nu(T_2)} \quad (8)$$

Temperature is also responsible for the phase change of water, point 7, and because of pore ice, as well as of the ice in frozen soil, infiltration rates and subsurface flows are significantly modified (Walvoord et al., 2012).

- Requirement III - To account for thermodynamic effects, temperature should be at least present in the R^2 equation as a parameter, as in Eq. (8). However, for a more accurate approximation of the water dynamics, the option to solve the water and energy budgets simultaneously must be present.

Soil thermal properties are important physical parameters in modelling land surface processes (Dai et al., 2019) since they control the partitioning of energy at the soil surface and its redistribution within the soil (Ochsner et al., 2001). For a multi-phase material, like soil, their definition is always problematic since they depend on the physical properties of each phase and their variations (Dai et al., 2019; Dong et al., 2015; Nicolsky and Romanovsky, 2018).

In literature different models have been proposed with such a scope, and further studies on it are recommended (Dai et al., 2019): nonetheless, when considering the phase change of water, the estimation of the unfrozen and frozen water fraction is still an unresolved issue for which different models, usually referred to as SFCC, Soil Freezing Characteristics Curve, have been proposed (Kurylyk and Watanabe, 2013). Thus, it is clear that the aspects related to the estimation of soil thermal properties fall fully within Requirement I too. Moreover, there are other reasons for which the equations of the water and energy budgets should be solved in a coupled manner (Rigon et al., 2006a): for instance, this makes it possible to include an appropriate treatment of evaporation and transpiration processes (Bisht and Riley, 2019; Bonan, 2019), as well as of the heat advection (Engeler et al., 2011; Frampton et al., 2013; Ronan et al., 1998; Walvoord and Kurylyk, 2016; Wierenga et al., 1970; Zhang et al., 2019).

1.4 HEAT TRANSPORT

Under the conditions defined above, the governing equation for the transport of energy in variably saturated porous media is given by the following energy conservation equation:

$$\frac{\partial h(\psi, T)}{\partial t} = \nabla \cdot [\lambda(\psi) \nabla T - \rho_w c_w (T - T_{ref}) J] \quad (9)$$

where h is the specific enthalpy of the medium $L^2 T^{-2}$, λ $ML\Theta^{-1}T^{-3}$ is the thermal conductivity of the soil, T Θ is the temperature, ρ_w ML^{-3} is the water density, c_w $L^2\Theta^{-1}T^{-2}$ is the specific heat capacity of water, T_{ref} Θ is a reference temperature used to define the enthalpy, and J_w is the water flux LT^{-1} . The first term in the right-hand-side is the heat conduction flux described by the Fourier's

law, the second term is the sensible heat advection of liquid water. The specific enthalpy of a control volume of soil $V_c \text{ L}^3$ can be calculated as the sum of the enthalpy of the soil particles and liquid water:

$$h = \rho_{sp}c_{sp}(1 - \theta_s)(T - T_{ref}) + \rho_w c_w \theta(\psi)(T - T_{ref}) \quad (10)$$

where ρ_{sp} and ρ_w are the densities of the soil particles and water, c_{sp} , c_w , are the specif heat capacity of the soil particles and water. Equation (9) is the so-called conservative form.

1.5 SOLUTES TRANSPORT

Besides the need to couple the energy and water budget, there is a great urge to model solutes transport according to the water movements. The range of applications for solute/tracer/pollutants spans from agriculture to industry to research itself. In fact, in recent years there has been a tumultuous growth of studies using tracers to asses the various pathways of water (Hrachowitz et al., 2016). However, so far these studies have mostly used lumped models with limited capability to investigate water age selection processes, processes that became very important in the most recent literature e.g. (Penna et al., 2018). Using more complex modelling can benefit both the investigation of the processes and the construction of more refined water budget closures. Even though in this paper we do not detail the work on tracers, they must be kept in mind in software design so that the modules to be implemented eventually.

1.6 ORGANISATION AND SCOPE

The thesis is structured as follows. After these introductory remarks, Chapter 2 presents the WHETGEO-1D model. Firstly, the Chapter presents general issues in solving the R^2 equation and the its coupling with the heat transport equation. Next, it conducts an extended critical analysis of the implementation of algorithms adopting an OOP and generic approach. The Chapter then provides information for users and developers. Finally, it concludes by presenting some test cases for the R^2 and the heat transport equation. The heat transfer problem in frozen ground is addressed by Chapter 3. In particular, this Chapter firstly reviews established approaches to study freezing and thawing phenomena in soils and points to relevant issues. Then, it critically describes the new approach we propose. It details the discretization of the governing equation and the NCZ algorithm used to solve the resulting nonlinear numerical system, and it presents the some analytical benchmarks, and its performance is compared over a range of spatial and temporal resolutions. Finally, it briefly presents the inclusion of freezing and thawing processes in WHETGEO-1D and possible future outlooks. Chapter 4 deals with presentation of the ongoing development of WHETGEO-2D model. The Chapter starts presenting the problem of storing the grid information. Then, it discusses the algorithm required to solve a PDE in a bi-dimensional domain and a critical analysis of their implementation adopting the OOP and generic programming approach. At the end, Chapter 4 briefly concludes with some test cases for the R^2 equation. Conclusions and future perspective are finally presented in Chapter 5.

2

WHETGEO-1D

Contents

2.1	General issues of the R^2 equation	18
2.1.1	The discretization of the R^2 equation	20
2.1.2	Surface boundary condition	21
2.2	Heat transport and numerics issues	24
2.2.1	The discretization of the heat equation	25
2.2.2	Driving the heat equation with the surface energy budget	27
2.3	Algorithms	29
2.3.1	The NCZ algorithm	30
2.3.2	The scalar case	34
2.4	Informatics	36
2.4.1	Design requirements	36
2.4.2	The software organisation	40
2.4.3	Generic Programming at work	47
2.5	Information for Users and Developers	52
2.5.1	Workflow for Users	54
2.5.2	Inputs and outputs	55
2.5.3	Workflow for Developers	58
2.6	R^2 test cases	61
2.6.1	Analytical solution of Srivastava and Yeh (1991)	61
2.6.2	Analytical solution of Vanderborgh et al. (2005)	66
2.6.3	Surface boundary condition	66
2.6.4	Energy budget	79

2.7	Code availability	80
2.8	Conclusion remarks	80

This Chapter describes the implementation and the content of the software WHETGEO-1D (Water, HEat and Transport in GE-Oframe) in observance of requirements I to V and aware of the hydrologic facts described in points 1-7. Further requirements derive from Numerics and Mathematics as argued below. We do not treat transport since its numerics is slightly different from those of the water and energy budget and this topic will be covered in a future work.

2.1 GENERAL ISSUES OF THE R^2 EQUATION

Equation (2) is said to be written in “mixed form” because it is expressed in term of θ and ψ (and uses the SWRC to connect the two variables).

The “ ψ -based form” is derived from Eq. (2) by applying the chain rule for derivatives:

$$c(\psi) \frac{\partial \psi}{\partial t} = \nabla \cdot [K(\psi) \nabla(\psi + z)] \quad (11)$$

where

$$c(\psi) = \frac{\partial \theta(\psi)}{\partial \psi} \quad (12)$$

with dimension L^{-1} , is the specific moisture capacity, also called hydraulic capacity. Even though Eq. (2) and Eq. (11) are analytically equivalent under the assumption that the water content is a differentiable variable, this is not generally true in the discrete domain where the derivative chain rule is not always valid (Farthing and Ogden, 2017). Because of this the ψ -based form may

suffer from large balance errors in the presence of big nonlinearities and strong gradients, as discussed in (Casulli and Zanolli, 2010; Farthing and Ogden, 2017; Zha et al., 2019) and literature therein. The specific moisture capacity c , which appears in the storage term, itself depends on ψ and so is not constant over a discrete time interval during which ψ changes value. Let us discretise the time derivative in Eq. (11) by using the backward Euler scheme and obtain:

$$\tilde{c}_i \frac{\psi_i^{n+1} - \psi_i^n}{\Delta t} \quad (13)$$

where \tilde{c}_i is the discrete operator of the soil moisture capacity, $c(\psi)$. In order to preserve the chain rule of derivatives at the discrete level, i.e. the equality $c\partial\psi/\partial t = \partial\theta(\psi)/\partial t$, \tilde{c}_i has to satisfy the requirement (Roe, 1981)

$$\tilde{c}_i(\psi_i^{n+1} - \psi_i^n) = \theta(\psi_i^{n+1}) - \theta(\psi_i^n) \quad (14)$$

As can be seen from the above equation, the right definition of \tilde{c}_i depends on the solution itself. To overcome this problem, in literature different techniques have been presented to improve the evaluation of \tilde{c}_i , but none ensures mass conservation (Farthing and Ogden, 2017).

There is a third form of Eq. (2), the so-called “ θ -based form”, it is obtained as

$$\frac{\partial\theta}{\partial t} = \nabla \cdot \left[K(\theta) \frac{\partial\theta}{\partial\theta} \nabla\psi \right] + \nabla \cdot [K(\theta)\nabla z] \quad (15)$$

defining

$$D(\theta) = K(\theta) \frac{\partial\psi}{\partial\theta} \quad (16)$$

where D is the soil-water diffusivity L^2T^{-1} . Finally we get

$$\frac{\partial\theta}{\partial t} = \nabla \cdot [D(\theta)\nabla\theta] + \nabla \cdot [K(\theta)\nabla z] \quad (17)$$

The first term on the right-hand-side represents the water flow due to capillary forces, while the second term is the contribution due to gravity (Farthing and Ogden, 2017). The θ -based form is mass-conserving and it can be solved perfectly by mass conservative methods (Casulli and Zanolli, 2010). However, its applicability is limited to the unsaturated zone since water content varies between θ_r and θ_s , whereas water suction is not bounded. This formulation is intrinsically not suited to fulfilling our requirement III. Moreover, water content is discontinuous across layered soil since the SWRCs are soil specific, whereas water suction is continuous even in inhomogeneous soils (Bonan, 2019; Farthing and Ogden, 2017).

In WHETGEO, we directly use the conservative form of the R^2 equation (Celia et al., 1990), Eq. (2), which seems the easiest way to deal with both the mass conservation issues and the extension of the equation to the saturated case.

2.1.1 The discretization of the R^2 equation

The implicit finite volume discretization of Eq. (2) reads as:

$$\theta_i(\psi_i^{n+1}) = \theta_i(\psi_i^n) + \Delta t \left[K_{i+\frac{1}{2}}^{n+1} \frac{\psi_{i+1}^{n+1} - \psi_i^{n+1}}{\Delta z_{i+\frac{1}{2}}} + K_{i+\frac{1}{2}}^{n+1} - K_{i-\frac{1}{2}}^{n+1} \frac{\psi_i^{n+1} - \psi_{i-1}^{n+1}}{\Delta z_{i-\frac{1}{2}}} - K_{i-\frac{1}{2}}^{n+1} + S_i^n \right] \quad (18)$$

where Δt is the time step size,

$$S_i = \int_{\Omega_i} S d\Omega \quad (19)$$

is an optional source/sink term in volume, and $\theta_i(\psi)$ is the i th water volume given by

$$\theta_i(\psi) = \int_{\Omega_i} \theta(\psi) d\Omega. \quad (20)$$

Equation (18) can be written in matrix form as

$$\vec{\theta}(\vec{\psi}) + \mathbf{T}\vec{\psi} = \vec{b} \quad (21)$$

where $\vec{\psi} = \{\psi_i\}$ is the tuple of unknowns, $\vec{\theta}(\vec{\psi}) = \theta_i(\psi_i)$ is a tuple-function representing the discrete water volume, \mathbf{T} is the flux matrix, and \vec{b} is the right-hand-side vector of Eq. (18), which is properly augmented by the known Dirichlet boundary condition when necessary. For a given initial condition ψ_i^0 , at any time step $n = 1, 2, \dots$, Eq. (18) constitutes a nonlinear system for ψ_i^{n+1} , with the nonlinearity affecting only the diagonal of the system and being represented by the water volume $\theta_i(\psi_i^{n+1})$. This set of equations is a consistent and conservative discretization of Eq. (2). Therefore, regardless of the chosen spatial and temporal resolution, ψ_i^{n+1} is a conservative approximation of the new water suction.

2.1.2 Surface boundary condition

The definition of the type of surface boundary condition (Neumann vs. Dirichlet) for the R^2 equation is a non trivial task since it can depend on the state of the system. In literature several approaches are used (Furman, 2008). These approaches are mainly based on a switch of the type of the boundary condition from a prescribed head to prescribed flux and viceversa. This switching often causes numerical difficulties that need to be addressed (Furman, 2008).

To overcome this problem we have included an additional computational node at the soil surface. As will be made clear in the following, for it we prescribe an “equation state” like that presented in (Casulli, 2009):

$$H(\psi) = \begin{cases} \psi & \text{if } \psi > 0 \\ 0 & \text{otherwise} \end{cases} \quad (22)$$

where H is the water depth, which also represents the pressure if the ponding is assumed to happen in hydrostatic conditions. By doing so, it is possible to prescribe as the surface boundary condition the rainfall intensity (Neumann type) without resorting to any switching techniques to reproduce infiltration excess or saturation excess processes. In this case the system, Eq. (21), must to be modified to account for the additional computational node describing the state of the soil surface:

$$\left\{ \begin{array}{l} H_N(\psi_N^{n+1}) - \Delta t \left[0 - K_{N-\frac{1}{2}}^n \frac{\psi_N^{n+1} - \psi_{N-1}^{n+1}}{\Delta z_{N-\frac{1}{2}}} \right] \\ \quad = H_N(\psi_N^n) + \Delta t [J^n - K_{N-\frac{1}{2}}^n] \quad \text{if } i == N \\ \theta_i(\psi_i^{n+1}) - \Delta t \left[K_{i+\frac{1}{2}}^n \frac{\psi_{i+1}^{n+1} - \psi_i^{n+1}}{\Delta z_{i+\frac{1}{2}}} - K_{i-\frac{1}{2}}^n \frac{\psi_i^{n+1} - \psi_{i-1}^{n+1}}{\Delta z_{i-\frac{1}{2}}} \right] \\ \quad = \theta_i(\psi_i^n) + \Delta t [K_{i+\frac{1}{2}}^n - K_{i-\frac{1}{2}}^n] \quad \text{if } i = 1, 2, \dots, N-1 \end{array} \right. \quad (23)$$

where J^n is the rainfall intensity and represents the Neumann boundary condition used to drive the system at the soil surface. For any time step, Eq. (23) can be written in matrix form, similar to (Eq. (21)), as:

$$\vec{V}(\vec{\psi}) + \mathbf{T}\vec{\psi} = \vec{b} \quad (24)$$

where $\vec{\psi} = \{\psi_i\}$ is the tuple of unknowns, $\vec{V}(\vec{\psi}) = (\theta_i(\psi_i))$ for $i = 1, 2, \dots, N-1$ and $V_N(\psi) = H(\psi)$ is a tuple-function representing

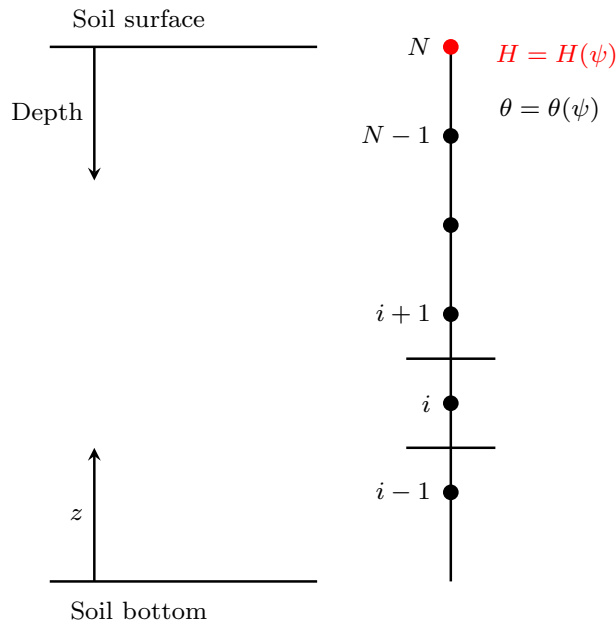


Figure 2.1: Scheme of the computational domain to solve the Richards equation in 1D. The uppermost node represents the water depth at the soil surface. By considering this additional computational node the boundary condition does not change its nature depending on the solution.

the discrete water volume, \mathbf{T} is the flux matrix, and \vec{b} is the right-hand-side vector of Eq. (18), which is properly augmented by the known Dirichlet boundary condition when necessary. For a given initial condition ψ_i^0 , at any time step $n = 1, 2, \dots$ Eq. (24) constitutes a nonlinear system for ψ_i^{n+1} , with the nonlinearity affecting only the diagonal of the system and being represented by the water volume $V_i(\psi_i^{n+1})$. Therefore, regardless of the chosen spatial and temporal resolution, ψ_i^{n+1} is a conservative approximation of the new water suction.

2.2 HEAT TRANSPORT AND NUMERICS ISSUES

Equation (9) is said to be written in conservative form and expresses an important property, which is the conservation of the scalar quantity, in this case the specific enthalpy. It is interesting to note that by making use of the mass conservation equation, Eq. (2), Eq. (9) can be written in an analytically equivalent form, the so called non-conservative form (Šimůnek et al., 2005; Sophocleous, 1979). The time derivative can be expressed as

$$\begin{aligned} \frac{\partial h}{\partial t} = c_T \frac{\partial T}{\partial t} + \rho_w c_w (T - T_{ref}) \frac{\partial \theta}{\partial t} + \rho_w l \frac{\partial \theta}{\partial t} = \\ c_T \frac{\partial T}{\partial t} + \rho_w [l + c_w (T - T_{ref})] \frac{\partial \theta}{\partial t} \end{aligned} \quad (25)$$

and substituting in Eq. (9)

$$c_T \frac{\partial T}{\partial t} + \rho_w [l + c_w (T - T_{ref})] \frac{\partial \theta}{\partial t} = \nabla \cdot [\lambda \nabla T - \rho_w c_w (T - T_{ref}) J] \quad (26)$$

where J is the Darcian flux defined by Eq. (1). Developing the right-hand-side term

$$c_T \frac{\partial T}{\partial t} + \rho_w [l + c_w(T - T_{ref})] \frac{\partial \theta}{\partial t} = \lambda \nabla^2 T - \rho_w c_w (T - T_{ref}) \nabla \cdot J - \rho_w c_w J \nabla T \quad (27)$$

and by making use of the continuity equation for the mass, the Richards' equation, it becomes

$$c_T \frac{\partial T}{\partial t} = \lambda \nabla^2 T - \rho_w c_w J \nabla T \quad (28)$$

Equation (28) expresses another important property which is the maximum principle (Casulli and Zanolli, 2005), i.e. the analytical solution is always bounded, above and below, by the maximum and minimum of its initial and boundary values, as shown in casulli1988numerical.

Although Eq. (9) and Eq. (28) are analytically equivalent, once they are discretized the corresponding numerical solution will, in general, either be conservative or satisfy a discrete max-min property (Casulli and Zanolli, 2005), but not both as would be required.

As in the case of the water flow, thermal budget issues can be subdivided into three aspects: the discretization of the equation, the inclusion of the appropriate boundary conditions, and the implementation of some closure equation for the thermal capacity and conductivity.

2.2.1 The discretization of the heat equation

The key feature (Casulli and Zanolli, 2005) to obtaining a numerical solution for the heat transport equation that is both conservative and possesses the max-min property is to solve the conservative form of the heat equation by using the velocity field obtained in solving the continuity equation Eq. (2). By making use

of the up-wind scheme for the advection part and the centered difference scheme for the diffusion part we have:

$$\begin{aligned}
 C_{T_i}^{n+1} T_i^{n+1} = C_{T_i}^n T_i^n - \rho_w c_w \Delta t \left[\right. \\
 & \frac{1}{2} J_{1+\frac{1}{2}}^{n+1} \left(T_{i+1}^{n+1} + T_i^{n+1} \right) - \frac{1}{2} \left| J_{1+\frac{1}{2}}^{n+1} \right| \left(T_{i+1}^{n+1} + T_i^{n+1} \right) \\
 & \left. - \frac{1}{2} J_{1-\frac{1}{2}}^{n+1} \left(T_i^{n+1} + T_{i-1}^{n+1} \right) + \frac{1}{2} \left| J_{1-\frac{1}{2}}^{n+1} \right| \left(T_{i+1}^{n+1} + T_i^{n+1} \right) \right] \\
 & + \Delta t \left[\lambda_{i+\frac{1}{2}}^n \frac{T_{i+1}^{n+1} - T_i^{n+1}}{\Delta z_{i+\frac{1}{2}}} - \lambda_{i-\frac{1}{2}}^n \frac{T_i^{n+1} - T_{i-1}^{n+1}}{\Delta z_{i-\frac{1}{2}}} \right] \quad (29)
 \end{aligned}$$

where

$$C_{T_i} = \int_{\Omega_i} \rho_{sp} c_{sp} (1 - \theta_s) + \rho_w c_w \theta(\psi) d\Omega \quad (30)$$

When heat equation does not consider water phase changes, it is decoupled from the R^2 equation and the finite volume discretisation leads to a linear algebraic system of equations. However, once freezing and thawing processes are considered, the heat equation is fully coupled with the R^2 equation, as in (Dall'Amico et al., 2011) for instance, and the enthalpy function becomes nonlinear. At this point, since the enthalpy function is nonlinear the NCZ algorithm is required to linearise it, as shown in (Tubini et al., 2020). So far, we have not considered the problem of water flow in freezing soils, however being aware of this issue is important for the future developments and code design.

2.2.2 Driving the heat equation with the surface energy budget

At the soil surface the heat equation is driven by the surface energy balance. The heat flux exchanged between the soil and the atmosphere, the surface heat flux, \mathcal{F} MT^{-3} , is given as:

$$\mathcal{F} = S_{in} + S_{out} + L_{in} + L_{out} + \mathcal{H} + LE \quad (31)$$

where S_{in} is the incoming short wave radiation, S_{out} is the outgoing short wave radiation, L_{in} is the incoming longwave radiation, L_{out} is the outgoing longwave radiation, and \mathcal{H} and LE are respectively the turbulent fluxes of sensible heat and latent heat. Fluxes are positive when directed toward the soil surface and all have the dimension of an energy per unit area per unit time MT^{-3} .

Similarly to the definition of the surface boundary condition for the water flow, the surface boundary condition for the energy equation is also system dependent. In fact, in Eq. (31) the only fluxes that do not depend on the soil temperature and/or moisture are the incoming shortwave and longwave radiation fluxes, S_{in} and L_{in} . The outgoing shortwave radiation flux is usually parameterized as:

$$S_{out} = \alpha S_{in} \quad (32)$$

where the surface albedo α – can be assumed to vary with the soil moisture content (Saito et al., 2006) and radiation wavelength. The outgoing longwave surface radiation is:

$$L_{out} = (\epsilon - 1)L_{in} - \epsilon\sigma T_s^4 \quad (33)$$

where T_s [$^\circ\text{C}$] the temperature of the topmost layer of soil, ϵ is the soil emissivity, and σ is the Stefan-Boltzmann constant. The sensible heat flux \mathcal{H} is taken as:

$$\mathcal{H} = -\frac{\rho_a c_a}{r_H} (T_a - T_s) \quad (34)$$

where ρ_a is the air density ML^{-3} , and c_a is the thermal capacity of air per unit mass $\text{L}^2\text{T}^{-2}\Theta^{-1}$. Regarding the aerodynamic resistances r_H [T L^{-1}], it should be noted that it can be evaluated with different degrees of approximation and may require a specific modelling solution. For instance, the aerodynamic resistance r_H can be evaluated with models ranging from semi-empirical models to the the Monin-Obukov similarity (Liu et al., 2007), or even by solving the turbulent dynamics with direct methods (McDonough, 2004; Raupach and Thom, 1981).

The latent heat flux is taken here as given by a formula of the type:

$$LE = l\rho_a E_P \frac{r_H r_v}{r_H + r_v} \quad (35)$$

where l ML^2T^{-2} is the specific latent heat of vaporisation of water, E_P is the potential evapotranspiration, r_H and r_v TL^{-1} are respectively the aerodynamic resistance and the soil surface resistance to water vapour flow. The latent heat flux it is the sum of two distinct processes evaporation and transpiration. Compared to the other fluxes, latent heat flux presents further complications because evaporation is both an energy and a water limited process, and transpiration depends also on the physiology of trees (as well as root distribution/growth and leaf cover). The latent heat flux is associated to the water flux that must be accounted in the R^2 equation. Here we present a simplified treatment of the latent heat flux as an external driving force. A more exhaustive and physically based treatment of the latent heat flux, and the related water flux, is addressed in the ongoing development of the Lysimeter GEO model by Concetta D'Amato.

Including the surface energy budget boundary condition requires the computation of additional quantities such as the incoming radiation fluxes, the shortwave radiation and the longwave radiation, and the potential evapotranspiration flux. These quantities can be easily computed within the GEOframe system in which

WHETGEO-1D is embedded. The proper estimation of the incoming radiation fluxes is far from being a simple task and it is often oversimplified in hydrological problems. Our approach is to use the tools already developed inside the system GEOframe which were tested independently and accurately (Formetta et al., 2013; Formetta et al., 2014a). Similarly the evapotranspiration can be computed with other GEOframe components (Bottazzi, 2020; Bottazzi et al., 2021).

2.3 ALGORITHMS

By using a numerical method, here the finite volume method, a partial differential equation is transformed into a system of non-linear algebraic equations, as has already been shown. The system has to be solved with iterative methods and, at their core, these reduce the problem to using a linear systems solver. The solver can be of various types, according to the dimension of the problem. For instance in 1D, the final system of finite volume problems we present is tridiagonal and can be conveniently solved with the Thomas algorithm (Campbell et al., 1995; Quarteroni et al., 2010), which is a fast direct method. In 2D or 3D, the final matrix is not tridiagonal and a different solution method must be used, for instance the conjugate gradient (Shewchuk et al., 1994). These algorithms are well known and do not need to be explained here.

However, the reduction of a nonlinear system to a linear one is not trivial. We illustrate the issues by taking the R^2 equation as an example. As discussed in depth in Zha et al. (2019) and Farthing and Ogden (2017), and references therein, the linearisation of the R^2 equation is challenging. Following the work of Celia et al. (1990), a lot of advancements have been made in this direction: Hydrus, CATHY, and ParFlow use variants of the Newton

and Picard iteration methods (Paniconi and Putti, 1994; Zha et al., 2019), while GEOtop 2.0 implements a suitable globally convergent Newton method (Kelley, 2003). Although current algorithms are relatively stable, they may fail to converge or require a considerable computational cost (Zha et al., 2019). This has a significant impacts both on the reliability of the solution, which can have mass-balance errors, and on the computational cost to produce it (Farthing and Ogden, 2017; Zha et al., 2019). Since Casulli and Zanolli (2010) and Brugnano and Casulli (2008), a new method was found, called nested Newton by the authors and NCZ in the following, that guarantees convergence in any situation, even with the use of large time steps and grid sizes.

2.3.1 The NCZ algorithm

As clearly pointed out by Casulli and Zanolli (2010), what makes the linearisation of the R^2 equation difficult is the non-monothonic behaviour of the soil moisture capacity. A mathematical proof of convergence for NCZ exists (Brugnano and Casulli, 2008, 2009; Casulli and Zanolli, 2010, 2012), which is not repeated here. However, we take the time to illustrate this new algorithm with care.

Let us start again from the nonlinear system (Casulli and Zanolli, 2012):

$$\vec{V}(\vec{\psi}) + \mathbf{T}\vec{\psi} = \vec{b} \quad (20)$$

where $\vec{\psi} = (\psi_i)$ is the tuple of unknowns, $\vec{V}(\vec{\psi}) = (V_i(\psi_i))$ is a nonnegative vectorial function and where the $V_i(\psi_i)$ are defined for all $\psi_i \in \mathbb{R}$ and can be expressed as:

$$V_i(\psi_i) = \int_{-\infty}^{\psi_i} a_i(\xi) d\xi \quad (36)$$

For all $i = 1, 2, \dots, N$, the following assumptions are made on the functions $a_i(\psi)$ (we are here quite literally following (Casulli and Zanolli, 2010)):

- A1 : $a_i(\psi)$ is defined for all $\psi \in \mathbb{R}$ and is a nonnegative function with bounded variations;
- A2 : There exists $l_i, u_i \in \mathbb{R}$ such that $a_i(\psi)$ is non-decreasing in $(-\infty, l_i]$ and non-increasing in $[u_i, +\infty)$.

\mathbf{T} in (Eq. (20)) is the so-called matrix flux and it is a symmetric and (at least) positive semidefinite matrix satisfying one of the following properties:

- T1 : \mathbf{T} is a Stieltjes matrix, i.e., a symmetric M-matrix, or
- T2 : \mathbf{T} is irreducible, $\text{null}(\mathbf{T}) \equiv \text{span}(\vec{v})$, with $\vec{v} > \vec{0}$ (componentwise), and $\mathbf{T} + \mathbf{D}$ is a Stieltjes matrix for all diagonal matrices $\mathbf{D} \succeq \mathbf{O}$, with \mathbf{O} denoting the null matrix.

Finally \vec{b} is the vector of the known terms. When \mathbf{T} satisfies property T2, then for Eq. (20) to be physically and mathematically compatible, the following assumption about \vec{b} is required:

$$0 < \vec{v}^\top \vec{b} < \vec{v}^\top \vec{V}^{Max} \quad (37)$$

where $\vec{V}^{Max} = \int_{-\infty}^{+\infty} a_i(\xi) d\xi$.

Having assumed that the $a_i(\psi)$ are non-negative functions of bounded variations, they are differentiable almost everywhere, admit only discontinuities of the first kind, and can be expressed as the difference of two non-negative, bounded, and non-decreasing functions, say $p_i(\psi)$ and $q_i(\psi)$, such that:

$$\begin{aligned} a_i(\psi) &= p_i(\psi) - q_i(\psi) \geq 0 \\ 0 &\leq q(\psi) \leq p(\psi) \end{aligned} \quad (38)$$

for all $\psi \in \mathbb{R}$. When $a(\psi)$ satisfy assumptions A1 and A2, the corresponding decomposition (known as the Jordan decomposition (Chistyakov, 1997) and presented in Figure 2.2), is given by:

$$\begin{aligned} p_i(\psi) &= a_i(\psi) & q_i(\psi) &= 0 & \text{if } \psi &\leq \psi_i^* \\ p_i(\psi) &= a_i(\psi_i^*) & q_i(\psi) &= p_i(\psi) - a_i(\psi) & \text{if } \psi &> \psi_i^* \end{aligned} \quad (39)$$

where ψ_i^* is the position of the maximum of p_i . Thereafter, $\vec{V}(\vec{\psi})$ can be expressed as

$$\vec{V}(\vec{\psi}) = \vec{V}_1(\vec{\psi}) - \vec{V}_2(\vec{\psi}) \quad (40)$$

where the i -th component of $\vec{V}_1(\vec{\psi})$ and $\vec{V}_2(\vec{\psi})$ are defined as

$$V_{1,i}(\psi_i) = \int_{-\infty}^{\psi_i} p_i(\xi) d\xi \quad V_{2,i}(\psi_i) = \int_{-\infty}^{\psi_i} q_i(\xi) d\xi \quad (41)$$

By making use of Eq. (40) the algebraic system in Eq. (20) can be written as

$$\vec{V}_1(\vec{\psi}) - \vec{V}_2(\vec{\psi}) + \mathbf{T}\vec{\psi} = \vec{b} \quad (42)$$

It is necessary here to point out exactly how the nonlinear system, Eq. (20), reads when considering only the R^2 equation and when the water depth function is used to properly define the surface boundary condition. In the first case, i.e. when Neumann or Dirichlet boundary conditions are used, the vectorial function is defined as $\vec{V}(\vec{\psi}) = (\theta_i(\psi_i))$ for $i = 1, 2, \dots, N$.

Instead, when we consider the water depth function to describe the computational node at the soil surface, the vectorial function is defined as $\vec{V}(\vec{\psi}) = (\theta_i(\psi_i))$ for $i = 1, 2, \dots, N - 1$ and $V_N(\psi) = H(\psi)$. Therefore, the nonlinear system in Eq. (42) is valid to describe both the subsurface and surface waters when the symbols are appropriately understood.

This aspect, the use of two different equation states, and the fact that the NCZ algorithm can be successfully reused to solve other

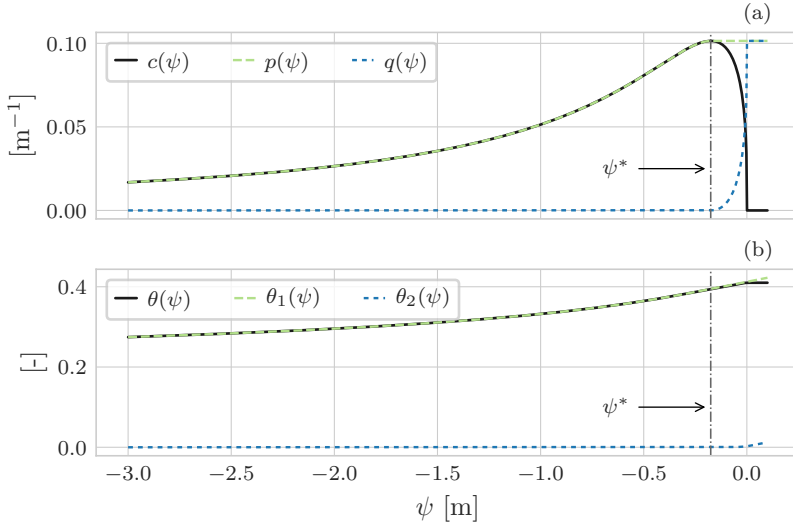


Figure 2.2: Graphical representation of the Jordan decomposition for soil water content using the SWRC model by Van Genuchten (Van Genuchten, 1980) for a clay loam soil (Bonan, 2019). (a) shows the Jordan decomposition of $c(\psi)$, (39). For $\psi = \psi^*$, $c(\psi)$ presents a maximum: for $\psi < \psi^*$ it is increasing, and for $\psi > \psi^*$ it is decreasing. This non monothonic behaviour causes problems when solving the nonlinear system. $c(\psi)$ is thus replaced by $p(\psi)$ (in green) and $q(\psi)$, in blue, two monothonic functions whose difference is the original function c . Consequently, (b), $\theta(\psi)$ is replaced by $\theta_1(\psi)$ and $\theta_2(\psi)$, Eq. (40).

problems (Casulli and Zanolli, 2012; Tubini et al., 2020), requires a careful design of its implementation, as discussed in the following sections.

2.3.2 The scalar case

In this section we apply the NCZ algorithm for solving a scalar problem and we provide a graphical representation of the nested iterations.

Let us consider the following scalar problem

$$\theta(\psi) = b \quad (43)$$

where $\theta(\psi)$ is the Van Genuchten model and $b \in [\theta_r, \theta_s]$. In this case the Jordan decomposition reads as:

$$\begin{aligned} p_i(\psi) &= c_i(\psi) & q_i(\psi) &= 0 & \text{if } \psi \leq \psi_i^* \\ p_i(\psi) &= c_i(\psi_i^*) & q_i(\psi) &= p_i(\psi) - c_i(\psi) & \text{if } \psi > \psi_i^* \end{aligned} \quad (44)$$

where

$$\psi^* = -\frac{1}{\alpha} \left(\frac{n-1}{n} \right)^{\frac{1}{n}} \quad (45)$$

and the specific moisture capacity reads as

$$c_i(\psi) \begin{cases} \alpha_i m_i n_i \frac{\theta_{s,i} - \theta_{r,i}}{[1 + |\alpha_i \psi|^{n_i}]^{m_i}} |\alpha_i \psi_i|^{n_i-1} & \text{if } \psi \leq 0 \\ 0 & \text{if } \psi > 0 \end{cases} \quad (46)$$

This problem can be easily solved by using the NCZ algorithm, Fig. (2.3). The initial guess ψ^0 is chosen in such a way that $\psi^0 < \psi^*$, thus $\theta_2(\psi) = 0$. Then the inner-iteration starts. $\psi^{0,3}$ solves the equation $\theta_1(\psi)$, and it is set as the result of the first the outer-iteration. Now it is checked whether ψ^1 solves $\theta_1(\psi) - \theta_2(\psi) = b$, and in case the NCZ algorithm is terminated.

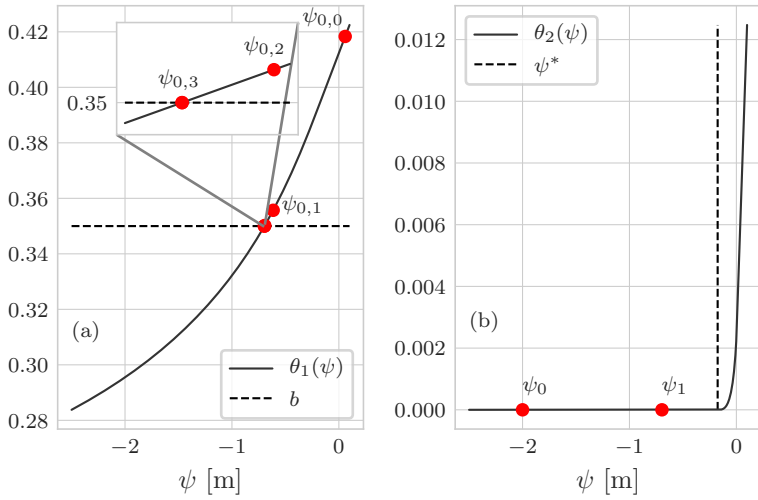


Figure 2.3: Graphical representation of the NCZ iterations. Panel (a) plots the function $\theta_1(\psi)$, while panel (b) plots the function $\theta_2(\psi)$. For this problem we set $\theta_s = 0.41 \text{ m}^3 \text{ m}^{-3}$, $\theta_s = 0.095 \text{ m}^3 \text{ m}^{-3}$, $\alpha = 1.9 \text{ m}^{-1}$, $n = 1.31$ -, and $b = 0.35$ -.

This problem can be solved also with the Newton-Raphson algorithm but in this case it is not possible to define a suitable interval to pick the initial guess that ensure the convergence of the algorithm.

2.4 INFORMATICS

The concepts and requirements previously illustrated must be cast into a software whose usability, expandability and inspectability are demanded by good software design, which adds further requirements. As discussed in Serafin (2019), codes were usually developed as monolithic code with severe drawbacks for maintainability and developments to improve the description of environmental processes, as has been proven by our own experience with the model GEOtop (Endrizzi et al., 2014; Rigon et al., 2006a), and by the experiences of other modelling frameworks (Bisht and Riley, 2019; Clark et al., 2015b; Clark et al., 2021). Based on these experiences, the WHETGEO-1D code has been developed by adopting an Object-Oriented-Programming (OOP) approach and it has been integrated into OMS₃. Information on OMS₃ is provided in Appendix A. Furthermore, WHETGEO-1D is part of the system of interoperable components called GEOframe, a short description of which is given in Appendix B. The utility of GEOframe has been partially discussed previously, when treating the surface energy budget.

2.4.1 Design requirements

One of the major difficulties encountered by a research group concerns the development and reuse of scientific software (Berti, 2000) and the writing of structurally clean code, i.e. a code that

is easily readable and understandable, with objects that have a specified, and possibly unique, responsibility (Martin, 2009).

An Object-Oriented-Programming approach, with the adoption of standard design patterns (DPs) (Freeman et al., 2008; Gamma et al., 1995) and the creation of new ones, has been adopted for the internal classes design and hierarchy.

The design principles followed by the WHETGEO-1D software can be summarised as follows:

- A. The software should be open source to allow inspection and improvements by third parties;
- B. For the same reason it should be organised into parts, each with a clear functional meaning and possibly a single responsibility.
- C. The software can be extended with minimal effort and without modifications (according to the “open to extensions, closed to modifications” principle Freeman et al., 2008). In particular, the parts to be modified are those that, according to the discussion of the previous sections, could be changed to try new closures, i.e. the SWRC and the hydraulic conductivities in the case of the R^2 equation, and the thermal capacity and thermal conductivity in the case of the energy budget. Adding a new SWRC type or a new conductivity functions should be easy.
- D. The largest set of boundary conditions should be smoothly manageable
- E. The implementation of equations should be abstract, according to the principle of “programming to interfaces and not to concrete classes”, which is the core of contemporary OOP (Gamma et al., 1995). The different equations describing the

processes should be implemented within the set of classes by implementing a common interface.

- F. The implementation of algorithms should not depend on the data formats of inputs and outputs.

Another requirement has to do with the user experience. In fact, solvers of PDEs (Menard et al., 2020) tend to be complex to understand and run when features are added. In particular, the number of inputs grows exponentially when features are added, and the user has to overcome a steep learning curve before being able to use these software packages to appreciate all the cases implemented and their physics.

- G. To simplify this situation, WHETGEO-1D has to be implemented in such a way that any of the alternative implementations must come only with their own parameters and variables, and appear to the user as simple as possible, though not too simple.

There is finally a last requirement to consider:

- H. For computational and research purposes, there will be one, two and three dimensional (1D, 2D, 3D) implementations of the aforementioned equations. Therefore, as much as possible of the code should be shared across these. In particular, the NCZ and Newton algorithms should be shareable across the various applications.

This requirement implies that the geometry of the domain, as well as the topology, be specified in an abstract manner to cope with the specifics of each dimensionality.

The rest of this section is organised to respond to points from A to H. A is actually responded to in the next section describing where the software can be downloaded and with which open

license. Points B and C are accomplished by studying an appropriate design of classes and the use of design patterns (Freeman et al., 2008; Gamma et al., 1995). For D, generic programming is used and specific classes are implemented. E is resolved by deploying a set of classes that implement a common interface with an extension that allows it to obtain the required functionalities.

To respond to the issues raised in F and G, WHETGEO-1D is implemented as various components of OMS₃, as shown below, each one with its own inputs. Therefore, the number of flags to check and the number of unused inputs are reduced to the minimum required by the solvers and parameterizations that the user chooses. If users want to solve the R^2 equation alone, for instance, they can pick out the appropriate component and do not need to know about the inputs and details of the energy budget. The separation into components has two other advantages. First, it eases the testing of a single process against available analytical solutions and against other models results (Bisht and Riley, 2019). Second, it improves the model structure, facilitating the representation of new processes (Clark et al., 2021).

Point H is solved by deploying new components for the 1D, 2D, and 3D cases. In the following section we mainly deal with points B to E. Before discussing details of some classes, a few general choices have to be reported. Data of any type are stored internally in vectors of doubles, in turn encapsulated in appropriate Java objects. OOP good practice would suggest that an object should be immutable (Bloch, 2001), but we decided that the main classes have to be mutable and allocated once forever as singletons (Freeman et al., 2008; Gamma et al., 1995). This potentially exposes the software to side effects but frees it to allocate new objects at any time step and decreases the computational burden and memory occupancy generated by deallocating unused obsolete objects

at runtime. This approach may be considered a specific design pattern for partial differential equation solvers.

2.4.2 The software organisation

The more visible effect of our choices is that we have built various OMS₃ components:

- whetgeo1d-1.0-beta
- netcdf-1.0-beta
- closureequation-1.0-beta
- buffer-1.0-beta
- numerical-1.0-beta

Internally, the classes are assembled by using some interfaces and abstract classes, since WHETGEO-1D is coded using the Java language.

In order to improve the re-usability of the Java code we adopted a generic programming approach (Berti, 2000) that consists in decoupling of algorithm implementations from the concrete data representation while preserving efficiency. The generic approach has been balanced with domain-specific ones that can improve the computational efficiency of the software, as is the case of the previously mentioned Thomas algorithm used in 1-D implementations.

Another requirement regards the division of software classes into three main groups, as the lack of a proper separation between the parameterisation of physical processes and their numerical solutions has been recognised as one of the weak points of existing land surface models (Clark et al., 2015b; Clark et al., 2021). One group describes the mathematical-physical problem, the second one implements the numerical solution (Berti, 2000), and the

third one contains the growing group of concrete classes. The first group contains the SWRC, and hydraulic and thermal conductivity, and it forms a stand-alone library since its content can eventually be reused in the 2D and 3D version of WHETGEO-1D. Similarly, we grouped the classes that solve linear and nonlinear algebraic systems, containing the Thomas, conjugate gradient, and the various Netwon types of algorithms, in a second stand-alone library. The third group of classes gathers the concrete implementations and the variety of OMS₃ components that are deployed.

The classes used, and their repository for third parties inspection, are illustrated in the oo_Notebooks referred in section 4 and in the supplemental material. However, there are three pivotal groups of classes that we want to mention here: These contain the description of the geometry of the integration domain, the closure equation, and the state equation.

Computational domain, i.e. the Geometry class

One of the key aspects to have in a generic solver regards the management of the grid and, in particular, the definition of its topology, or how grid elements are connected to each other. In the 1D case the description of the topology is quite simple since it can be implicitly contained in the vector representation: each element of the vector corresponds to a control volume of the grid and it is only connected with the elements preceding and following it. It is worth noting that this approach is peculiar to 1D problems and cannot be adopted for the 2D and 3D domains, where, especially when unstructured grids are used, the grid topology requires a smart implementation of the incidence and adjacency matrices.

For each control volume it is necessary to store its geometrical quantities, their position and dimension, its variables, its parameter set, and the form of the equation to be solved there, referred to in the following as “equation state”. The appropriate arrangement

of information together with the internal design of the classes allows us to create a generic finite volume solver.

Closure equations, i.e. the `ClosureEquation` abstract class

The `ClosureEquation` class is shown in the UML diagram of Fig. (2.4). As explained in the Introduction, one of the core concepts of modelling water and heat transport in soils is the SWRC. Soil is a multi-phase material, thus knowledge of its composition is of crucial importance in defining its unsaturated hydraulic conductivity and its thermal properties, specific internal energy and thermal conductivity.

An abstract class `ClosureEquation` is defined to contain only abstract methods that would be overwritten by the concrete classes implementing it. The `ClosureEquation` class essentially defines a new data-type. A closer inspection of Fig. (2.4) reveals that the `ClosureEquation` is composed by aggregation with the `Parameter` class, which contains all the physical parameters of the model. Moreover, the `Parameter` class is implemented by using the Singleton pattern (Freeman et al., 2008). This design pattern is functional to have only one instance of the `Parameter` class shared by all the `ClosureEquation` objects and to provide a global point of access to the `Parameter` instance.

The Simple Factory pattern `SoilWaterRetentionCurvesFactory` accomplishes the task of implementing the concrete classes accordingly with the OO principles: “Program to an interface, not an implementation” and “open for extension but close for modification” Freeman et al., 2008; Gamma et al., 1995. By preferring polymorphism to inheritance and using the Factory pattern (Freeman et al., 2008; Gamma et al., 1995), the developers can easily include and extend existing code or new formulations or parametrisations of SWRC. Besides, the Simple Factory fulfils the dependency inversion principle (Eckel, 2003), thus new extensions cannot affect

the functioning of existing code. The same closure equation, for instance a particular SWRC, can be used to compute the soil water volume, when solving the R^2 equation, and the specific enthalpy of the soil, when solving the heat equation.

Conductivity models, i.e. the `ConductivityEquation` abstract class

The abstract class `ConductionEquation` defines the interface to implement the hydraulic conductivity models and the thermal conductivity models. In Fig. (2.5) is reported the UML diagram. The `ConductionEquation` is composed by aggregation with the `ClosureEquation` class.

To include in WHETGEO the dependence of the soil hydraulic conductivity on temperature with adopted the Decorator pattern (Freeman et al., 2008; Gamma et al., 1995). The Decorator pattern extends an object's behaviour without subclassing it but defining a new class that wraps the original class. The decorator pattern fulfils the "Single Responsibility Principle" and the "Open-Closed principle". In Fig. (2.6) the base decorator class, `UnsaturatedHydraulicConductivityTemperatureDecorator`, implements the `ConductivityEquation` interface and contains a reference to the `ConductivityEquation` object. The `Ronan1998` is concrete class implementing the `UnsaturatedHydraulicConductivityTemperatureDecorator` and defines the implementation of the abstract methods.

Equation state, i.e. the `EquationState` class

The `EquationState` class in Fig. (2.7) contains the implementation of the discretised form of the equation state of the PDE under scrutiny. It contains a reference each to the `ClosureEquation` object, to the `Geometry` and `ProblemVariables` objects.

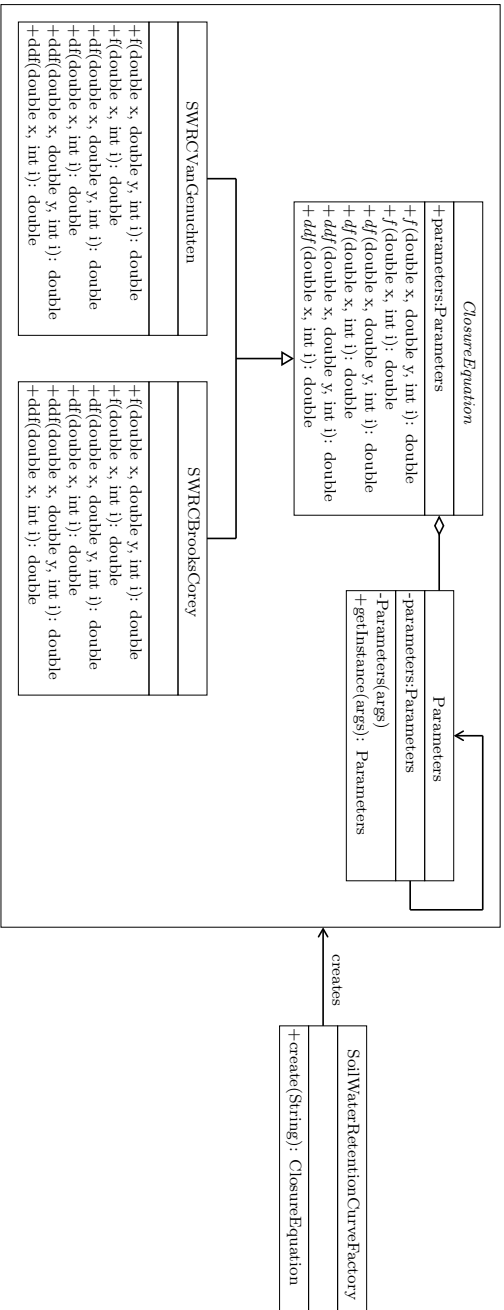


Figure 2.4: UML class diagram for the Java Simple Factory applied for the choice of the SWRC model. The ClosureEquation defines the interface that is implemented by the concrete classes SWRCVanGenuchten and SWRCBrooksCorey. The ClosureEquation is aggregated with the class Parameters containing the physical parameters of the model. The Parameters is implemented by using the Singleton pattern and its instance is inherited by the concrete classes SWRCVanGenuchten and SWRCBrooksCorey.

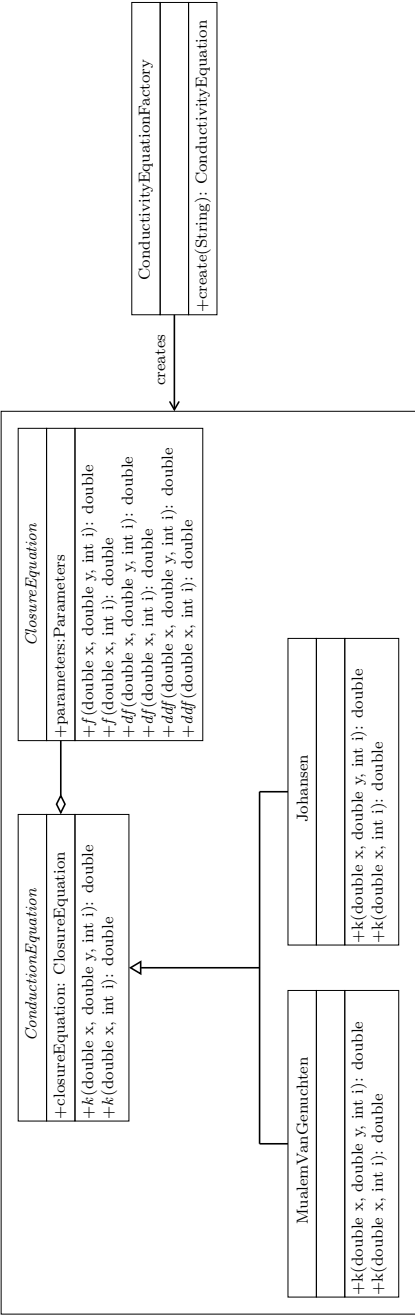


Figure 2.5: UML class diagram for the Java Simple Factory applied for the choice of the hydraulic conductivity model and of the thermal conductivity model. The `ConductivityEquation` defines the interface that is implemented by the concrete classes `MualemVanGenuchten`, implementing the Mualem-Van Genuchten model for the unsaturated hydraulic conductivity (Mualem, 1976), and `Johansen`, implementing the Johansen model for the soil thermal conductivity (Johansen, 1977). The `ConductivityEquation` is aggregated with the class `ClosureEquation` containing the SWRC model.

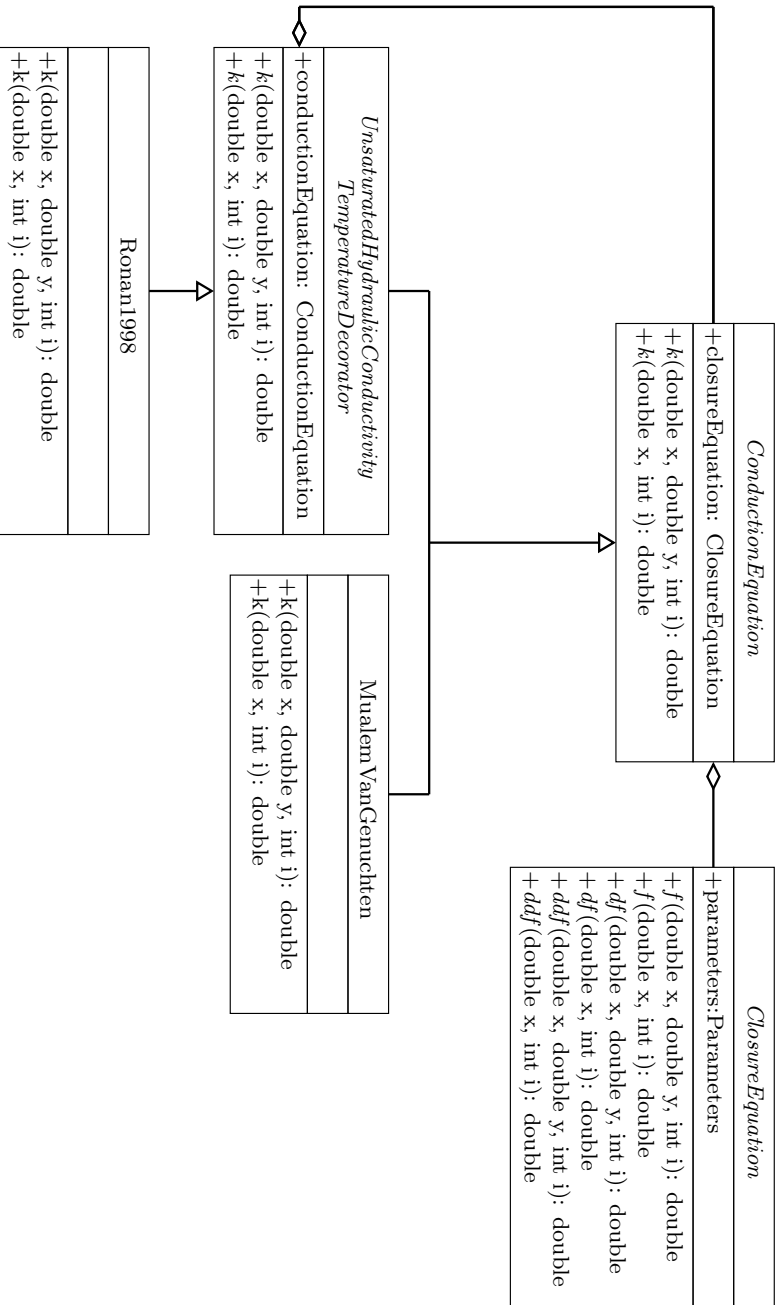


Figure 2.6: UML class diagram for the Decorator pattern applied to include the dependence of the soil hydraulic conductivity on the temperature. The `UnsaturatedHydraulicConductivityTemperatureDecorator` is the base decorator class. It implements the `ConductivityEquation` interface and contains a reference to the `ConductivityEquation` object. `Roman1998` is concrete implementing the `UnsaturatedHydraulicConductivityTemperatureDecorator`.

Notably, the solver of a PDE problem can refer to the abstract class and to its abstract object without implying the specific concrete equation to be solved or its concrete parameterisations. Moreover, the compositionality of the `EquationState` allows the creation of new solvers from existing closures without the need to add new subclasses. As shown in the UML of Figure 4, the `EquationState` class defines methods used to linearise the PDE when it is nonlinear. For instance, it computes the first and second derivatives, and the functions necessary to define the Jordan decomposition as required by the NCZ algorithm. Specifically, these methods are `p`, `q`, `pIntegral`, `qIntegral`, `computeXStar`, and `initialGuess`.

In our code design the `ClosureEquation` class is limited to computing a physical parameterisation, whereas the `EquationState` class is used to discretise the equation state of the PDE, and whenever required to properly linearise it. Any new concrete `EquationState` subclass can either have the same physics of another with a different solver or a different physics with the same solver.

2.4.3 Generic Programming at work

As explained in Section 2.1.2, the definition of the surface boundary condition for the R^2 equation can require the introduction of an additional computation node at the soil surface to simulate the water depth. This means that we have two different equation states, one for the soil water content and one for the water depth. On the other hand, when considering the Neumann or Dirichlet boundary condition we have only one equation state, for the soil water content. The nonlinear solver of the NCZ algorithm must work seamlessly with any type of boundary condition used, and with any type of equation involved in the problem.

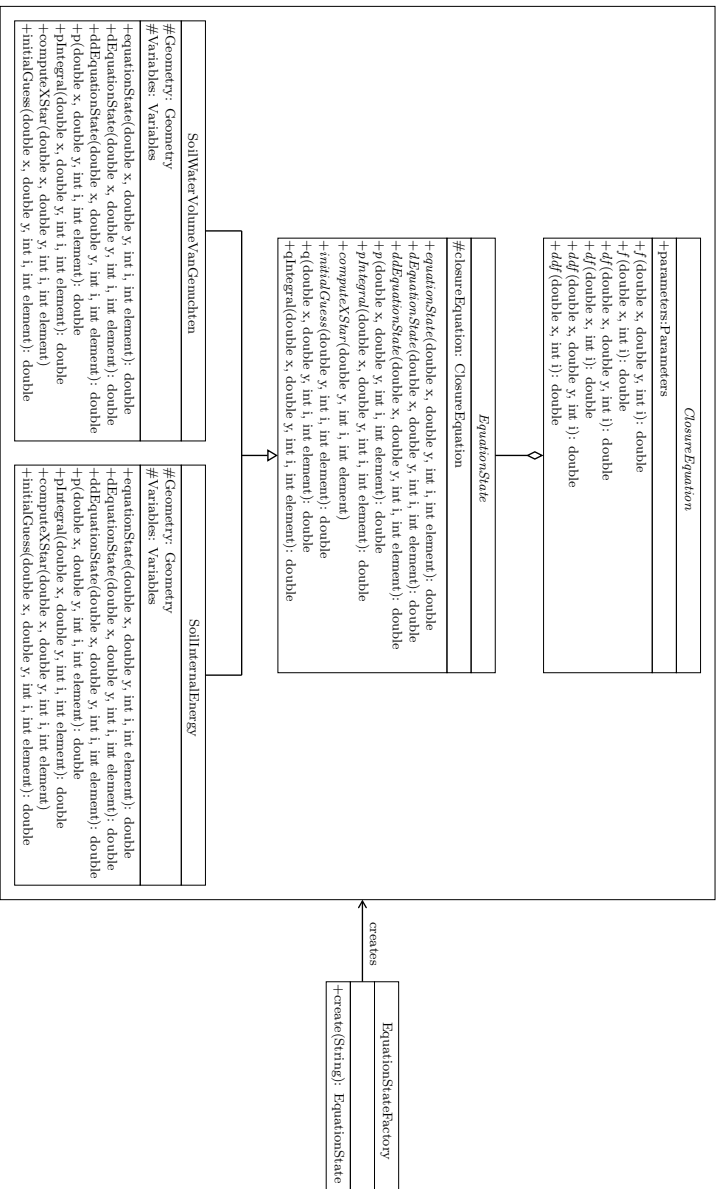


Figure 2.7: UML class diagram for the Java Simple Factory applied for the choice of the EquationState model. The EquationState defines the interface that is implemented by the concrete classes SoilWaterVolumeVanGenuchten and SoilInternalEnergy. The EquationState contains a reference to a ClosureEquation object.

Let us consider, for example, the case of the R^2 equation with water depth as the surface boundary condition. Figure (2.8) reports the pseudocode for computing the nonlinear functions in the NCZ algorithm using a procedural approach. When traversing the computational grid we need to resort to an `if-else` statement to compute the nonlinear function of each control volume: the control volume N represents the control volume for the surface water and in this case we need to use the water depth equation state, $H(\psi)$ in Fig. (2.8). The remaining control volumes represent the soil moisture and for them we need to use the SWRC equation state, $\theta(\psi)$ in Fig. (2.8). The main limit of this approach is that the computation of the nonlinear functions, $H(\psi)$ and $\theta(\psi)$, is hard-wired into the code of the NCZ algorithm. This presents a shortcoming for the reusability of the code since, as the boundary condition changes and the physical problem changes, it is necessary to modify the `for` loop and the name of the objects computing the nonlinear functions.

Adopting the OOP and generic programming approach, Fig. (2.9), it is possible to implement the NCZ algorithm in such a way that enhances its reusability. The key feature is the decoupling of the computational grid from the `algorithm(data)` (Berti, 2000). This is achieved through two elements. The first consists in creating a container of the objects that deal with the equation states of the problem, `equationState`, `eS` in Fig. (2.9). Second, we use a label `equationStateID`, `eSID` in Fig. (2.9), to specify the behaviour of each control volume. So, the behaviour of each control volume is determined by this label and not by the position of the element in the grid. Specifically, when we traverse the grid we use the `equationStateID` to determine which object inside the container `equationState` to use.

The NCZ algorithm has been implemented in the `NestedNewtonThomas` class. The `NestedNewtonThomas` contains a reference to the `Thomas`

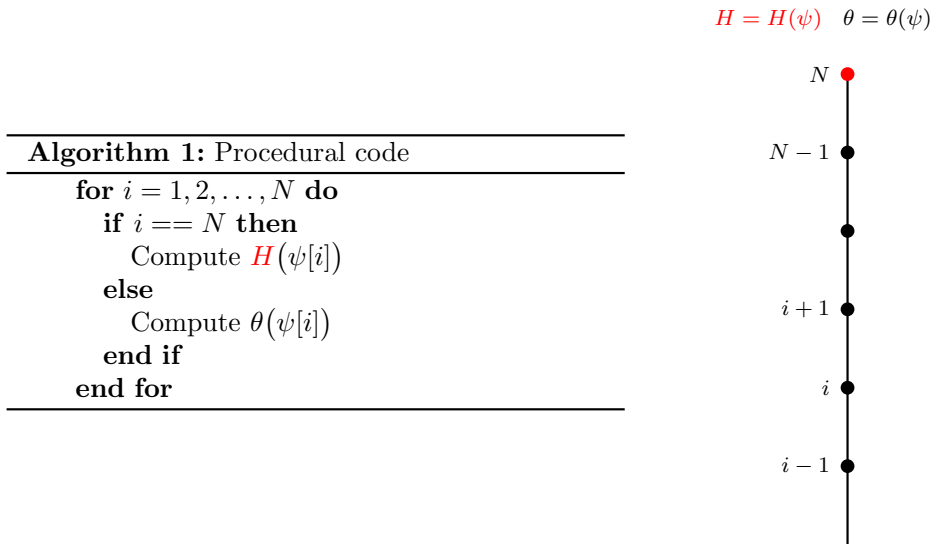


Figure 2.8: Adopting a procedural approach, the computation of the equation states is hard-wired into the code. The behaviour of each control volume is determined by an if-else statement according to the position of the element in the grid. In this case the properties of the grid, here the equation state, are joined with the topology. Here the non linear function $V(\psi)$ is replaced with either $H(\psi)$ or $\theta(\psi)$ according with the position of the node. To keep the pseudocode short, $H(\psi)$ and $\theta(\psi)$ stand for all the nonlinear function used in the NCZ algorithm, and the method `f` stands for one of the methods defined in the `EquationState` class.

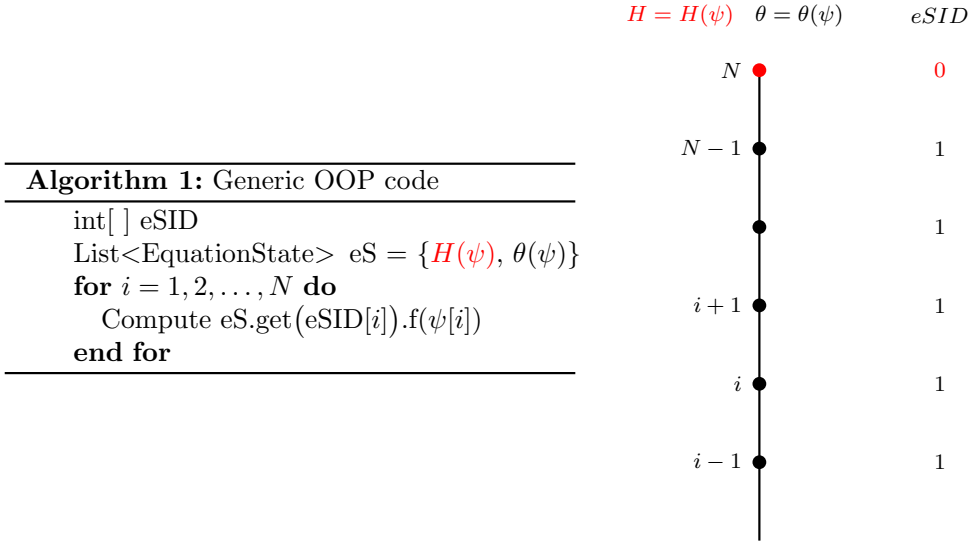


Figure 2.9: Adopting OOP with a generic programming approach, the computation of the equation states is independent from the grid. In fact, the behaviour of each control volume is determined by the vector $eSID$ - $eSID$ - equationStateID in the code - that determines which object belonging to the class `EquationState` of eS - eS - equationState in the code - must be used to compute the equation state. In this manner it is possible to traverse the computation domain without resorting to the `if-else` statement. Here the non linear function $V(\psi)$ is consistently replaced with either $H(\psi)$ or $\theta(\psi)$ according to the position of the node. To keep the pseudocode short, $H(\psi)$ and $\theta(\psi)$ stand for all the nonlinear function used in the NCZ algorithm, and the method `f` stands for one of the methods defined in the class `EquationState`.

object, whose task is to solve a linear system, and to a list of EquationState objects, Fig. (2.10). Considering the ubiquity of nonlinear problems in Hydrology and the robustness of the NCZ algorithm, the NCZ algorithm has been encapsulated in a stand-alone library.

The example has been illustrated in 1D but it becomes even more effective when working on 2D or 3D, especially with an unstructured grid.

2.5 INFORMATION FOR USERS AND DEVELOPERS

While most of the what written so far is of general application, the deployment shown here is 1D. Information on WHETGEO-1D for users and developers is provided in the supplemental material, where there is a Jupyter Notebook that contains the guidelines for executing the codes for any of the components. Its name starts with "oo_" and we call it "Notebook Zero" of the components. The latest executable code can be downloaded from

- <https://github.com/geoframecomponents/WHETGEO-1D>

and can be compiled by following the instructions therein. The version of the OMS₃ compiled project can be found here https://github.com/GEOframeOMSProjects/OMS_Project_WHETGEO1D. The code can be executed in the OMS₃ console, which can be downloaded and installed according to the instructions given at:

- <https://geoframe.blogspot.com/2020/01/the-winter-school-on-geoframe-system-is.html>

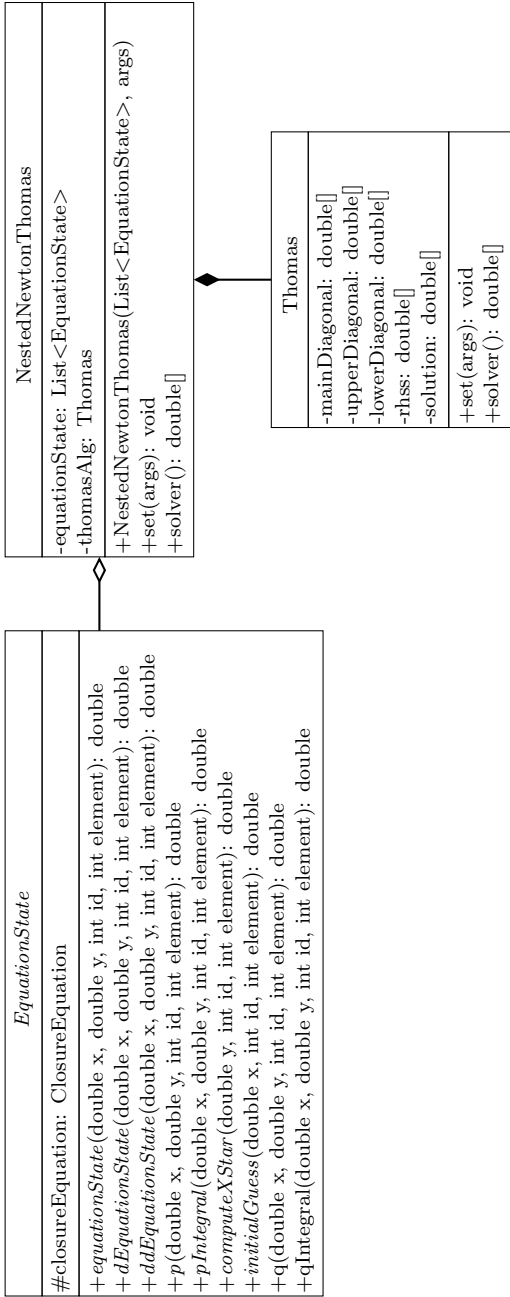


Figure 2.10: UML class diagram of the `NestedNewtonThomas` class. This class deals with the solution of the nonlinear system. The `NestedNewtonThomas` contains a reference each to the `Thomas` object, whose task it is to solve a linear system, and to a list of `EquationState` objects.

Some brief information about GEOframe can be found in Appendix B, and more comprehensive information is at:

- <https://abouthydrology.blogspot.com/2015/03/jgrass-new-age-essentials.html>
- <https://geoframe.blogspot.com/2020/01/gsw2020-photos-and-material.html>

To run the tests, please follow the instructions on the Github repository of the GEOframe components. If a user wants to compile the code themselves, they can use the appropriate Gradle script that guarantees independence from any IDE. For further information about input and output formats for WHETGEO-1D, please see the Notebook `00_WHETGEO1D_Richards.ipynb` in the folder Documentation of the Zenodo distribution.

2.5.1 Workflow for Users

Examples of uses of WHETGEO-1D can be found in the form of Python Notebooks in the directory Notebooks/Jupyter. Documentation can be found in form of Python Notebooks in the directory Documentation. Simulations with WHETGEO-1D are run as OMS₃ simulations. Therefore, the first operation to accomplish is to prepare the appropriate `.sim` files. For new users, many simulation files are available in the directory simulation of the Zenodo distribution. As shown in Fig. (2.11), in the modelling solutions that involve WHETGEO-1D, there is always a “Main” component that is in charge of running the core code for solving the PDE. The inputs and the outputs are treated by other OMS₃ components. They are tied together by a Domain Specific Language (DSL) based on Groovy. This allows for great flexibility in using various input and output formats.

2.5.2 Inputs and outputs

Input data can be broadly classified into time series, computational grid data, and simulation parameters. Time series are used to specify the boundary conditions of the problem. Time series are contained in .csv files with a specific format that is OMS3 compliant (David, [n.d.](#)). With computational grid data we refer to the domain discretisation, initial condition, and soil parameters. All these data are stored in a netCDF file. Time series and computational grid data are elaborated with dedicated Python modules distributed under the `geoframepy` package (Tubini and R, [2021](#)). The simulation parameters, such as the start date and end date of the simulation, time step size, and file paths, are specified by the user in the OMS3 .sim file.

For the design of the output workflow we took advantage of the OMS3 system that allows the user to connect stand-alone components. Figure (2.11) shows the output workflow for saving output data and where Main, Buffer, and netCDF writer are the stand-alone OMS3 components. Main stands for the generic component having the responsibility of solving the PDE. Buffer has the responsibility of temporarily storing output data, and Writer handles the saving of data to the disk. The Buffer component has the sole purpose of storing data and this has two important advantages. The first is that it limits the number of accesses to the disk to save output, i.e. reducing the computational time. The second is that it introduces a layer separating the Main component from the netCDF writer. This increases the flexibility of the modelling solution, as future developers can adopt different file formats, or develop different writer components that, instead of saving all the outputs, can save discrete outputs or aggregated outputs. The advantage is that developers need only know the legacy of the Buffer component and customise the both output file format and memory optimisation strategy, such as chunking, according to

their need. Currently all outputs are stored in a netCDF-3 format (Unidata, 2021). netCDF is a self-describing portable data format developed and maintained by UCAR Unidata. netCDF is commonly used by the Geo-science community and there is an ever-growing number of tools for processing and visualisation.

The choice of including the Buffer component in the workflow of the modelling solution is motivated by earlier experiences of the GEOTop community with the GEOTop model, and by more recent experience with the FreeThaw1D model (Tubini et al., 2020), where long spin-ups of the model (~ 1500 years) were required with consequent large output files (~ 100 GB). Furthermore, in anticipation of the 2D and 3D developments, the netCDF-3 format is probably not the most appropriate and could be abandoned in favour of more performing file formats Unidata, n.d.-a, n.d.-b, such as netCDF-4 or HDF5.

WHETGEO-1D can be integrated with the built-in calibration component LUCA (Formetta et al., 2014a; Hay et al., 2006) and the Verification component, as shown in Fig. (2.12). The former is used to calibrate optimal parameters, the latter to compute the indices of goodness of simulated data versus measured data. Besides the LUCA component and the Verification component, it is necessary to add two more components, specifically the Buffer calibration parameters and the Measurement point data. The Buffer calibration parameters is needed to interface the Main component with the LUCA component. In fact, in the WHETGEO-1D Main component, physical parameters are stored as vectors, whilst LUCA handles calibration parameters as scalars (single value). The Buffer calibration component receives the optimal parameters set from the LUCA component and returns them packed in appropriate vectors. The Verification component receives as input two, OMS3-compliant time series: one for measured data and one for simulated data. In this case it is necessary to extract from the

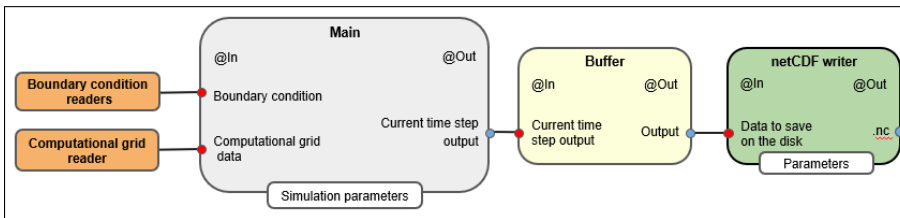


Figure 2.11: Workflow of WHETGEO-1D. The boundary condition readers, computational grid reader, Main, Buffer, and netCDF writer are stand-alone OMS₃ components. Main stands for the generic component with the responsibility of solving the PDE, the Buffer temporarily stores output data that later are passed to the netCDF writer component, which in turn saves data to the disk. The Buffer component has the sole purpose of storing data. This has two advantages: the first one is to limit the number of accesses to the disk to save output, i.e. reducing the computational time, and the second one is to introduce a layer separating the Main component, which handles the numerical solution of the PDE, and the component responsible for saving outputs.

simulation output only the simulated data at the measurement points of the variable used to calibrate the model. These data are then saved as OMS3 time series. It is interesting that the integration of WHETGEO-1D with the OMS3 built-in calibration components is achieved by adding two new, stand-alone components without modifying the source code of the existing components, i.e. the Main component, the Buffer component, and the netCDF writer.

2.5.3 Workflow for Developers

Here, as an example, we present how to add the Brooks-Corey (Brooks and Corey, 1964) model as an extension of the code base. The constitutive relationships are given by:

$$\theta(\psi) = \begin{cases} \theta_r + (\theta_s - \theta_r) \left(\frac{\psi_d}{\psi} \right)^n & \text{if } \psi \leq \psi_d \\ \theta_s & \text{if } \psi > \psi_d \end{cases} \quad (47)$$

$$K(\psi) = K_s \left[\frac{\theta(\psi) - \theta_r}{\theta_s - \theta_r} \right]^{3 + \frac{2}{n}} \quad (48)$$

where θ_s and θ_r are, respectively, the saturated and residual values of the volumetric water content, ψ_d is the air-entry water suction value, n is the pore size distribution index, and K_s is the saturated hydraulic conductivity at saturation.

The standard approach to adding a new SWRC parametrization, here the Brooks and Corey model, requires the definition of a new class that extends the abstract class `ClosureEquation`. This new class, `SWRCBrooksCorey`, provides the implementation of the abstract methods defined in the super class `ClosureEquation`, and inherits the association with the `Parameters` class. Specifically, the `SWRCBrooksCorey` class overrides the following methods:

- `f` calculates the water content for a given water suction value and set of parameters, Eq. (47);

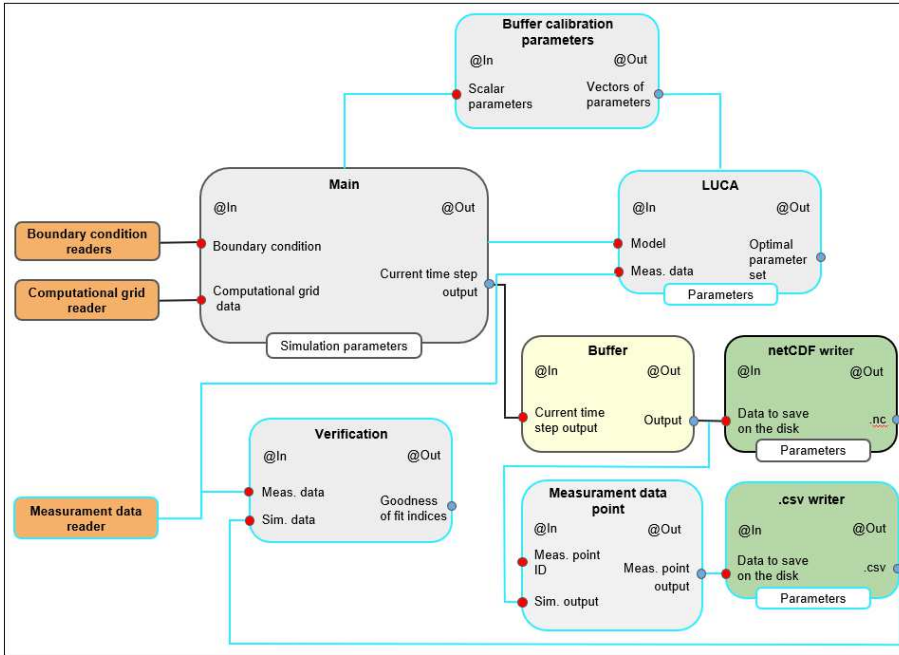


Figure 2.12: Workflow of WHETGEO-1D integrated with LUCA. The cyan lines identify those components required to integrate WHETGEO-1D with LUCA. The LUCA and Verification components are built-in OMS₃ components. The former is used to calibrate optimal parameters, the latter to compute the indices of goodness of simulated data versus measured data. To integrate WHETGEO-1D with the OMS₃ calibration components it is necessary to add two other components into the workflow, specifically the Buffer calibration parameters component and the measurement point data component. LUCA handles scalar parameters whilst WHETGEO-1D uses vectorial parameters. The Buffer calibration parameters creates an interface between these two components, simply creating vectorial parameters from scalar parameters. The Verification component requires the input time series as a .csv file of simulated data at the measurement points. To accomplish this requirement, it is necessary to modify the output strategy: the Buffer component passes output data to the Measurement points data component. This component extracts only the simulated variables at the measurement points and passes them to the OMS₃ time series writer, .csv writer, which save the simulated time series as a .csv file.

- `df` calculates the first derivative of Eq. (47);
- `ddf` calculates the second derivative of Eq. (47).

In order to use the Brooks-Corey model in the Richards' equation it is necessary to define a new class, `SoilWaterVolumeBrooksCorey`, that extends the abstract class `StateEquation`. Specifically the `SoilWaterVolumeBrooksCorey` class overrides the following methods:

- `equationState` calculates the water volume using the Brooks-Corey model for a given water suction value and set of parameters, Eq. (20).
- `dEquationState` calculates the first derivative of the `equationState` function, in this the moisture capacity function. This method is used within the linearisation algorithm.
- `ddEquationState` calculates the second derivative of the `equationState` function. This method is relevant for those models where the ψ^* cannot be computed analytically but requires the application of a root finding method such as the bisection method. An example is the soil internal energy function when considering the phase change of water Tubini et al., 2020.
- `p` calculates the p function of the Jordan decomposition.
- `pIntegral` calculates the V_1 function of the Jordan decomposition.
- `computeXStar` calculates the ψ^* value to properly define the functions p and V_1 .
- `initialGuess` calculates the initial guess for the linearisation algorithm.

2.6 R² TEST CASES

In this section we test the solver of the R² equation against the analytical solutions presented by Srivastava and Yeh (1991) and by Vanderborght et al. (2005). Then we present and discuss two “behavioural” test cases to try out WHETGEO-1D in simulating both the infiltration excess and the saturation excess process.

2.6.1 Analytical solution of Srivastava and Yeh (1991)

Srivastava and Yeh (1991) derived an analytical solution describing the one-dimensional transient infiltration in an homogeneous and layered soil. The hydraulic properties of the soil are described by the following constitutive relations:

$$K(\psi) = K_s e^{\alpha\psi} \quad (49)$$

$$\theta(\psi) = \theta_r + (\theta_s - \theta_r) e^{\alpha\psi} \quad (50)$$

where K_s is the saturated hydraulic conductivity, θ_r is the residual water content, θ_s is the saturated water content, and α is the soil pore-size distribution parameter, representing the desaturation rate of the SWRC. The lower boundary condition is represented by the water table, $\psi = 0$ m, while the upper boundary condition is subjected to a constant flux, q . The initial condition corresponds to the steady state profile due to a prescribed initial flux at the soil surface and prescribed pressure at the lower boundary. The analytical solution is derived by linearising Richards' equation and using Laplace's transformation. Details on the analytical solution can be found in (Srivastava and Yeh, 1991).

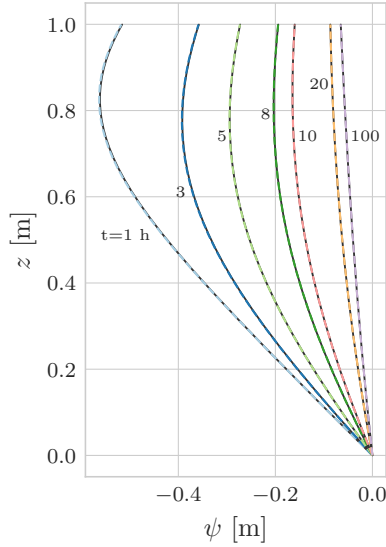


Figure 2.13: Comparison between the analytical and numerical solutions for the test problem TP1.

Homogeneous soil

We consider a one-dimension homogeneous soil layer of 1 m depth (TP1). The saturated hydraulic conductivity value is assumed to be $2.778 \times 10^{-6} \text{ m s}^{-1}$, with $\theta_s = 0.45 \text{ m}^3 \text{ m}^{-3}$, $\theta_r = 0.2 \text{ m}^3 \text{ m}^{-3}$, and $\alpha = 1 \text{ m}^{-1}$. The initial condition is determined by imposing as lower boundary condition $\psi = 0 \text{ m}$ and a constant water flux at the soil surface $q_A = 2.776 \times 10^{-7} \text{ m s}^{-1}$. For times greater than 0 the water flux at the soil surface is $q_B = 2.5e - 6 \text{ m s}^{-1}$. The domain is discretised with a uniform grid space $\Delta z = 0.001 \text{ m}$ and the time step is $\Delta t = 60 \text{ s}$. The model accuracy is enhanced by allowing two Picard iterations per time step. Figure (2.13) shows a comparison between the numerical and the analytical solutions.

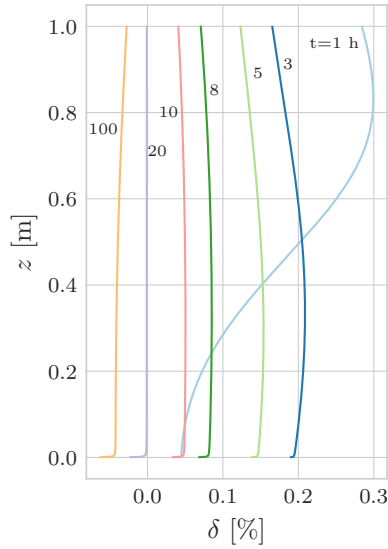


Figure 2.14: Relative water suction error for the test problem TP1.

Layered soil

In this numerical problem (TP2) we consider one-dimensional vertical infiltration toward the water table through a layered soil. The initial condition is determined by imposing as lower boundary condition $\psi = 0$ m and a constant water flux at the soil surface $q_A = 2.776 \times 10^{-7} \text{ m s}^{-1}$. For times greater than 0 the water flux at the soil surface is $q_B = 2.5 \times 10^{-6} \text{ m s}^{-1}$. The domain is discretised with a uniform grid space $\Delta z = 0.001$ m and the time step is $\Delta t = 60$ s. The model accuracy is enhanced by allowing two Picard iterations per time step. The hydraulic conductivity at the interface is computed as the harmonic mean of the neighbours (Romano et al., 1998). Comparison between the numerical and the analytical solution for water suction is shown in Fig. (2.15).

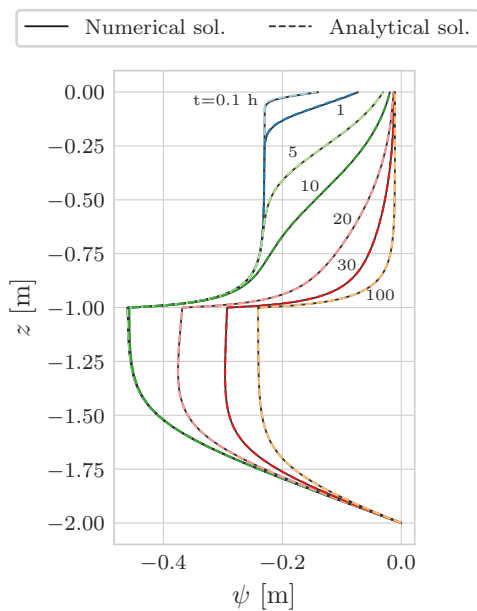


Figure 2.15: Comparison between the analytical and numerical solutions for the test problem TP2.

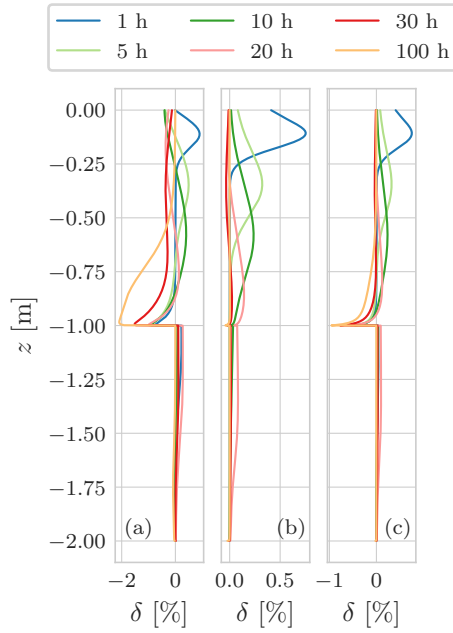


Figure 2.16: Comparison of relative water suction error δ for the test problem TP2 using different interface hydraulic conductivity algorithms. Panel (a) is computed with max., panel (b) with harmonic mean, and panel (c) with geometric mean. As reported in (Romano et al., 1998), the harmonic mean offers the best agreement with the analytical solution. This is particularly evident at the interface between the two layers.

Table 2.1: Hydraulic properties for the three soil types used in the Vanderborght test case (TP₃).

Soil type	$\theta_s \text{ m}^3 \text{ m}^{-3}$	$\theta_r \text{ m}^3 \text{ m}^{-3}$	$\alpha \text{ m}^{-1}$	$n -$	$K_s \text{ m s}^{-1}$
Sand	0.43	0.045	15.0	3	1.16×10^{-4}
Loam	0.43	0.08	4.0	1.6	5.79×10^{-6}
Clay	0.4	0.1	1.0	1.1	1.16×10^{-6}

2.6.2 Analytical solution of Vanderborght et al. (2005)

The next test case was defined by Vanderborght et al. (2005) to evaluate the steady-state flux in layered soil profiles. For this numerical problem (TP₃) we consider a soil column of 2 m depth with one soil type for depth 0 m – 0.5 m overlying another soil type for depth 0.5 m – 2 m, specifically for loam over sand, sand over loam, and clay over sand. The soil parameters are defined in Tab. (2.1). The initial condition for water suction is a uniform profile with $\psi = -20$ m, the surface boundary condition is a constant flux $q = 5.79 \times 10^{-8} \text{ m s}^{-1}$, and at the bottom we impose a free drainage boundary condition. The domain is discretized with a uniform grid space $\Delta z = 0.01$ m and the time step is $\Delta t = 3600$ s. In order to reach the steady state condition the simulation lasts 2 years. Comparison between the numerical and the analytical solution is shown in Fig. (2.17).

2.6.3 Surface boundary condition

The definition of the surface boundary condition is a nontrivial task since it is a system-dependent boundary condition. The infiltration rate through the soil surface depends on precipitation, rainfall intensity J , and on the moisture condition of the soil. Because of this, the surface boundary condition may change from the Dirichlet type - prescribed water suction - to the Neumann type

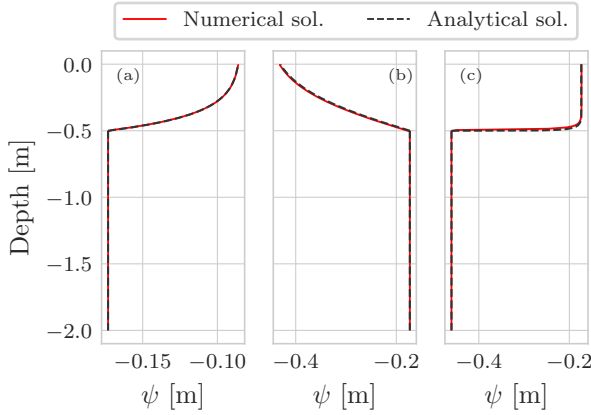


Figure 2.17: Comparison between the analytical and the numerical solution for the test problem TP₃. The three panels show the vertical profile of water suction at steady state for a constant flow rate of $5.79 \cdot 10^{-8} \text{ m s}^{-1}$: (a) clay-sand soil profile, (b) loam-sand soil profile, and (c) sand-loam soil profile.

- prescribed flux - and vice-versa. The works by Horton (1933) and Dunne and Black (1970) establish the conceptual framework to explain the runoff generation.

The infiltration excess or Horton runoff occurs when the rainfall intensity is larger than infiltration capacity of the soil:

$$|J| > \left| -K(\psi) \frac{\partial}{\partial z} (\psi + z) \right|_{z=0} \quad (51)$$

Infiltration excess is most commonly observed with short-duration, intense rainfall.

The saturation excess or Durnian runoff occurs when the soil is saturated and additional water cannot infiltrate through the soil surface. Saturation excess generally occurs with long-duration, moderate rainfall, or with a series of successive precipitation events. In this case the soil depth or the presence of a bedrock are deter-

Table 2.2: Hydraulic properties of the silty clay loam soil (Bonan, 2019) for the Horton runoff numerical experiment.

θ_r m ³ m ⁻³	θ_s m ³ m ⁻³	α m ⁻¹	n -	K_s m s ⁻¹
0.089	0.43	1.0	1.23	1.9447×10^{-7}

mining factors for saturation excess. Another possible cause is the rise of the water table up to the soil surface.

Infiltration excess

In this numerical experiment we consider a homogeneous soil of 3 m depth. Soil hydraulic properties are described with the Van Genuchten's model, Table (2.2).

The initial condition is assumed to be hydrostatic with $\psi = 0$ m at the bottom. The surface boundary condition is a synthetic rainfall, as in Fig. (2.18) (a), lasting 15 min with constant intensity of 0.028 mm s^{-1} . At the bottom we prescribed a Dirichlet boundary condition with constant $\psi = 0$ m so the transient is driven only by the surface boundary condition. In Fig. (2.18) panel (a), the time is indicated when it would be necessary to switch from the Neumann type to the Dirichlet type boundary condition.

Figure (2.18) shows a comparison of water ponding at the soil surface considering two different initial conditions of the soil, wet and dry. For the wet case, the initial condition is hydrostatic with $\psi = 0$ m at the bottom. For the dry case, the initial condition is hydrostatic with $\psi = -100$ m at the bottom. In the wet initial condition the hydraulic conductivity is higher than for the dry initial condition, however, in the dry case the capillary gradient is larger and because of this the soil infiltration capacity is higher, as in Fig. (2.18) panel (a). With regards to the water ponding, the maximum value is almost the same in both cases, 1 mm higher in the wet case, but the time evolution is different: in the wet case

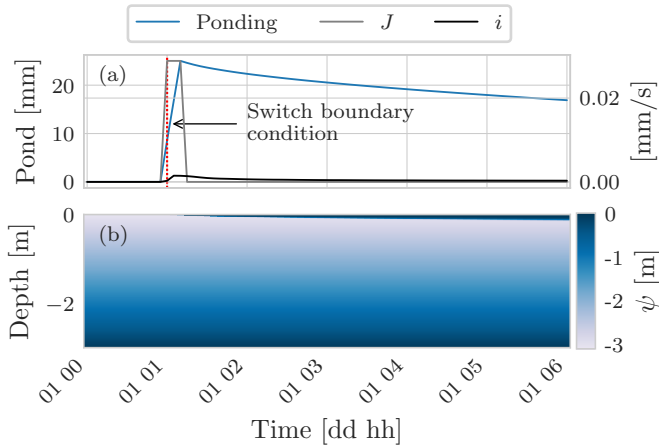


Figure 2.18: Panel (a) shows a comparison between the rainfall intensity J and actual soil infiltration i . The rainfall intensity exceeds the actual infiltration rate so water builds up at the soil surface (blue line). Panel (b) shows the time evolution of the water suction within the soil. From the numerical point of view, as water builds up at the soil surface it would be necessary to switch the boundary condition, from Neumann type to Dirichlet type.

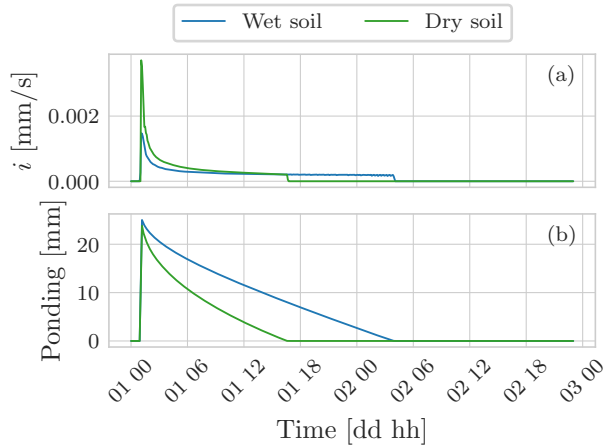


Figure 2.19: Panel (a) shows a comparison between the infiltration rate for two cases: wet and dry initial condition. In the dry case, soil infiltration is greater than the wet case even though the hydraulic conductivity is smaller. This is due to the higher capillary gradients that develop in the soil. Panel (b) shows the time evolution of the water ponding at the soil surface.

the water only infiltrates completely 13 h later than the dry case. This delay may seem counter-intuitive since wetter conditions are associated with higher values of hydraulic conductivity, Fig. (2.19), but in the wet soil the capillary gradients are smaller than in the dry soil, Fig. (2.20).

In Fig. (2.22) we compare the water ponding as the soil temperature varies. The temperature-hydraulic conductivity relationship is model using the model presented in Ronan et al. (1998). The soil temperature in these simulation is kept constant over time. As temperature is lower the reference value of $T = 20\text{ }^{\circ}\text{C}$ the infiltration is slower because the hydraulic conductivity is lower the reference value, whereas when temperature is higher the infiltration is faster. From this synthetic experiment it is clear how

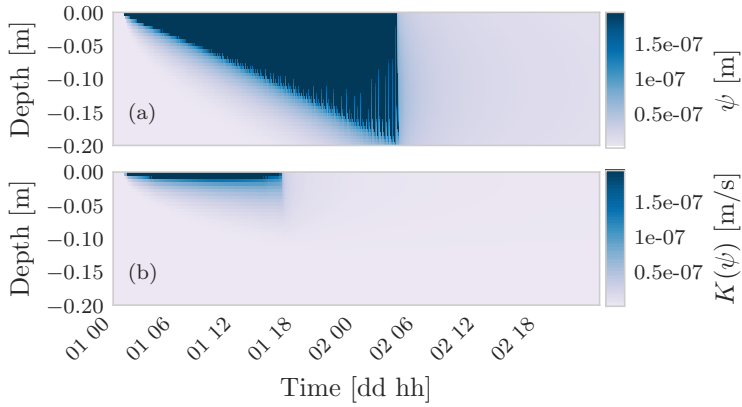


Figure 2.20: Panel (a) shows the hydraulic conductivity field for the case of wet soil, while panel (b) shows the hydraulic conductivity field for the case of dry soil.

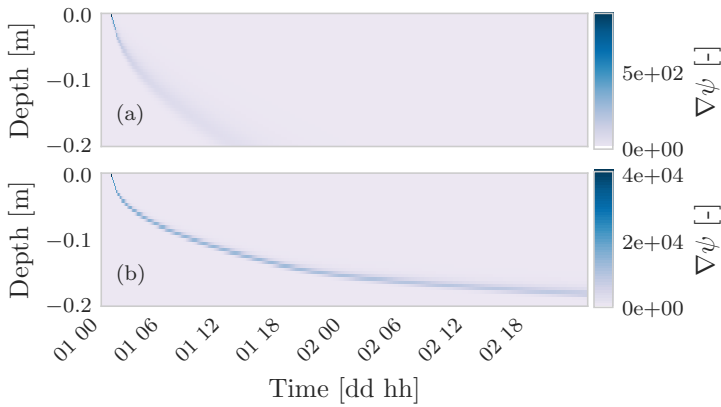


Figure 2.21: Panel (a) shows the capillary gradient for the case of wet soil, panel (b) shows the the capillary gradient for the case of dry soil. As can be seen, in the dry soil the capillary gradient is two orders of magnitude larger than in the wet soil. Because of this higher gradient water infiltrates faster in the dry soil than in the wet soil.

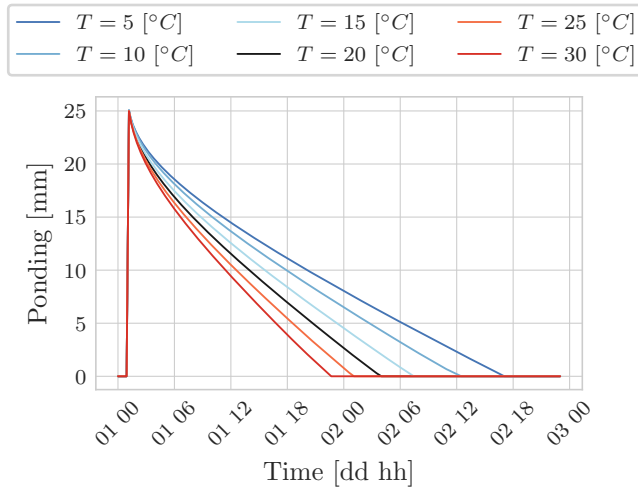


Figure 2.22: Comparison of the water ponding time evolution considering different soil temperatures. The temperature in these simulations is uniform and kept constant over time. The reference value of for temperature is $T = 20$ °C. As soil temperature is lower the reference value the infiltration is lower, vice-verse when temperature is higher.

temperature can affect the water infiltration and thus simulate the coupled water and energy budget.

Saturation excess

In this section we present two numerical experiments to simulate the saturation excess process. Saturation excess is more critical, in terms of simulation stability, than the infiltration excess (Forums, [n.d.](#)). We consider two cases: one in which the water table reaches the soil surface; and another in which the total rainfall amount is larger than the maximum water holding capacity but the rainfall intensity is less than the maximum infiltration rate.

Table 2.3: Hydraulic properties of the loam layer and clay layer, respectively, (Bonan, 2019) for the numerical experiment on Dunnian runoff due to water table rising.

θ_r m ³ m ⁻³	θ_s m ³ m ⁻³	α m ⁻¹	n -	K_s m s ⁻¹
0.078	0.43	3.6	1.56	2.8889×10^{-6}
0.068	0.38	0.8	1.09	5.5556×10^{-7}

Table 2.4: Hydraulic properties of the loamy sand layer and clay layer, respectively, (Bonan, 2019) for the numerical experiment on Dunnian runoff due rainfall.

θ_r m ³ m ⁻³	θ_s m ³ m ⁻³	α m ⁻¹	n -	K_s m s ⁻¹
0.057	0.41	12.4	2.28	4.0528×10^{-5}
0.068	0.38	0.8	1.09	5.5556×10^{-7}

Firstly, we consider a layered soil of 3 m depth. The thicknesses of the loamy layer and clay layer are, respectively, 0.5 m, and 2.5 m. The soil hydraulic properties are described with the Van Genuchten's model, Tab. (2.3). The initial condition is assumed to be hydrostatic with $\psi = 0$ m at the bottom. At the surface boundary condition we prescribe no rainfall, while at the bottom a variable Dirichlet boundary condition is prescribed Fig. (2.23) (a). The transient is driven by variation of the water table. In Fig. (2.23) panel (a) the time is indicated when it would be necessary to switch the surface boundary condition from the Neumann type to the Dirichlet type boundary condition and vice-versa.

Secondly, we consider a layered soil of 3 m depth. The thicknesses of the loamy sand layer and the clay layer are, respectively, 0.3 m, and 2.7 m. The soil hydraulic properties are described with the Van Genuchten's model, Tab. (2.4). The initial condition is assumed to be hydrostatic with $\psi = -2$ m at the bottom. The surface boundary condition is a synthetic rainfall Fig. (2.21) (a), at the bottom we prescribed a Dirichlet boundary condition with constant

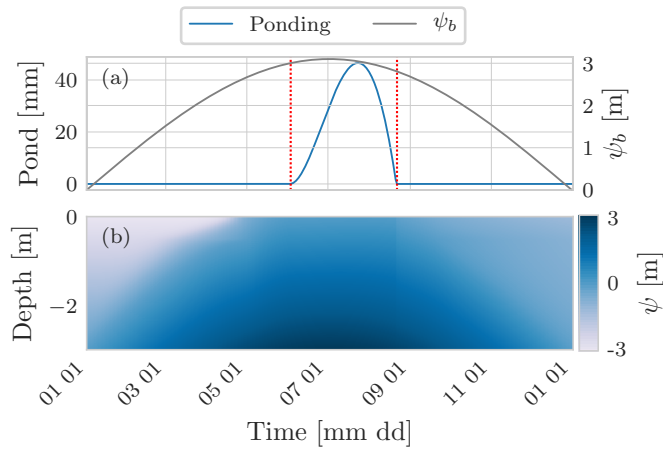


Figure 2.23: Panel (a) shows the water table position, Dirichlet boundary condition, and the water ponding at the soil surface. The dotted red lines indicate the times at which the boundary condition at the soil surface should be switched. The first line indicates the switch from the Neumann type to the Dirichlet type since water starts building up. The second line indicates the switch from the Dirichlet type to the Neumann type because there is no water at the soil surface. Panel (b) shows the time evolution of the water suction within the soil.

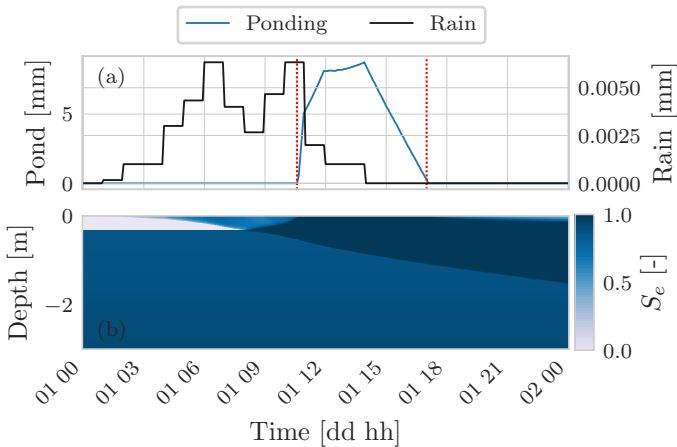


Figure 2.24: Panel (a) shows the rainfall and the water ponding at the soil surface. Initially rainfall can infiltrate into the soil and no water builds up at the soil surface. As the uppermost layer of the soil saturates water starts ponding at the soil surface. The dotted red lines indicate the times at which the boundary condition at the soil surface should be switched. Panel (b) shows the time evolution of the saturation degree within the soil.

$\psi = -2$ m so the transient is driven only by the surface boundary condition. Figure (2.24) panel (b) shows the time evolution of the degree of saturation within the soil. Initially water infiltrates in the soil but then the clay layer, which is characterised by a lower conductivity than the loam-sand layer, limits the deep infiltration causing the saturation of the loam-sand layer from below.

Figure (2.25) presents the aforementioned numerical test taking in account the effect of soil temperature on the hydraulic conductivity. As before the temperature is uniform and kept constant over time.

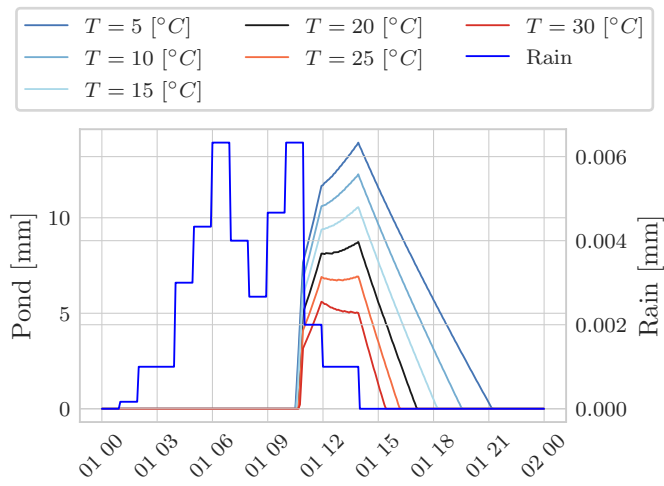


Figure 2.25: In this numerical experiment the run-off varies with soil temperature. As the soil becomes colder the maximum for water ponding increases and water takes more time to infiltrate.

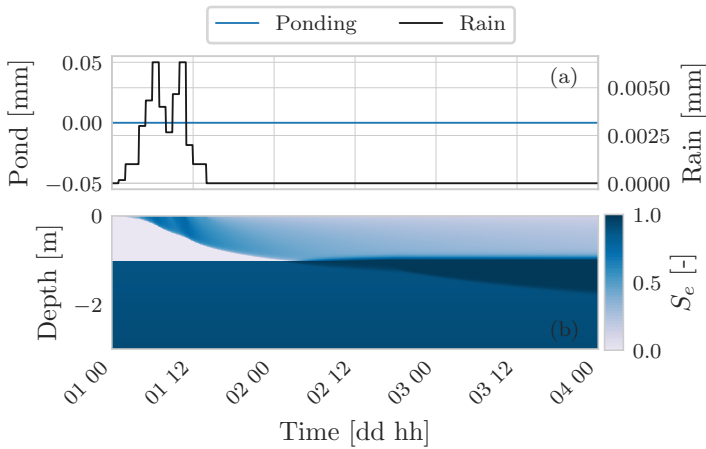


Figure 2.26: In this numerical experiment there is no saturation excess since the greater thickness of the uppermost layer ensure a sufficient water storage capacity for the forcing rainfall.

Repeating the above numerical experiment with a thicker loam-sandy layer, Fig. (2.26), there is no water ponding at the soil surface. In this case all the rainfall can infiltrate into the loam-sandy layer thanks to the increased water storage capacity.

Example of a calibration with

In this section I present an application of WHETGEO-1D combined with the LUCA component to calibrate some measurements of water content (Formetta et al., 2016b). This is meant to be a calibration exercise. The calibration process is described in Fig. (2.12). Figure (2.27) shows a comparison between measurements and simulated values for site C₁. As can be seen WHETGEO-1D is able to reproduce the stable soil moisture patterns both at low and high saturation levels, as well as the main wetting front. Table 2.5 reports the indices of goodness-of-fit for the four depths.

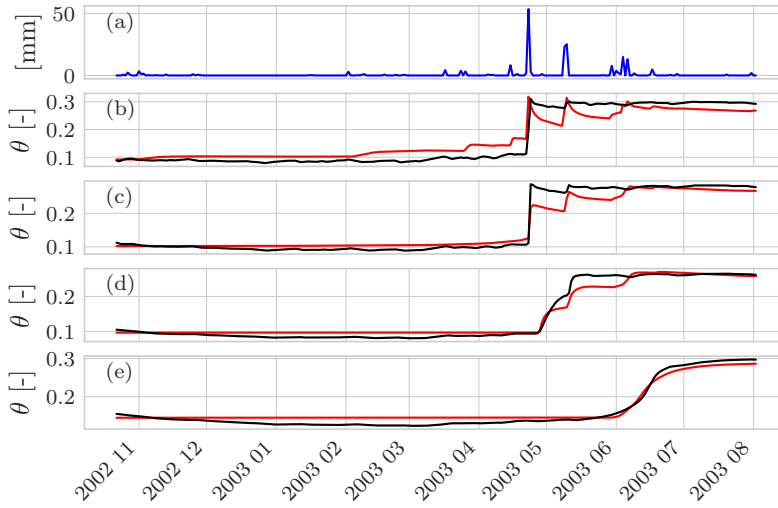


Figure 2.27: Comparison between measurement data of soil moisture, black, and simulated values, red, for location C1. Panel (a) shows the rainfall, panel (b), soil moisture dynamics at depth 0.3 m, panel (c) at depth 0.6 m, panel (c) at depth 0.9 m, panel (c) at depth 1.2 m.

Table 2.5: Kling-Gupta Efficiency (KGE) coefficient and root mean squared error (RMSE) values quantify the model godness of fit.

Depth m	KGE	RMSE $\text{m}^3\text{m}^{-3}\%$
0.3	0.69	3.05
0.6	0.82	1.86
0.9	0.89	1.39
1.2	0.82	1.29

Table 2.6: Optimal parameter set estimated by using the LUCA calibration algorithm. D_z is the depth of each layer measured from the soil surface.

D_z m	K_s m s ⁻¹	θ_r m ³ m ⁻³	θ_s m ³ m ⁻³	α m ⁻¹	n -
0.15	2.1×10^{-3}	0.553	0.061	11.36	2.919
0.45	7.1×10^{-5}	0.550	0.031	1.90	1.374
0.75	8.4×10^{-5}	0.530	0.044	2.10	1.364
1.05	8.9×10^{-5}	0.550	0.056	2.15	1.425
1.35	1.9×10^{-6}	0.536	0.070	2.10	1.314
2.35	3.1×10^{-6}	0.498	0.069	2.40	1.360

2.6.4 Energy budget

This Section presents some behavioural test case on the pure heat conduction considering the surface energy balance, and on the couple water and energy budget.

Pure heat diffusion with surface energy budget

The soil column is 30 m deep and the initial condition is a constant temperature profile $T = 12$ °C. Figure (2.28) panel (a) shows the components of the surface energy fluxes and the thermal regime of the uppermost 2 m of the soil column. As can be seen in panel (b), the soil temperature falls below 0 °C; therefore it is not reasonable to neglect freezing and thawing processes.

Coupled water and energy budget

In this it is presented a simulation of coupled water and heat transport in soil.

2.7 CODE AVAILABILITY

The source code is written in Java using the object-oriented programming paradigm. It can be found at <https://github.com/geoframecomponents/WHETGEO-1D>. The OMS3 project can be found at https://github.com/GEOframeOMSProjects/OMS_Project_WHETGEO1D. A frozen version of the OMS project used can be found at <https://zenodo.org/record/4749319>.

2.8 CONCLUSION REMARKS

In this chapter we discussed the issues raised by implementing a new expandable system to model the Earth's CZ. Firstly, mathematical issues were discussed and then the software-engineering aspects were faced. The implementation has been shown to solve the issues presented in 7 observations, 3 requirements, and A to H design specifications. Each of these was analysed and informed the choice of algorithms and code implementation. The first deployment of the concepts was the 1D stand-alone water budget and the coupled water and energy budgets WHETGEO versions.

The water budget was tested against analytical solutions presented in (Srivastava and Yeh, 1991) and (Vanderborgh et al., 2005). Some behavioural simulations were also performed to show some features of the code, such as the ability to deal with switching boundary conditions. Moreover some synthetic simulations has been presented about the pure heat diffusion and the heat advection-diffusion. As noted further development is required to properly include freezing and thawing processes in soils.

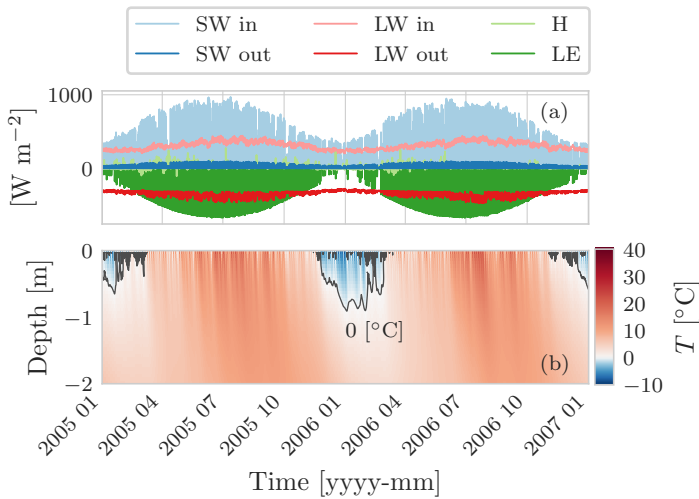


Figure 2.28: Behavioural test case of pure heat conduction in soil considering the surface energy budget. Panel (a) shows the surface energy fluxes driving the simulation. The external fluxes, incoming shortwave and longwave radiation, and the latent heat flux, are computed with existing GEOframe components. Panel (b) shows the thermal regime of the uppermost 2 m of the soil column. As can be seen, during winter the temperature of the uppermost layer goes below $0\text{ }^{\circ}\text{C}$, the grey line is the $0\text{ }^{\circ}\text{C}$ isotherm, therefore, it is not reasonable to overlook the phase change of water.

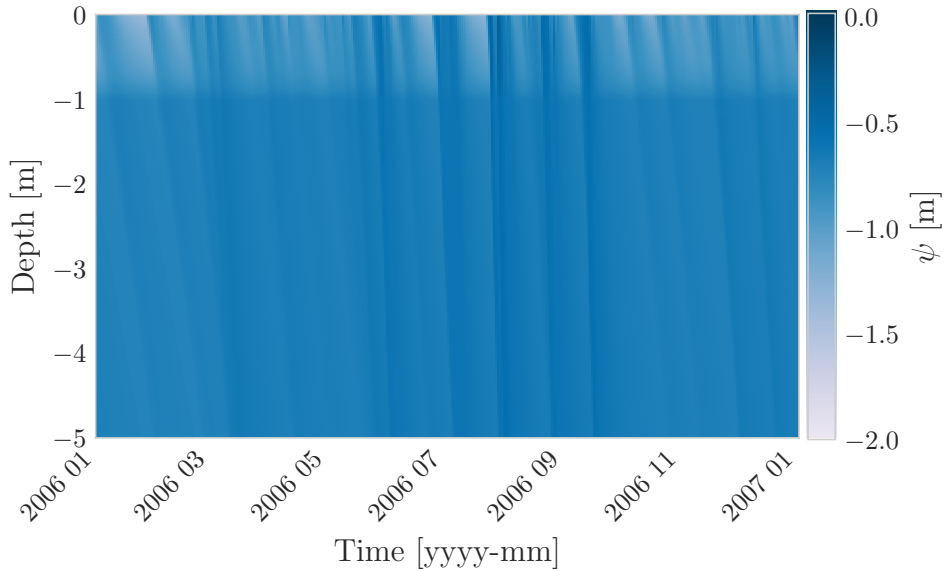


Figure 2.29: Behavioural test case of pure heat conduction in soil considering the surface energy budget. Panel (a) shows the surface energy fluxes driving the simulation. The external fluxes, incoming shortwave and longwave radiation, and the latent heat flux, are computed with existing GEOframe components. Panel (b) shows the thermal regime of the uppermost 2 m of the soil column. As can be seen, during winter the temperature of the uppermost layer goes below $0\text{ }^{\circ}\text{C}$, the grey line is the $0\text{ }^{\circ}\text{C}$ isotherm, therefore, it is not reasonable to overlook the phase change of water.

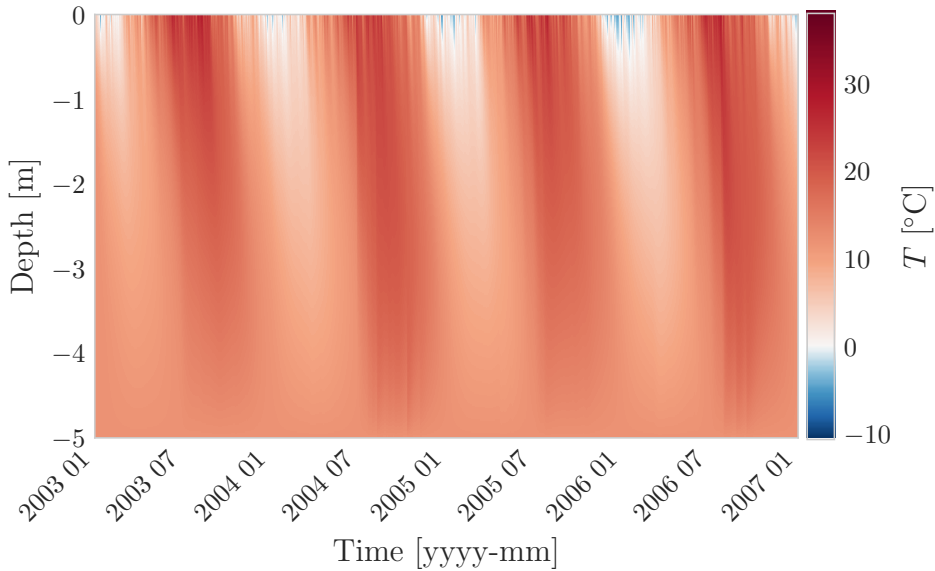


Figure 2.30: Behavioural test case of pure heat conduction in soil considering the surface energy budget. Panel (a) shows the surface energy fluxes driving the simulation. The external fluxes, incoming shortwave and longwave radiation, and the latent heat flux, are computed with existing GEOframe components. Panel (b) shows the thermal regime of the uppermost 2 m of the soil column. As can be seen, during winter the temperature of the uppermost layer goes below $0\text{ }^{\circ}\text{C}$, the grey line is the $0\text{ }^{\circ}\text{C}$ isotherm, therefore, it is not reasonable to overlook the phase change of water.

3

HEAT CONDUCTION IN FROZEN SOIL 1D

Contents

3.1	Introduction	85
3.2	The governing equations and their numerical issues	89
3.3	Discretization of the enthalpy equation	93
3.4	Analytical benchmarks	95
3.4.1	Neumann analytical solution	95
3.4.2	Lunardini analytical solution	102
3.5	Numerical test	106
3.6	FreeThaw-1D and WHETGEO-1D	115
3.7	Commonly used simulation software	123
3.8	Code availability	132
3.9	Conclusion remarks	133

3.1 INTRODUCTION

Freezing and thawing of soils affect a wide range of biogeochemical and hydrological (Schuur et al., 2015; Walvoord and Kurylyk, 2016) processes and interact with engineered structures in cold regions. Correspondingly, the simulation of freezing and thawing soil is an important and well-researched topic (Harris et al., 2009; Streletskiy et al., 2019). Climate change brings additional urgency and new phenomena of interest to these studies. It is thus not a surprise that many models of freezing and thawing soil and

ice exist, some of which are reviewed in Appendix 3.7. Here, we propose a solution to a central challenge that these models have in common.

Published models can be categorized as empirical, analytical, or numerical (Riseborough et al., 2008). Empirical methods relate ground temperature or thawing/freezing depth (TFD) to simple topoclimatic factors (Riseborough et al., 2008; Zhang et al., 2008) and are relatively simple to apply. By contrast, analytical and numerical models are based on the conservation of mass and energy and can be divided in two broad groups (Tan et al., 2011). The first group focuses primarily on freezing and thawing, commonly known as the Stefan problem. The governing equation describes energy conservation with the heat flux modelled using the Fourier law. The second group considers the coupled problem of heat transfer and water flow in soils. In this case energy-enthalpy conservation equation includes also the advective heat flux and it is coupled with the mass conservation equation. For both groups, the latent heat transfer during phase change of water leads to problems related to convergence, conservation, and restrictions to discretization of space and time (Bao et al., 2016).

Historically (Hu and Argyropoulos, 1996; Vuik, 1993), the first attempts to solve the problem of heat conduction considering the phenomena of solidification and melting date back to the studies by Lamé and Clapeyron in 1831, and the analytical solutions presented by Stefan around 1890, and Neumann in 1921. Later, other analytical solutions were proposed in order to overcome some simplifications that were too restrictive (Riseborough et al., 2008; Walvoord and Kurylyk, 2016; Zhang et al., 2008). These analytical solutions, however, are limited to one dimensional problems and constrained in their initial and boundary conditions as well as the description of soil characteristics (Kurylyk et al., 2014a).

By contrast, numerical models can accommodate complex processes or configurations, including soil heterogeneities, complicated temperature boundary conditions, intermittent freeze-thaw and temporally variable thermal properties. Accurately representing phase transitions, however, is a non-trivial task and several different methods have been published. They can be broadly cast in two general groups: the so-called front-tracking methods and the fixed-grid methods (Voller et al., 1990). Even though this contribution is focused on modelling heat transfer in frozen soil or ice, the following review includes, and is relevant for, other fields of research that involve phase change.

Front-tracking methods are suitable whenever the two phases are divided by a spatially smooth and continuous front and thus the state of the system can be conveniently described by the position of this interface (Voller et al., 1990). The moving front is tracked defining a continuity ('Stefan') condition on the heat flux across it. For example, the one-dimensional model by Goodrich (1978, 1982) uses front-tracking in modelling frozen soil and the SICOPOLIS model (Greve, 1997a, 1997b; Greve and Blatter, 2016) uses it to model polythermal ice sheets.

In frozen soil, however, a significant proportion of water can remain liquid at temperatures well below 0 °C. This depression of the melting temperature is due to the presence of solutes (Bouyoucos, 1920; Bouyoucos, 1923; Bouyoucos, 1913; Bouyoucos and McCool, 1915), surface effects in the interaction between water and soil particles as well as water and ice (Anderson and Tice, 1972; Clow, 2018), and the Gibbs-Thomson effect (Rempel et al., 2004; Watanabe and Mizoguchi, 2002). To some degree, also polycrystalline ice has a temperature-dependent liquid water content (Langham, 1974). The gradual phase change over a range of temperatures in soils is commonly described with the soil freezing characteristic curve (SFCC) (Kurylyk and Watanabe, 2013). More-

over the presence of a partially frozen region is also common in ice and snow where liquid and solid phase coexist in thick isothermal layers.

With phase change occurring over a range of temperatures, rather than at one specific temperature, front-tracking methods become computationally expensive (Voller et al., 1990) and conceptually ambiguous. This is the case in many industrial (Voller and Cross, 1981) and environmental problems. Additionally, front tracking is complicated because it requires either a deforming grid or a transformed coordinate system (Aschwanden and Blatter, 2009). By contrast, fixed-grid methods can accurately describing the thermodynamics of the problem without requiring additional complications in handling the computational domain. For these reasons, fixed-grid methods are generally preferable to front-tracking methods when simulating frozen soil.

Fixed-grid methods include the latent heat of fusion in their governing equation, avoiding the necessity to define a continuity condition across the moving boundary and related implementation problems. All contemporary fixed-grid methods we reviewed aim to solve the numerical integration using globally convergent algorithms. Three differing approaches for treating the latent heat of fusion exists: the enthalpy method, using a source term, and using apparent heat capacity. As analytical expressions, these methods look the same because their governing equations can be obtained from each other by the chain rule of derivation. As we will illustrate in the next section, problems can arise in the discrete domain where this rule is not always valid.

Here we present a numerical model of heat conduction with freezing and thawing in soils without water flow that guarantees exact energy conservation for any time step size and for a wide range of soil freezing characteristics. It is novel in using the nested Newton-Casulli-Zanolli (NCZ) algorithm (Casulli and

Zanolli, 2010) for solving the nonlinear system obtained from discretizing the governing equation, written in terms of the specific enthalpy, using a semi-implicit finite volume scheme. The NCZ algorithm has previously been applied to solving water flow in soils and to our knowledge this is first application for solving the heat equation. Long time steps, such as hours or days, are desirable in several applications including permafrost thaw, or surface components of climate models, and models dedicated to avalanche prediction.

3.2 THE GOVERNING EQUATIONS AND THEIR NUMERICAL ISSUES

The governing equation of the problem in the first of the three approaches is written in terms of both the total enthalpy and temperature

$$\frac{\partial h(T)}{\partial t} = \nabla \cdot [\lambda(T)\nabla T] \quad (52)$$

where $h(T)$ is the specific enthalpy, T is temperature, $\lambda(T)$ is the thermal conductivity, and t is the time.

In the approach relying on apparent heat capacity, the governing equation is

$$C_a \frac{\partial T}{\partial t} = \nabla \cdot [\lambda(T)\nabla T] \quad (53)$$

where

$$C_a = \frac{\partial h}{\partial T} = C_T + \rho_w l_f \frac{\partial \theta_w}{\partial T} \quad (54)$$

is the apparent heat capacity that is the sum of the actual heat capacity C_T and a term representing the additional thermal capacity arising from phase change with the local derivative of the SFCC (Dall'Amico, 2010).

In the approach using a source term for latent heat, it is considered as a heat source

$$C_T \frac{\partial T}{\partial t} = \nabla \cdot [\lambda(T) \nabla T] - \rho_w l_f \frac{\partial \theta_w}{\partial T}, \quad (55)$$

and in this equation, there are two unknowns: the temperature, and the liquid fraction θ_w appearing in the source term.

The specific enthalpy per unit mass is defined as

$$h = u + pv \quad (56)$$

where u is the specific internal energy, p is pressure, and v is the specific volume, the inverse of density. Assuming that the heat transfer occurs at constant pressure and volume the differential of the specific energy and of the specific enthalpy are equal (Appendix C). However, since the term enthalpy method is commonly used in the literature, we will refer to enthalpy instead of internal energy.

When considering freezing and thawing processes, the specific enthalpy of a control volume of soil V_c can be calculated as the sum of the enthalpy of the soil particles, liquid water and ice (Dall'Amico et al., 2011):

$$h = h_{sp} + h_w + h_i \quad (57)$$

Defining a reference temperature T_{ref} the above terms becomes

$$\begin{aligned} h_{sp} &= \rho_{sp} c_{sp} (1 - \theta_s) (T - T_{ref}) \\ h_w &= \rho_w c_w \theta_w (T) (T - T_{ref}) + \rho_w l_f \theta_w (T) \\ h_i &= \rho_i c_i \theta_i (T) (T - T_{ref}) \end{aligned} \quad (58)$$

where l_f is the specific latent heat of fusion, ρ_{sp} , ρ_w and ρ_i are the densities of the soil particles, water, and ice, c_{sp} , c_w , c_i are the specif heat capacity of the soil particles, water, and ice, $\theta_w(T)$ is

the unfrozen water content, and $\theta_i(T)$ is the ice content. The liquid water content and the ice content are evaluated using SFCCs (Dall'Amico et al., 2011) which are dependent on temperature and, in the general case, on temperature and water saturation. Usually the reference temperature, T_{ref} , is set to 273.15 K, the melting temperature of pure water at standard atmospheric pressure. By using Eq. (58) the enthalpy Eq. (57) can be rewritten as

$$h = C_T(T - T_{ref}) + \rho_w l_f \theta_w(T) \quad (59)$$

where $C_T = \rho_{sp} c_{sp}(1 - \theta_s) + \rho_w c_w \theta_w(T) + \rho_i c_i \theta_i(T)$ is the bulk heat capacity of the soil volume V_c .

SFCCs have an inflection point (Bao et al., 2016; Hansson et al., 2004) causing a sharp change in their derivative. This non-linear behaviour gives rise to convergence problems during the solution of the system of equations resulting from the numerical approximation of the governing equation (Casulli and Zanolli, 2010; Voller, 1990). This is true for any method used such as finite differences (Bao et al., 2016; Sergueev et al., 2003; Westermann et al., 2016), finite elements (McKenzie et al., 2007), and finite volumes (Dall'Amico et al., 2011). As a consequence, the robustness (stability) of the numerics used is a fundamental and important issue in frozen soil models.

There is a more subtle aspect in the integration though. Analytically, Eq. (52), Eq. (53) and Eq. (55) are equivalent because Eq. (53) and Eq. (55) are derived from Eq. (52) by applying the chain rule of derivative on the enthalpy under the general assumption that the enthalpy is a differentiable variable. However, this is not necessarily so in the discrete domain where the derivative chain rule is not always valid. This is a known issue when dealing with hyperbolic equations (Roe, 1981), but often overlooked when treating the parabolic ones.

The apparent heat-capacity approach, Eq. (53) can suffer from large balance errors in the presence of high nonlinearities and

strong gradients (Casulli and Zanolli, 2010). The key to deriving a conservative numerical method here concerns the discretization of the apparent heat capacity, and Nicolsky et al. (2007a) as well as Voller et al. (1990) discussed suitable techniques. It is worth to note that the solution of the apparent heat-capacity approach presents the same issue of the ψ -based form of the R^2 .

The source-term approach presents problems analogous to those of the apparent heat-capacity formulation. Specifically, Eq. (55) is derived from Eq. (53) by moving the latent heat term to the right-hand-side of the equation. Equation (55) can be solved numerically using an iterative procedure (Voller et al., 1990) or the Decoupled Energy Conservation Parametrization method (DECP) (Zhang et al., 2008). As pointed out by Voller et al. (1990), the numerical solutions based on an iterative procedure may suffer from non-convergence problem unless under-relaxation is wisely applied, and additionally, it necessary to guarantee that the liquid fraction is in the range $(0, 1)$. With DECP, the energy equation is first solved without latent heat. Then, soil temperature and the liquid and solid fractions are readjusted to ensure energy conservation during phase change. This method is mainly used in land-surface models (LSMs) (Dai et al., 2003; Foley et al., 1996; Verseghy, 1991). In this case, Nicolsky et al. (2007b) showed that it results in an artificial stretch of the phase change region, with consequent inaccuracies in the simulation of active-layer thickness. A summary of relevant models is given in Table 3.1 and more details in Appendix 3.7.

In summary, the governing equation can be written using three different approaches that are equivalent analytically, but not in their discrete formulation. Of the three, the enthalpy approach remains conservative, even when discretized, and should be preferred. An additional fundamental problem is the solution of the nonlinear system of equations. Current algorithms either require

time step adaptation or may fail to converge, leading to unstable simulations and reduced computational efficiency (Casulli and Zanolli, 2010). Here we address this fundamental challenge by using the NCZ algorithm to solve the nonlinear system of equations. Compared to other algorithms, it guarantees convergence of the solution for any integration time step. When the time step is not constrained by numerical issues, it can be chosen to better match the time scale of the process under investigation.

3.3 DISCRETIZATION OF THE ENTHALPY EQUATION

The implicit finite volume discretization of Eq. (52) reads as

$$h_i(T_i^{n+1}) = h_i(T_i^n) + \Delta t \left[\Lambda_{i+\frac{1}{2}}^{n+1} \frac{T_{i+1}^{n+1} - T_i^{n+1}}{\Delta z_{i+\frac{1}{2}}} - \Lambda_{i-\frac{1}{2}}^{n+1} \frac{T_i^{n+1} - T_{i-1}^{n+1}}{\Delta z_{i-\frac{1}{2}}} + S_i^n \right] \quad (60)$$

where Δt is the time step size,

$$S_i^n = \int_{\Omega_i} S d\Omega \quad (61)$$

is an optional source/sink term in volume, and $h_i(T)$ is the i th enthalpy given by

$$h_i(T) = \int_{\Omega_i} h(T) d\Omega. \quad (62)$$

Equation (60) can be written in matrix form as

$$\mathbf{h}(\mathbf{T}) + \mathbf{A}\mathbf{T} = \mathbf{b} \quad (63)$$

Table 3.1: Diversity of formulations and solvers in current models of heat transfer and phase change in the cryosphere. Theoretical limitations do not necessarily affect the usability of models for their intended purpose. More details are in Section 3.7.

Model	Form	Time discretization	Nonlinear solver	Theoretical limitations
CLM	N. L. H ^a	Crank-Nicolson	DECP ^f	Artificial stretch of phase change region ^h and non-convergence ⁱ .
CoupModel	A. H. C ^b	Explicit	Not required	Monotonicity time step restriction.
CryoGrid	A. H. C ^b	Implicit	Newton based algorithm	Stability time step restriction.
GEOtop	A. H. C ^b	Implicit	Globally convergent Newton algorithm	Nonlinear solver ^g .
GIPL-2.0	E. F. ^c	Implicit	Newton algorithm with Godunov splitting	Nonlinear solver ^g .
Goodrich	N. L. H. ^a	Implicit	Front tacking method	Computationally expensive. Problems arise when the phase change occurs over a range of temperatures.
Hydrus 1D	A. H. C ^b	Implicit	Picard iteration	Nonlinear solver ^g .
MarsFlow	E. F. ^c	Implicit	Newton-Raphson algorithm	Nonlinear solver ^g .
NEST	S. T. ^d	Explicit	Not required	Stability time step restriction.
SoilVision	A. H. C ^b	Explicit and implicit	Newton-Raphson algorithm	Nonlinear solver ^g .
SUTRA	A. H. C ^b	Implicit	Picard iteration	Nonlinear solver ^g .
Crocus	E. F. ^c	Implicit	DECP ^f	Artificial stretch of phase change region due to the DECP ^h and non-convergence ⁱ .
SNOWPACK	S. T.	Implicit	DECP ^f	Artificial stretch of phase change region ^h and non-convergence ⁱ .
ORCHIDEE	N. L. H. ^a	Explicit	DECP ^f	Artificial stretch of phase change region ^h and non-convergence ⁱ .
JSBACH	S. T. ^d	Implicit	DECP ^f	Artificial stretch of phase change region ^h and non-convergence ⁱ .
Aschwanden Blatter	E. G. M. ^c	Implicit	Newton based algorithm	Nonlinear solver ^g .
SICOPOLIS	N. L. H. ^a	Implicit	Front tracking method with a transformed coordinate system	Computationally expensive.
Schoof Hewitt	E. F. ^c	Implicit and explicit	Not required	Requires the partition of the domain in cold and temperate regions.

^aThe governing equation is written in only in terms of temperature and the latent heat is not included. ^bApparent heat capacity formulation. ^cEnthalpy formulation. ^dSource term formulation. ^eThe heat flux is written in terms of enthalpy and not of temperature as in the enthalpy formulation. ^fDecoupled Energy Conservation Parametrization. ^gConvergence of the nonlinear solver can be problematic (Casulli and Zanolli, 2010, 2012). ^h(Nicolosky et al., 2007a). ⁱ(Voller et al., 1990).

where $\mathbf{T} = \{T_i\}$ is the vector of unknowns, $\mathbf{h}(\mathbf{T}) = h_i(T_i)$ is a vectorial function representing the discrete enthalpy, \mathbf{A} is the energy flux matrix, and \mathbf{b} is the right-hand-side vector of Eq. (60), which is properly augmented by the known Dirichlet boundary condition when necessary. For a given initial condition T_i^0 , at any time step $n = 1, 2, \dots$ Eq. (60) constitutes a nonlinear system for T_i^{n+1} , with the nonlinearity affecting only the diagonal of the system and being represented by the enthalpy $h_i(T_i^{n+1})$. This set of equations is a consistent and conservative discretization of Eq. (52). Therefore, regardless of the chosen spatial and temporal resolution, T_i^{n+1} is a conservative approximation of the new temperature.

3.4 ANALYTICAL BENCHMARKS

The numerical model is compared for the problem of a column of freezing water, i.e. the Stefan problem, with the analytical solution presented by Neumann (cited in Kurylyk et al., 2014b), and for the problem of a column of soil with the three-zone with the analytical solution presented by Lunardini (1988).

3.4.1 Neumann analytical solution

The Neumann analytical solution gives the solution of unilateral freezing of a semi-infinite domain for both the temperature profile and the position of the moving boundary. Kurylyk et al. (2014b) recommended the Neumann solution due to its ability to represent differences between the thermal diffusivities of the thawed and frozen zones. Here we consider the freezing of pure water instead of soil since it is more numerically demanding. Consider a semi-infinite domain of pure water at temperature $T(z, 0) = T_0$ where $T_0 > T_m$, Fig. (3.1). At the surface a Dirichlet boundary

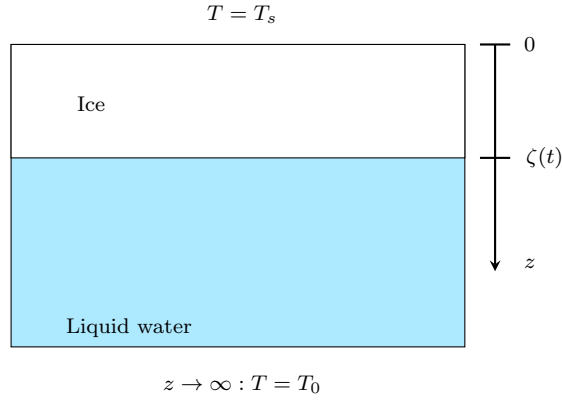


Figure 3.1: Scheme showing the setting of the Neumann solution for the freezing case. Initially all water is liquid, $T_0 > T_m$. Because of the surface boundary condition, $T_s < T_m$, a freezing front, ζ , propagates downward.

condition is imposed $T(z = 0, t) = T_s$, with $T_s < T_m$. As a consequence a freezing front ζ propagates downward separating the solid and the liquid phase. The governing equations are

$$\frac{\partial h}{\partial t} = \lambda \frac{\partial^2 T}{\partial z^2} \quad (64)$$

$$T(\zeta, t) = T_m \quad (65)$$

$$\lambda_i \frac{\partial T}{\partial z} \Big|_{z=\zeta^-} dt = \lambda_w \frac{\partial T}{\partial z} \Big|_{z=\zeta^+} dt + l_f \rho d\zeta \quad (66)$$

At the moving boundary $\zeta(t)$, the temperature is equal to the melting temperature of water, and the time evolution of $\zeta(t)$ is described by the third equation, the Stefan condition. This condition states that the difference of the heat fluxes at the interface of the two substances is consumed for the phase change. The derivation of the analytical solution is reported in Appendix (D). The parameters used in the comparison are given in Table (D.1). The

Table 3.2: Maximum error m of the freezing front position from the numerical solution with the NCZ algorithm for different space and time discretizations relative to the Neumann analytical solution. For the numerical solution the position of the freezing front has been reconstructed from the linear interpolation of the temperature profile.

	$\Delta t = 60 \text{ s}$	$\Delta t = 300 \text{ s}$	$\Delta t = 3600 \text{ s}$
$\Delta z = 0.001 \text{ m}$	0.00737	0.00153	0.00739
$\Delta z = 0.005 \text{ m}$	0.00271	0.00302	0.00714
$\Delta z = 0.01 \text{ m}$	0.00536	0.00553	0.00905

numerical model is able to simulate the freezing problem of water well as seen in Fig. (3.2) and Fig. (3.3).

For comparison, Kurylyk et al. (2014b) tested the numerical model SUTRA against the Neumann analytical solution considering a soil porosity of $0.50 \text{ m}^3 \text{m}^{-3}$. For their test the time step was of $0.04 - 0.4 \text{ s}$, the vertical spatial discretization 0.001 m , and the parameter ϵ was increased to $-0.01 \text{ }^\circ\text{C}$ to match the analytical solution. The maximum absolute error of the freezing front position was 0.00099 m .

In our model, the choice of a small melting temperature range $\epsilon = 0.0001 \text{ }^\circ\text{C}$ does not affect the quality of the numerical solution even at a large time step of 3600 s . Looking at Table (3.2) it is clear that the choice of the time step size is somehow related to the choice of the spatial discretization: using a small time step with a coarse grid does not necessarily improve the accuracy of the position of the freezing front.

We use the Neumann analytical solution to assess the robustness of the NCZ algorithm in comparison with the Newton-Raphson and globally-convergent Newton methods. As reported by Dall'Amico et al. (2011), Figure (3.4) represents a well known case for which the Newton-Raphson algorithm can not converge.

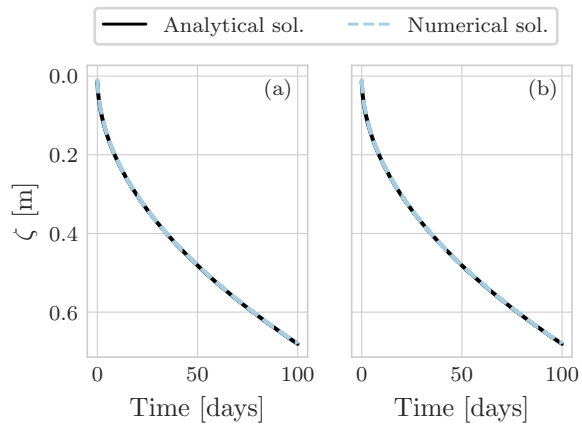


Figure 3.2: Propagation of the freezing front compared between the Neumann analytical and the numerical solution with the NCZ algorithm. Two space discretizations are used: (a) $\Delta z = 0.005$ m, and (b) $\Delta z = 0.001$ m. The integration time step is $\Delta t = 3600$ s.

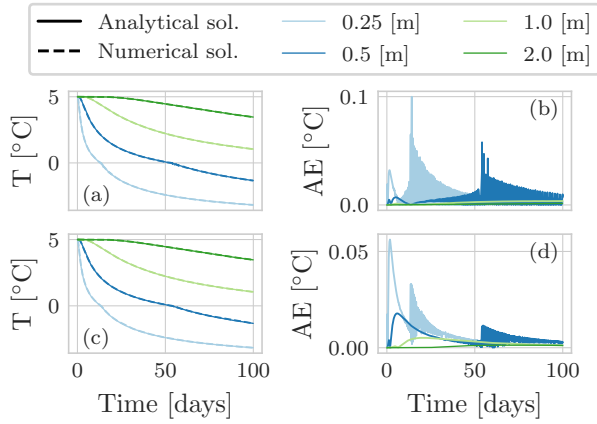


Figure 3.3: Panels (a) and (c) show the temperature evolution for the Neumann analytical and the numerical solution with the NCZ algorithm at various depths for a spatial discretization $\Delta z = 0.005$ m and $\Delta z = 0.001$ m respectively. The integration time step is $\Delta t = 3600$ s. Panels (b) and (d) show the absolute error.

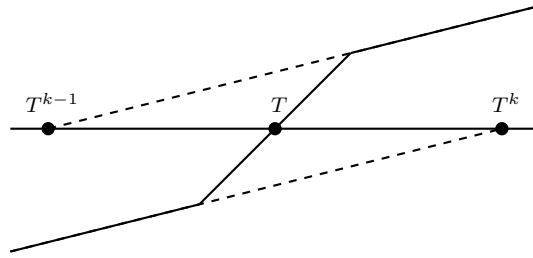


Figure 3.4: A scheme of problem which illustrates how the Newton-Raphson method can not converge towards T (Dall’Amico, 2010). In this case, the Newton-Raphson method fails to converge to T since it cycles between T^k and T^{k+1} values.

Instead, the solution continuously cycles between the iterates T^{k-1} and T^k . While the Newton-Raphson algorithm converges to the exact solution if a good initial guess for T^k exists, this represents a severe constraint for the reliable application for an iterative algorithm in a numerical model. An improvement of the Newton-Raphson algorithm can be obtained using the globally convergent Newton scheme (Dall’Amico et al., 2011). It uses the Newton-Raphson algorithm to provide the right search direction and, in order to avoid overshooting, a reduction factor δ is used to find the new estimate. This represents an improvement over the Newton-Raphson method, but its ability to converge depends on the choice of the parameter δ and on the treatment of the apparent heat capacity (Dall’Amico et al., 2011; Hansson et al., 2004; Nicolsky et al., 2007a). As such, this algorithm does not guarantee to converge for any time step size and the requirements for small time steps can become a limiting factor. For example, in (Dall’Amico et al., 2011) the comparison between the Neumann solution and GEOtop has been done with a time step of 10 s.

A comparison of the numerical solutions obtained with the Newton-Raphson algorithm, globally convergent Newton algorithm, and the NCZ algorithm shows significant differences Fig. (3.5). Newton-

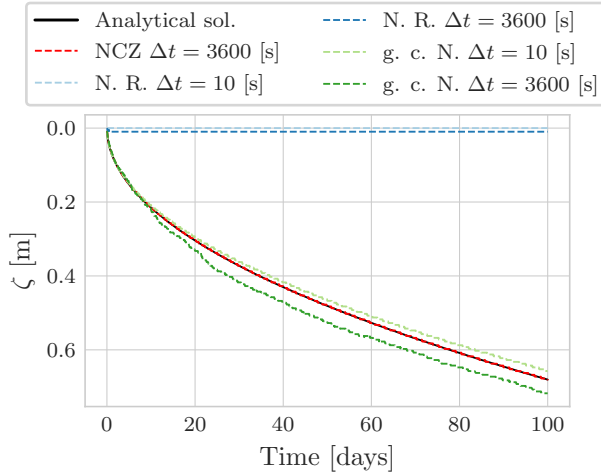


Figure 3.5: Comparison between the Neumann analytical solution and the numerical solution obtained with Newton-Raphson (N. R.), globally convergent Newton (g. c. N.), and NCZ algorithms. All the numerical simulations use the same spatial discretization $\Delta z = 0.005$ m.

Raphson cannot reproduce the analytical solution even if a time step of $\Delta t = 10$ s is used. The globally convergent Newton is in good agreement with the analytical solution if $\Delta t = 10$ s. With an hourly time step, however, the example with the globally convergent Newton method is not able to reproduce the position of the freezing front over longer periods of time. By contrast, the NCZ algorithm reproduces the analytical solution well using $\Delta t = 3600$ s. The quality of the solution obtained with the globally convergent Newton algorithm depends not only on the time step duration but also on the definition of the parameter δ , Fig. (3.6). The additional necessity for an arbitrarily chosen parameter in the globally convergent Newton algorithm further underscores the robustness of

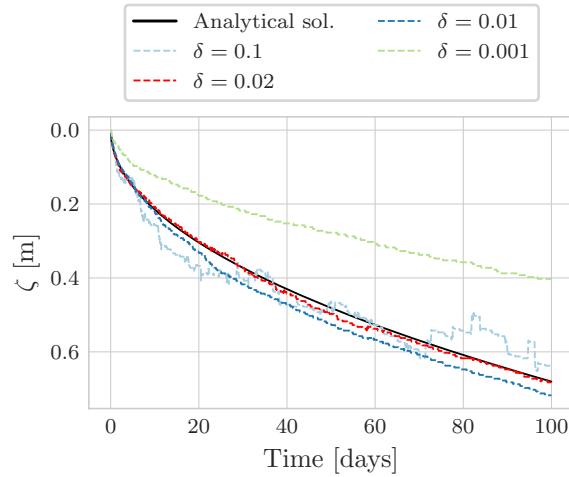


Figure 3.6: Comparison between the Neumann analytical solution and the numerical solution obtained with globally convergent Newton algorithm (g. c. N.). All the numerical simulations use the same spatial discretization $\Delta z = 0.005$ m and a time step size of $\Delta t = 3600$ s. This figure shows as the numerical solution depends on the choice of the parameter δ .

the NCZ algorithm, for which convergence only depends on the right definition of the Jordan decomposition.

3.4.2 Lunardini analytical solution

Lunardini (1988) derived an analytical solution (Appendix (E)) for the temporal evolution of temperature during the freezing of a semi-infinite and initially unfrozen soil column. In contrast to the Neumann analytical solution, in the Lunardini analytical solution the domain is divided into three regions Fig. (3.7) on the basis of temperature: unfrozen, $T < T_m$, partially frozen, $T_m < T < T_f$, and fully frozen, $T > T_f$. The domain is initially unfrozen

Table 3.3: Maximum absolute error °C of the temperature after 24 h from the numerical solution with the NCZ algorithm relative to the Lunardini analytical solution. The space resolution is $\Delta x = 0.01$ m.

	$T_m = -4$ °C	$T_m = -1$ °C	$T_m = -0.1$ °C
$\Delta t = 300$ s	0.00683	0.01419	0.11436
$\Delta t = 900$ s	0.01496	0.02448	0.11565
$\Delta t = 3600$ s	0.05115	0.08286	0.12116

with $T = T_0 = 4$ °C. At the left boundary condition a Dirichlet boundary condition is imposed with $T(x = 0, t) = T_s = -6$ °C, and the right boundary temperature is kept equal to the initial condition, $T(z \rightarrow \infty, t) = T_0$. Because the left boundary condition, $T_s < 0$ °C, a freezing front propagates from left to right.

We computed benchmark T1 proposed by the InterFrost project (InterFrost Project, n.d.), parameters are given in Table (E.1). The model agrees well with the analytical solution for all the three cases of T_m in terms of both the temperature profile, Fig. (3.8) and Table (3.3), and the freezing front position, Fig. (3.9) and Table (3.4), even with an hourly time step.

For comparison, McKenzie et al. (2007) compared the numerical model SUTRA against the Lunardini analytical solution for the cases $T_m = -4$ °C and $T_m = -1$ °C using a time step size of 900 s and a space resolution of 0.01 m. For the first test case the maximum absolute error was 0.01 °C, and for the second 0.1 °C. Their parameters, however, differ from those suggested by the InterFrost consortium, making performance comparisons difficult. In particular, their porosity was $0.05 \text{ m}^3\text{m}^{-3}$, whereas InterFrost uses $0.336 \text{ m}^3\text{m}^{-3}$. As this determines the amount of latent heat involved in phase change, smaller errors are to be suspected to occur with the parameters used by McKenzie et al. (2007).

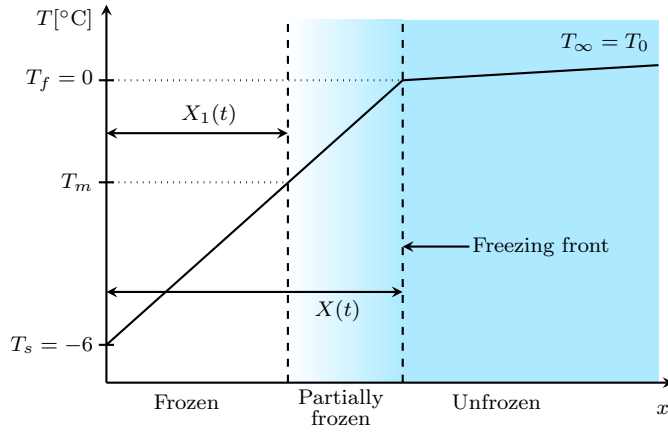


Figure 3.7: Scheme showing the setting of Lunardini problem (Ruhaak et al., 2015). Initially the domain is unfrozen with $T = T_0$. Because of $T_s < 0$ on the left boundary, a freezing front propagates from left to right. $X_1(t)$ and $X(t)$ identify respectively the isotherm corresponding to T_m , and T_f .

Table 3.4: Maximum error m of the freezing front position from the numerical solution with the NCZ algorithm relative to the Lunardini analytical solution. The space resolution is $\Delta x = 0.01$ m.

	$T_m = -4 \text{ }^\circ\text{C}$	$T_m = -1 \text{ }^\circ\text{C}$	$T_m = -0.1 \text{ }^\circ\text{C}$
$\Delta t = 300 \text{ s}$	0.00032	0.00051	0.00001
$\Delta t = 900 \text{ s}$	0.00043	0.00027	0.00016
$\Delta t = 3600 \text{ s}$	0.00062	0.00057	0.00047

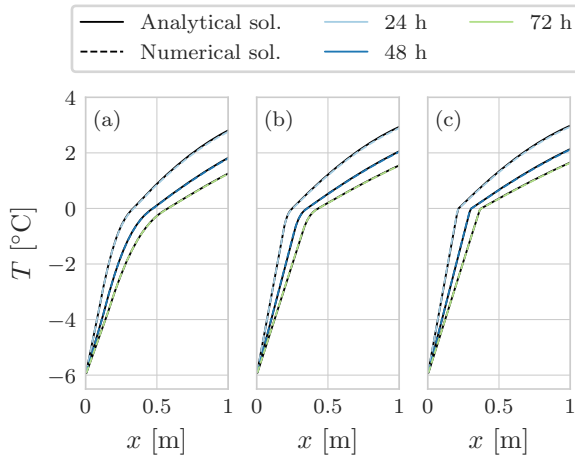


Figure 3.8: Comparison between the Lunardini solution and the numerical solution with the NCZ algorithm for the three cases of T1 benchmark: (a) $T_m = -4$ °C, (b) $T_m = -1$ °C, (c) $T_m = -0.1$ °C. The colours represent different times frame. The integration time step is $\Delta t = 3600$ s, and the space resolution is $\Delta x = 0.01$ m.

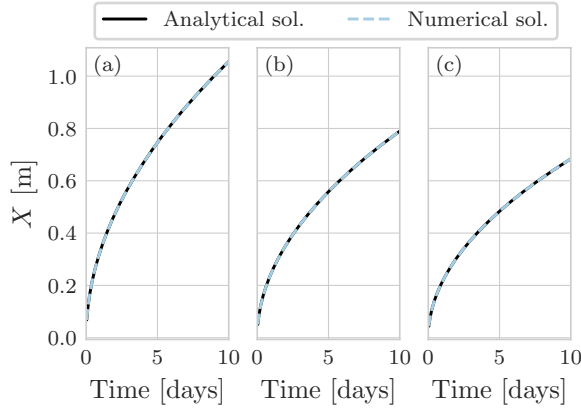


Figure 3.9: Propagation of the zero-isotherm for the Lunardini solution and the numerical solution with the NCZ algorithm for the three cases of T_1 benchmark: (a) $T_m = -4$ °C, (b) $T_m = -1$ °C, (c) $T_m = -0.1$ °C. The integration time step is $\Delta t = 3600$ s, and the space resolution is $\Delta x = 0.01$ m.

3.5 NUMERICAL TEST

In the previous sections, we have demonstrated that the proposed method can reproduce the Neumann analytical solution, as well as the Lunardini analytical solution, even when using larger time steps than other numerical models.

After comparing simulation results with analytical solutions, we now analyse the difference between solutions using hourly, daily, and 10-day time steps. The domain is a soil column of 20 m depth that is uniformly at $T = -3$ °C, initially. The bottom boundary condition is adiabatic and at the surface, we use a Dirichlet boundary condition. The original forcing has hourly resolution and for longer time steps, corresponding averages are computed. As temperature gradients and the influence of phase

change are usually greatest near the soil surface, the thickness Δz is parameterized with an exponential function (Gubler et al., 2013)

$$\Delta z_i = \Delta z_{min}(1 + b)^{i-1} \quad (67)$$

where Δz_{min} is the thickness of the first layer, b is the growth rate and i is the layer index, being one at the ground surface and increasing downward. The parameters used are reported in Table (3.5). All three simulations were spun-up for a period of 1400 years to reach a stable thermal regime. After spin-up, we performed a simulation of 100 years.

Figure (3.10) compares the zero-isotherm position computed after 100 years for the three different time steps.

Interestingly, there are no significant deviations in the results. The larger deviations occur when the zero-isotherm is shallow: at the beginning of the thawing season as well as the freezing one, Fig. (3.11) and Fig. (3.12). At the beginning of the thawing season, Fig. (3.11), there is a time lag of about one month between the beginning of the thawing season for the hourly simulation and the 10-days simulation. This can be attributed to different surface temperature used to drive the simulations. In particular, in the case of the hourly simulation it is possible to see the oscillations of the position of the zero-isotherm, panel (c), related to the oscillation of the surface temperature around 0 °C, panel (a). Figure (3.12) shows the detail of the freezing season. In panel (c) it is possible to note that when the zero-isotherm is deep there is a good agreement between the three simulations. The main differences occurs at the soil surface since with larger time steps the signal of the surface boundary condition is smoothed and does not oscillate around 0 °C. Moreover, by using an hourly time step and a daily time step it is possible to capture the joining of the downward and upward freezing front, while this is not possible with the 10-days time step since the joining occurs between two consecutive time steps. This can be attributed on one side to the diurnal

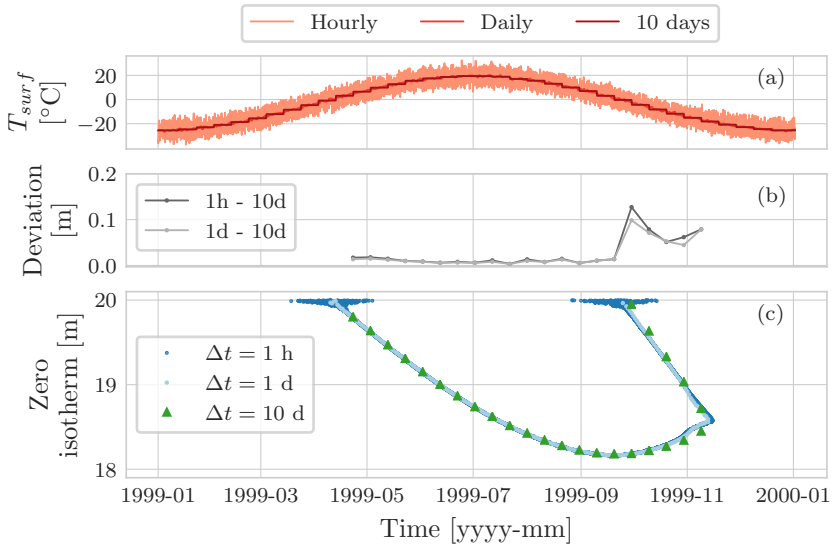


Figure 3.10: Comparison of the position of the zero-isotherm, panel (c), after 100 years of three simulations: using an hourly boundary condition with time step of $\Delta t = 1$ h, using a daily boundary condition with a time step of $\Delta t = 1$ day, and a 10-day boundary condition with a time step of $\Delta t = 10$ day. Panel (a) shows the surface temperature for the hourly, the daily and the 10-days simulations. Panel (b) shows the deviation of the position of the zero-isotherm after 100 years between the hourly and the 10-days simulation, and between the daily and the 10-days simulation.

cycles of surface boundary condition, and on the other side that using a larger time step we lose accuracy in capturing the timing of thawing/freezing even if we use the same boundary condition.

With larger time steps, we lose some of the information of the boundary conditions and the accuracy of the numerical model decreases because it is first-order accurate in time. The overall performance relative to simulations with smaller time steps, however, is largely preserved. While the order of accuracy can be increased to second order in time using the Crank-Nicholson method, this would incur a time step restriction to guarantee the monotonicity of the solution. As this restriction is proportional to the square of the space discretization, Δz^2 , the Crank-Nicholson method would represent a severe constrain whenever high spatial resolution is required.

Figure (3.13) compares the minimum, mean, and maximum temperature profile respectively for the three simulations. (a) shows the ground temperature envelope for the hourly simulation. The maximum envelop presents an 'elbow' that is due to the phase-change effects Fig. (3.13). As can be seen in (b) and (d), close to the soil surface the hourly simulation presents larger values for both the minimum and maximum temperature due the fact that the hourly boundary condition presents a greater amplitude that is smoothed computing the daily and 10-day average. The maximum temperature profile, Fig. (3.13) panel (d), presents an 'elbow' due to the so-called zero curtain effect. The zero curtain effect, Fig. (3.14), is the period of time during which the temperature remains nearly constant and very close to the freezing point because of the latent heat released during the phase change of water.

In the mean temperature profile, the 10 day simulation presents a larger deviation from the hourly simulation than the daily simulation. The large deviation can be explained with the interaction of

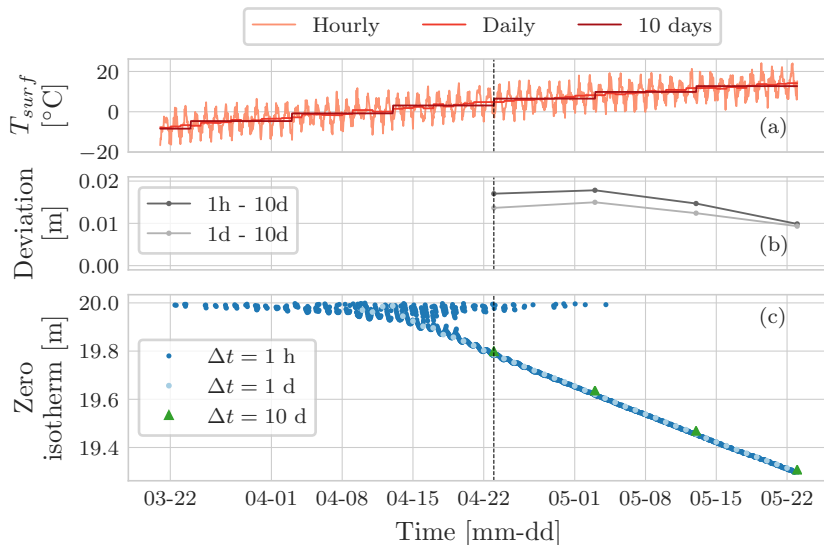


Figure 3.11: Detail of the beginning of the thawing season for the year 1999. Panel (a) shows the surface temperature for the hourly, the daily and the 10-days simulations. Panel (b) shows the deviation of the position of the zero-isotherm after 100 years between the hourly and the 10-days simulation, and between the daily and the 10-days simulation. Panel (c) shows the position of the zero-isotherm after 100 years for the three simulations. In (b) there is a time lag of about one month between the beginning of thawing season for the hourly simulation and the 10-days one, dashed grey line. This can be attributed to the different surface temperature used to drive the simulations.

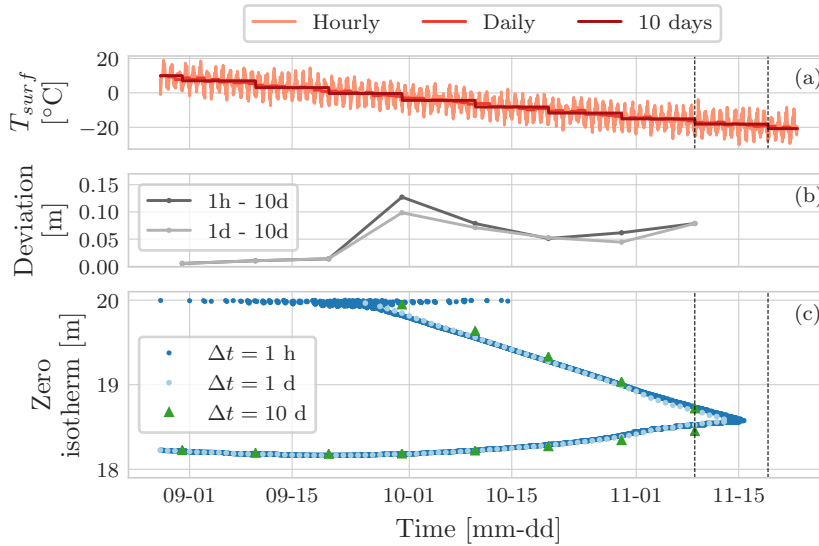


Figure 3.12: Detail of the beginning of the freezing season for the year 1999. Panel (a) shows the surface temperature for the hourly, the daily and the 10-days simulations. Panel (b) shows the deviation of the position of the zero-isotherm after 100 years between the hourly and the 10-days simulation, and between the daily and the 10-days simulation. Panel (c) shows the position of the zero-isotherm after 100 years for the three simulations. The joining of the downward and upward freezing front is captured by the hourly and the daily simulations, (c). It is interesting to note that for the 10-days simulation the joining occurs in-between of two consecutive time step.

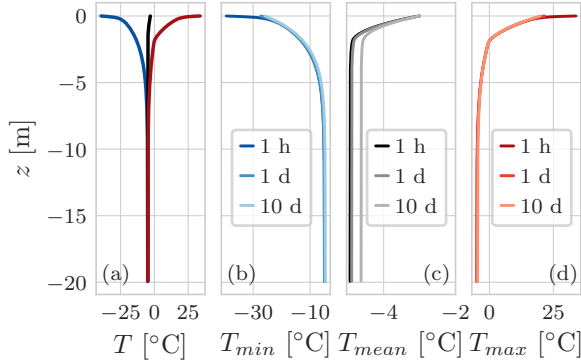


Figure 3.13: (a) The minimum, mean, and maximum temperature profile for the hourly simulation. (b), (c), (d) show the comparison of the minimum, mean, and maximum temperature profile respectively for the three simulations: with an hourly surface temperature boundary condition and $\Delta t = 1$ h, with a daily air temperature boundary condition and $\Delta t = 1$ day, with a ten day air temperature boundary condition and $\Delta t = 10$ day. All three simulations last 100 years. The maximum difference of T_{mean} between the hourly, and daily simulation is of 0.04 °C, while between the hourly, and ten-days simulation is of 0.3 °C.

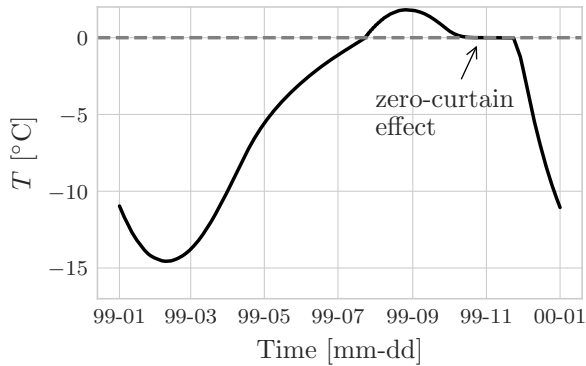


Figure 3.14: Hourly temperature at 1.5 m depth. Note the prolonged period of 43 days when temperature remained within ± 0.1 °C. This is the so-called zero-curtain effect, and it is due to latent heat of fusion that is continually released during the freezing of soil moisture.

the time-step size with the thermal offset effect, Fig. (3.13). If the thermal conductivity of water is set equal to that of ice, $\lambda_w = \lambda_i$, the maximum difference between the three profiles is reduced to 0.003 °C with a maximum deviation of 0.003 °C from the initial condition, that is also equal to the mean of the forcing boundary condition. It is interesting to note that mean temperature, panel (c), is constant throughout the soil column.

Regarding the spatial discretization Fig. (3.16) reports a comparison of the zero-isotherm position obtained using an hourly time step, a daily time step, and a 10 day time step. The results are still in good agreement, but it is interesting to note that the zero-isotherm presents some steps, independent of the size of the time step, and some details are missed, such as the joining of the downward and upward freezing fronts captured with the finer grid. These steps are caused by the greater thickness of the grid elements. Because temperature is computed in the middle of each

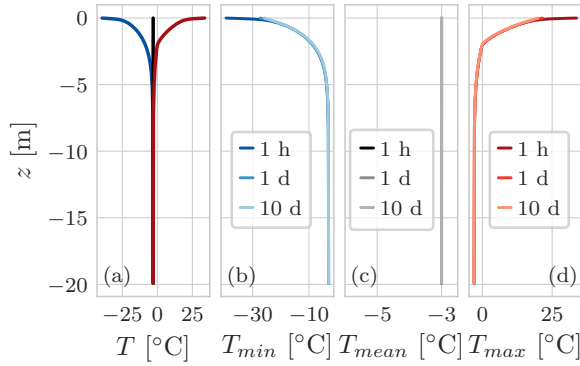


Figure 3.15: Temperature profile envelope considering $\lambda_w = \lambda_i$. (a) The minimum, mean, and maximum temperature profile for the hourly simulation. (b), (c), (d) show the comparison of the minimum, mean, and maximum temperature profile respectively for the three simulations: with an hourly surface temperature boundary condition and $\Delta t = 1$ h, with a daily surface temperature boundary condition and $\Delta t = 1$ day, with a ten day surface temperature boundary condition and $\Delta t = 10$ day. All three simulations last 100 years. Because $\lambda_w = \lambda_i$ the mean temperature, panel (c), is constant throughout the soil column and it is not possible to appreciate the thermal offset. The mean temperature is very close to the initial temperature profile, the maximum error is of 0.003 $^{\circ}\text{C}$.

control volume, more time is required to achieve complete phase change of water, resulting in slower variation of the zero-isotherm position. Moreover, the joining of the downward and upward freezing front is not captured neither by the hourly nor by the daily simulations.

For this numerical test we checked the mean number of iterations required to solve the nonlinear system with the NCZ algorithm, the Newton-Raphson algorithm, and the globally convergent Newton algorithm. We performed a simulation lasting 1 year with a time step $\Delta t = 1$ h and for different spatial discretizations. As can be seen in Table 3.6, neither the Newton-Raphson nor the globally convergent Newton converge: they always reach the maximum number of iterations allowed with a consequent increase of the computational cost.

These synthetic experiments demonstrate that spatial and temporal discretization can be chosen accordingly to the aim the study without any constraints due to the convergence and stability issues of the numerical scheme.

3.6 FREETHAW-1D AND WHETGEO-1D

This section is meant to show how to include FreeThaw-1D in WHETGEO-1D. Firstly it is necessary to implement a new concrete class of `ClosureEquation` implementing a SFC, as an example the SFC presented by Dall'Amico et al. (2011). Then we need of two more classes. One of type `ConductivityModel` implementing a soil thermal conductivity model for frozen soil. The other one is a concrete class derived from the abstract class `EquationState`. Compared to FreeThaw-1D, WHETGEO-1D enables to drive the simulation by using the surface energy balance.

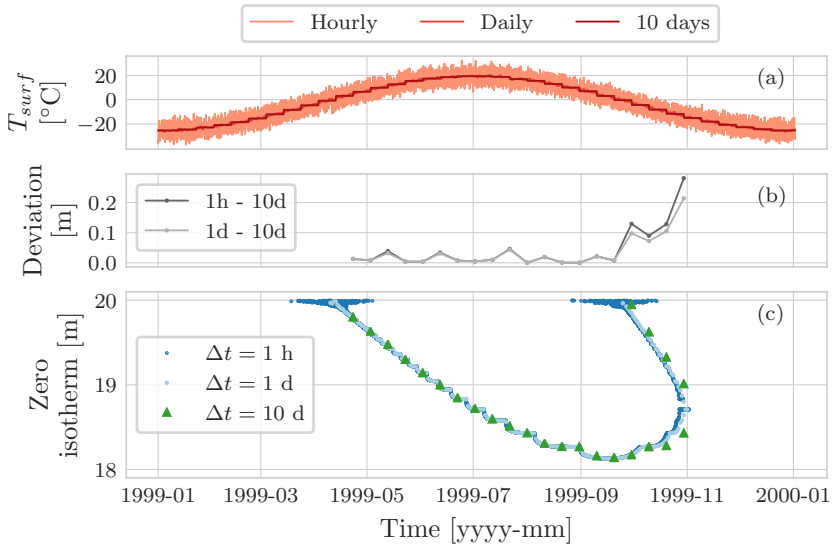


Figure 3.16: Comparison of the position of the zero-isotherm, panel (c), after 100 years of three simulations: using an hourly boundary condition with time step of $\Delta t = 1$ h, using a daily boundary condition with a time step of $\Delta t = 1$ day, and a 10-day boundary condition with a time step of $\Delta t = 10$ day. Panel (a) shows the surface temperature for the hourly, the daily and the 10-days simulations. Panel (b) shows the deviation of the position of the zero-isotherm after 100 years between the hourly and the 10-days simulation, and between the daily and the 10-days simulation. By using a coarser spatial discretization, the zero-isotherm presents some 'steps', panel (c), independently on the size of the time step. Another consequence of this is that the joining of the downward and upward freezing front is not captured neither by the hourly nor by the daily simulations.

Table 3.5: Input parameters for the numerical tests.

Symbol	Parameter	Value	Units
Δt	time step	3600, 86400, 864000	s
Δz_{min}^a	thickness of the first control volume	0.002, 0.005	m
b^a	growth rate ground depth	0.01, 0.1	—
z_{max}	maximal ground depth	20	m
l_f	latent heat of fusion	333700	J kg ⁻¹
c_w	specific heat of water	4188	J m ⁻³ °C ⁻¹
c_i	specific heat of ice	2117	J m ⁻³ °C ⁻¹
c_{sp}	specific heat of soil particles	1000	J m ⁻³ °C ⁻¹
ρ_w	water density	1000	kg m ⁻³
ρ_i	ice density	1000	kg m ⁻³
ρ_{sp}	soil particles density	2700	kg m ⁻³
λ_w	thermal conductivity of water	0.6	W m ⁻¹ °C ⁻¹
λ_i	thermal conductivity of ice	2.09	W m ⁻¹ °C ⁻¹
λ_{sp}	thermal conductivity of soil particles	3.0	W m ⁻¹ °C ⁻¹
θ_s	saturation water content	0.46	—
θ_r	residual water content	0.1	—
α	Van Genuchten parameter	1.5	m ⁻¹
n	Van Genuchten parameter	1.2	—
T_0	initial temperature	-3	°C
	SFCC	Dall'Amico	
	Thermal conductivity model	Johansen	

^a We used two different space discretizations. The thickness of the ground layer is parametrized as $dz_i = dz_{min}(1 + b)^{(i-1)}$ (Gubler et al., 2013).

	Number of control volumes				
	500	1000	2000	5000	10000
Mean number of iterations NCZ	12	3	14	16	18
Mean number of iterations N. R.	40	40	40	40	40
Mean number of iterations g. c. N.	40	40	40	40	40

Table 3.6: Summary of the mean number of iterations for the NCZ algorithm, the Newton-Raphson algorithm (N. R.), and the globally convergent Newton algorithm (g. c. N.). The simulation lasts 1 year with a time step $\Delta t = 1$ h. We considered different spatial discretizations. The tolerance $\varepsilon = 10e - 11$ has been rescaled with the water latent heat of fusion and the water density. The maximum number of iteration for each time step is 40. As can be seen the Newton-Rapshon and the globally convergent Newton does not converge so it always reaches the maximum number of iteration allowed.

Table 3.7: Parameters of the SFC model.

θ_r m ³ m ⁻³	θ_s m ³ m ⁻³	α m ⁻¹	n -
0.068	0.38	0.8	1.09

Here I reproduce the simulation presented in Section 2.6.4 considering the phase change of water. The soil column is 30 m deep and the initial condition is a constant temperature profile $T = 12$ °C. The parameters of the SFC are presented in Tab. (3.7) Figure (3.17) shows in panel (a) the components of the surface energy fluxes, and the thermal regime of the uppermost 2 m of the soil column. As can be seen in panel (b), the soil temperature fall below the 0 °C thus neglecting freezing and thawing processing results in a strong approximation. Figure (3.18) shows a comparison between the position of the 0 °C isotherm and the temperature at 0.05 m of the two simulation: considering the phase change of water and without it. Here it is worth to remark that as in FreeThaw-1D also in WHETGEO-1D the water flow is not allowed when considering the phase change.

Moreover, WHETGEO-1D thanks to the adoption of the generic programming approach allows to simulate the thermal regime of frozen soil underneath waterbodies (Langer et al., 2016; Ling and Zhang, 2003). In fact waterbodies are wide spread in the northern landscape (Pienitz et al., 2008) and they significantly affect the ground thermal regime (Arp et al., 2016; Langer et al., 2016; Vincent et al., 2017). In presenting this possible possible reasearch address of WHETGEO-1D I do not claim to be exhaustive and, but I would like to outline another advantage resulting from the code design I developed. At the base of studying the influence of shallow thaw lakes on the permafrost thermal regime model there is the solution of the enthalpy equation on two different domains: within the soil and in the waterbody. In this WHETGEO-1D offers a great advantage since, thanks to the generic approach, it is pos-

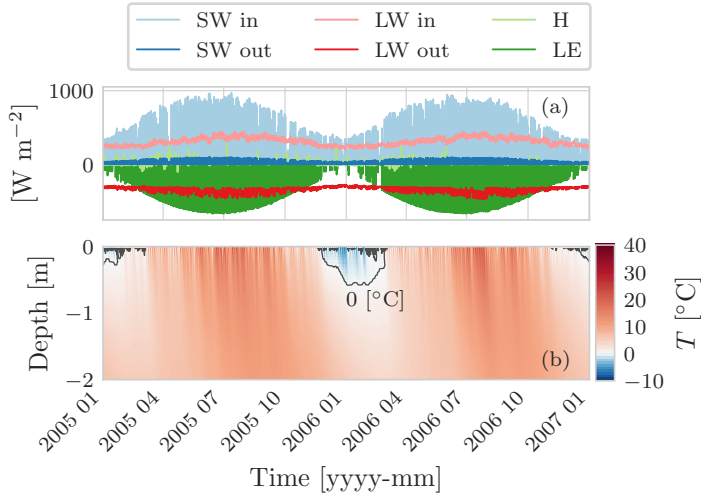


Figure 3.17: Behavioural test case of the pure heat conduction in soil considering the surface energy budget and the phase change of water. Panel (a) shows the surface energy fluxes driving the simulation. The external fluxes, incoming short-wave and longwave radiation, and the latent heat flux, are computed with existing GEOframe components. Panel (b) shows the thermal regime of the uppermost 2 m of the soil column.

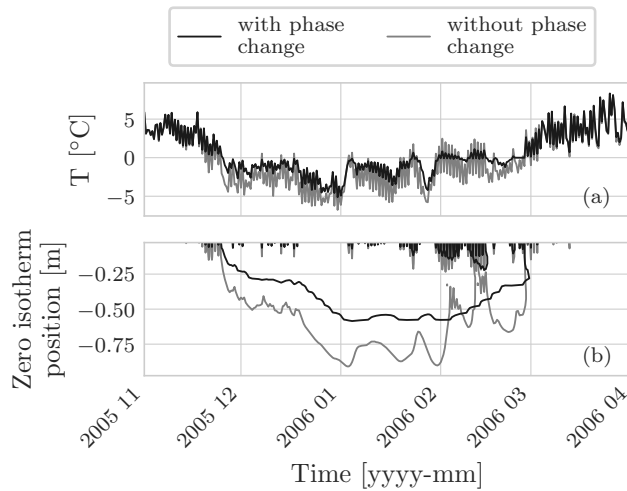


Figure 3.18: Panel (a) shows a comparison of the soil temperature at 0.05 m considering the phase change of water and without. As can be seen, in the latter case the soil temperature reaches lower value and fluctuates more: when considering the phase change of water we include in the problem the latent heat of water that increase the thermal inertia of the soil. Panel (b) shows a comparison of the position of the zero-isotherm in the two simulation. When the phase of water is not included the zero-isotherm does deeper into the ground.

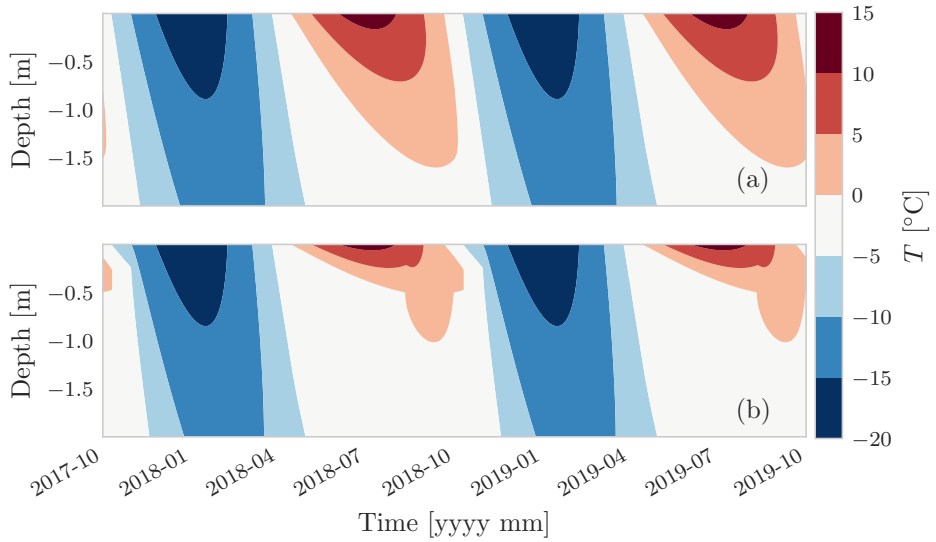


Figure 3.19: Panel (a) shows the case of only soil. Panel (b) shows the case with a waterbody of 1 m depth. As can be seen the presence of the surface water limits the propagation of the thawing front during the warm season due to the higher amount of heat required to completely thaw the frozen waterbody.

sible to solve in a coupled and conservative manner the enthalpy equation in both domains. Figure (3.19) shows a comparison between a simulation considering only soil, and the other one where a waterbody of 1 m depth is considered. The initial condition is a uniform temperature profile of $-1\text{ }^{\circ}\text{C}$. At top of the domain a Dirichlet boundary condition is imposed. The temperature oscillates around $-1\text{ }^{\circ}\text{C}$ with an amplitude of $15\text{ }^{\circ}\text{C}$. At the bottom a no flux boundary condition is prescribed. This is a first-order model since it neglects other processes that would be necessary to include in the model such as wind water mixing (Langer et al., 2016), thermal stratification, snow cover, subsidence and ac-

tive erosion (Ling and Zhang, 2003), and water flow. However, it is worth to remark that the solution of the nonlinear governing equation can be achieved with a small effort, simply adding the classes to describe the soil specific enthalpy and the water specific enthalpy.

3.7 COMMONLY USED SIMULATION SOFTWARE

The heat equation can be written in different forms that are analytically equivalent, but subject to differing numerical advantages and disadvantages. In the scientific literature, several simulators, i.e. software that implements a particular model (set of equations), for solving the heat equation with freezing and thawing have been presented. Here we review commonly used frozen soil models in terms of their governing equations and methods of finding numerical solutions.

Heat transfer with phase change of water is a cross-cutting problem existing in many geophysical phenomena other than frozen soil. This includes, for example, the seasonal snow pack, glaciers, and ice-sheets. Our contribution does not seek to present an improvement in the description of these problems and we ignore typical processes such as metamorphism and settling in seasonal snow or strain heating and deformation in glaciers and ice sheets. Nevertheless, corresponding models may benefit from the NCZ algorithm in the treatment of the nonlinearity arising from phase change and, furthermore, broadening our review to also include some snow and glacier models supports the generalisation of our findings.

CLM

The Community Land Model (CLM) is the LSM for the Community Earth System Model (Oleson et al., 2004). It includes a module to simulate the ground temperature considering freezing and thawing. The governing equation is written in the non-conservative form and does not include the latent heat term (Oleson et al., 2004) (Lawrence et al., 2019). The heat conduction equation is solved using a Crank-Nicholson method. The temperature profile is calculated adopting the DECP approach. This approach does not require to solve a nonlinear system, since the latent heat is treated in an explicit way, but Nicolsky et al. (2007b) have pointed out that this two-step procedure can overestimate the region where the phase change occurs, resulting in inaccuracies in the simulation of active-layer thickness.

CoupModel

The CoupModel (Jansson and Karlberg, 2011) is a one-dimensional numerical model to simulate the heat and water flow as well as carbon and nitrogen budgets in a soil-plant-atmosphere system (Hollesen et al., 2011). The governing equation for heat flow in the soil is defined using the apparent heat capacity, and solved with an explicit numerical method. This does not require to solve a non-linear system but sets a time step restriction to avoid numerical oscillation.

CryoGrid

CryoGrid 2 simulates the ground thermal regime based on conductive heat transfer in the soil and in the snowpack (Westermann et al., 2013). The heat equation is written using the apparent

heat capacity and solved using the method of lines (Westermann et al., 2013). The resulting system of ordinary differential equations is solved numerically with the package CVODE of Sundials that implements a modified Newton method, and Inexact Newton method, or a fixed-point solver to linearize the algebraic system resulting from the discretization of the heat transfer equation. The convergence of the Newton-type methods can be problematic (Casulli and Zanolli, 2012).

GEOtop

GEOtop (Endrizzi et al., 2014; Rigon et al., 2006a) is a physically based distributed model of the mass and energy balance of the hydrological cycle. It includes a module for solving the energy equation in freezing soil (Dall'Amico et al., 2011); this module can also be linked with the solver for the Richards equation. The governing equation for heat transfer is written in conservative form, but when solving the equation the apparent heat capacity formulation is used. A globally convergent Newton algorithm is used to deal with the non-linearities arising from phase change (Dall'Amico et al., 2011). The globally convergent Newton algorithm represents an improvement over the Newton-Raphson algorithm, however, as shown in Section (3.4.1) it does not perform as well as the NCZ algorithm, and additionally, the choice of the parameter δ is non trivial.

GIPL-2.0

GIPL-2.0 simulates the ground thermal regime by solving the heat equation with phase change numerically (Marchenko et al., 2008). The governing equation is written in the conservative form and Newton's method is used to linearize the energy equation.

To overcome convergence problems when solving the non-linear system, GIPL-2.0 implements a fractional time step approach, Godunov splitting. The key point of the solution regards the treatment of the enthalpy time derivative: in case of a non zero gradient of temperature exists the time derivative is approximated with a difference derivative, otherwise using the analytical representation.

Goodrich

Goodrich (1982) presented a one-dimensional model to simulate the ground thermal regime considering the phase change of water. The governing equation is written in the non conservative form and does not include the latent heat of fusion. Phase change is treated with the front tracking method, which offers good accuracy for problems in which phase change occurs at a fixed temperature (Goodrich, 1982). This model does not use a SFCC, and instead, the soil is represented as homogeneous layers with distinct frozen and thawed thermal properties.

Hydrus 1D

Hydrus 1D includes a module to simulate water flow and heat transport in frozen soil. The governing equation is written using the apparent heat capacity formulation and Picard iteration is used to linearize the algebraic nonlinear system. In their paper, Hansson et al. (2004) explain that during the Picard iteration the solution can easily oscillate whenever the temperature decrease below the melting temperature. To avoid these oscillation the temperature is reset to the critical value and iteration restarted. Hydrus 1D adopts an empirical time-step adaptation criterion. It is worthwhile to notice that the modified Picard iteration was pro-

posed by Celia et al. (1990) to solve the Richards equation – problem for which the NCZ algorithm was originally proposed (Casulli and Zanolli, 2010).

MarsFlo

MarsFlo is a three-phase numerical model to simulate the heat transfer and water flow in partially frozen, partially saturated porous media (Painter, 2011). The heat equation is written in the conservative form. The equation is solved using an implicit finite difference method, and the resulting nonlinear system is solved using a Newton-Raphson method. To overcome convergence and stability problems, three modifications were introduced (Painter, 2011). The convergence of the Newton-Raphson method can be problematic (Casulli and Zanolli, 2012).

NEST

Zhang et al. (2003) developed a one-dimensional physically based model of Northern Ecosystem Soil Temperature (NEST). The heat equation is written in the source term formulation and solved with the DECP approach. The numerical method is explicit in time, thus the maximum time step is of 30 minutes to prevent oscillations in the solution.

Sergueev et al.

This is a two dimensional model and the governing equation is written in the enthalpy form (Sergueev et al., 2003). This model implements a fractional time step approach (Godunov splitting): each time step is divided into two steps and at each step, a different dimension is treated implicitly. The system of finite difference

equations is non-linear and is solved with the Newton's method. As in GIPL-2.0, the time derivative of enthalpy is computed either using the difference derivative or the analytical derivative according with the gradient of the temperature field.

SoilVision

The heat equation is written using the apparent heat capacity. The equation are solved using a finite element solver, FlexPDE suite, both explicit and implicit in time. In case of implicit methods, the resulting non-linear system is solved using the Newton-Raphson method. The convergence of the Newton-Raphson method can be problematic (Casulli and Zanolli, 2012).

SUTRA

SUTRA is an established USGS groundwater flow and coupled transport model (Voss and Provost, 2002). McKenzie et al. (2007) and McKenzie and Voss (2013) have extended the model to simulate freezing and thawing processes in the soil. The heat equation is written using the apparent heat capacity formulation and non-linearities are solved using Picard iteration. The convergence of the Newton-type method can be problematic (Casulli and Zanolli, 2012).

Crocus

Crocus is a one-dimensional finite difference model that solves the mass and energy balance within the snowpack taking into account metamorphism and settling. The first versions of Crocus (Brun et al., 1992; Brun et al., 1989) were not enthalpy-based. The governing equation was written in terms of temperature and wa-

ter content. It was solved by using the Crank-Nicholson method, and the phase change is treated by using the DECP approach (Brun et al., 1992). After the integration within SURFEX (Vionnet et al., 2012), Crocus uses the enthalpy formulation and the numerical scheme is fully implicit, based on the numerics of ISBA-ES (Boone and Etchevers, 2001). Similarly to the previous version, the heat balance equation is solved adopting the DECP approach (Boone and Etchevers, 2001). Even though recent work Crocus is based on a simple bucket approach for liquid water percolation (Lafaysse et al., 2017; Morin et al., 2012), D'Amboise et al. (2017) implemented a routine for water flow in the snowpack based on the Richards equation, which is characterized by nonlinear behaviour like the enthalpy equation. To solve it, they adopted an approach based on Picard iteration with variable time steps (Paniconi and Putti, 1994).

SNOWPACK

SNOWPACK (Lehning et al., 1999) solves the heat transfer and creep/settlement equations using a Lagrangian finite element method. The governing equation is written using the source/sink formulation and it is solved using the DECP approach (Bartelt and Lehning, 2002; Lehning et al., 1999). Regarding the water flow, SNOWPACK implements three different schemes: a simple bucket-type approach, an approximation of Richards equation, and the full Richards equation (Wever et al., 2014). The full Richards equation is solved using Picard iteration with variable time steps (Paniconi and Putti, 1994).

ORCHIDEE

ORCHIDEE is terrestrial biosphere model and it is part of the IPSL-CM4 Earth system model developed by the Institute Pierre Simon Laplace (IPSL) (Krinner et al., 2005). In the version 1.9.6 the snow is described with a single layer of constant density (Wang et al., 2013). Because of the limitations of the this approach, Wang et al. introduce a three-layer snow model, ORCHIDEE-ES, largely inspired from ISBA-ES (Boone and Etchevers, 2001) to consider snow settling, water percolation, and water refreezing. The governing equation is written in the non-conservative form and does not include the latent heat term. The temperature profile is calculated adopting the DECP approach.

JSBACH

JSBACH is the land surface model developed by the Max Plank Institute (Ekici et al., 2014). It is a component of the Earth System Model (MPI-ESM) that also include ECHAM6 for the atmosphere and MPI-OM for the ocean. JSBACH simulates both the frozen soil and the snowpack. In both cases the heat conduction is assumed to be the dominant method of heat transfer. The governing equation is written in the source term formulation and solved with the DECP approach (Ekici et al., 2014).

Ice-sheet models

For glacier and ice-sheet models it is necessary to distinguish between cold and temperate ice. Following Aschwanden and Blatter (2005), “ice is treated as temperate if a change in heat content leads to a change in liquid water content alone, and is considered cold if a change in heat content leads to a temperature change alone.”

This means that cold ice is always below the melting temperature and thus the phase change does not occur. As result, present-day ice sheet models can be classified into: 'cold-ice method' models and polythermal models.

'Cold-ice method' does not consider the phase change of ice. Because of this the heat capacity can be assumed to be constant and therefore the governing equation can be written in terms of only temperature. These models are easy to implement, but their applicability is restricted since in general temperate zones can be present (Aschwanden and Blatter, 2009). In fact, since the phase change of ice is overlooked, locally, the 'cold-ice method' violates the energy conservation, overestimates the temperate region (Aschwanden and Blatter, 2009), and can not quantify the liquid water content that affects viscosity in temperate ice (Lliboutry and Duval, 1985).

By contrast, polythermal ice-sheet models consider the phase change of ice. Similar to freezing soil models, the polythermal ice-sheet models can be classified in two groups on the base of the treatment of the phase change: front tracking method and enthalpy method (Nedjar, 2002). SICOPLOIS (Greve, 1997a, 1997b; Greve and Blatter, 2016) is the only 'truly' polythermal ice sheet model. It employs the polythermal two-layer scheme (Greve, 1997b): the temperature field and the water content field are computed separately for the ice and temperate domain and a Stefan-type condition is applied at the cold-temperate surface (CTS). This model defines the CTS for both energy flux and mass flux. The drawback of this method relate to the implementation and restriction on the geometry and topology of the CTS (Aschwanden et al., 2012).

Aschwanden and Blatter (2009) presented an enthalpy gradient method. This is a fixed-grid method that differs from the enthalpy method commonly used for freezing soil in its definition of the energy flux. In the enthalpy method, the heat flux is expressed in

terms of the temperature gradient, whereas in the enthalpy gradient method it is expressed in terms of enthalpy, assuming that the heat capacity is constant (Aschwanden and Blatter, 2009). The enthalpy approach combines the advantage of solving one equation for the entire domain, cold-ice models, and the correct description of the thermodynamics of temperate ice (front tracking model). This model is implemented in COMSOL Multiphysics (Aschwanden and Blatter, 2009), where nonlinear problems are solved using either a Newton algorithm or a damped Newton algorithm. Also in this case the NCZ may represent a valid option to solve the nonlinear system. To the authors' knowledge, the enthalpy gradient method has not been used in freezing soil models.

Hewitt and Schoof (2016) presented an enthalpy-based finite volume method for polythermal ice. To solve the equation at each time step the computational domain is explicitly divided in the cold and temperate regions, and the energy equation is solved adopting a combination of implicit and explicit methods (Hewitt and Schoof, 2016). It is worth to note that in the temperate region, temperature is set equal to the melting temperature of the ice. This limits the application of this model to simulate freezing soil, where temperature can be larger than the melting temperature of water.

3.8 CODE AVAILABILITY

The source code is written in Java using the object-oriented programming paradigm. It can be found at <https://github.com/geoframecomponents/FreeThaw1D> (Tubini, 2020c). The OMS₃ project can be found at https://github.com/GEOframeOMSProjects/OMS_FreeThaw1D (Tubini, 2020b). A frozen version

of the OMS project used in (Tubini et al., 2020) can be found at <http://dx.doi.org/10.5281/zenodo.4017668> (Tubini, 2020a)

3.9 CONCLUSION REMARKS

We have presented a new model for simulating the ground thermal regime in the presence of freezing and thawing based on the heat-transfer equation and the application of the NCZ algorithm. To our knowledge, this is the only method that guarantees convergence while also permitting large time steps. The numerical model was implemented and verified against the Neumann and Lunardini analytical solutions. In both cases, the results were in good agreement even with an hourly integration time step. For the Neumann solution, we considered pure water instead of saturated soil since it is more numerically demanding, and no convergence problems were encountered despite choosing a narrow temperature range ($0.0001\text{ }^{\circ}\text{C}$) over which phase change occurs.

Numerical experiments demonstrated the robustness of the model by comparing results at differing temporal and spatial resolutions. Results obtained with time steps of 1 h, 1 day, and 10 days are consistent. The robustness of the numerics allows the user to choose both the space and time discretization without any restriction due to stability and convergence issues. As a consequence, this method is effective for simulating permafrost thaw, a phenomenon that occurs at depth, in response to seasonal and multi-annual cycles, and often over tens, hundreds or even thousands of years. Furthermore, phenomena like hysteresis or the variation of solute concentration upon freezing (Clow, 2018) can be included in the numerical model if the enthalpy function (i.e. its parameters) does not change within the current time step of integration.

While we presented a finite volume method, the NCZ algorithm can be also used with finite difference and finite element method. Beyond applications to frozen soil, it can be used to study other geophysical phenomena that involve phase change of a substance simply by changing the definition of the enthalpy function and the thermal conductivity function. Examples include, glacier dynamics (Aschwanden et al., 2012), snow pack evolution (Brun et al., 1992; Lehning et al., 1999), and magma bodies (De Lorenzo et al., 2006). This may be even further expanded to industrial problems involving phase change materials used in energy recovery systems (Mongibello et al., 2018; Nazzi Ehms et al., 2019) or casting problems of pure metals and alloys (Lewis and Ravindran, 2000).

4

RICHARDS 2D

Contents

4.1	Grid	136
4.2	Algorithms	141
4.2.1	Conjugate gradient method	141
4.2.2	Matrix-free algorithm	143
4.3	Code design	143
4.3.1	The matrix-vector product, Matop	144
4.3.2	The Conjugate gradient method, ConjugateGradient	144
4.3.3	The NCZ algorithm, NestedNewtonCG	146
4.4	Test cases	146
4.4.1	Analytical solution of Srivastava and Yeh (1991)	146
4.4.2	Test problem 1	150
4.4.3	Test problem 2	153
4.4.4	Test problem 3	159
4.5	Conclusion remarks	160

In this chapter I present the deployment of the first building block of WHETGEO-2D, i.e. the solver of the R^2 equation. Regarding the mathematical and numerical issues they are essentially the same of WHETGEO-1D and were deeply discussed in Chapter 2. Here we focus on the setting up of the geometrical support framework to solve a partial differential equation (PDE) and on the differences in the algorithms between the one-dimensional and the bi-dimensional cases. The definition and the storage of the computational grid is a key concept in solving any PDE in

a multidimensional domain Berti (2000). In the one-dimensional case the computational domain does not pose particular problems since the geometry is represented by a line and the topological information is embedded in the grid structure through the indexing system, i.e. the index of the grid element both account for the topology and geometry. At the same time, solving a PDE in a bi-dimensional domain requires new algorithms to solve the linearized system and a new method for assembling the matrix of the system. This Chapter is organized as follows. Section 4.1 discuss the problem related to the definition and the storage of the computational grid. Then, in Section 4.2 the algorithms as well as their implementation are presented, and finally in Section 4.4 WHETGEO-2D is tested against analytical solutions and compared with some benchmarks presented in literature.

4.1 GRID

In order to numerically solve a PDE the first step consists in the discretization of the physical domain. This requires to replace the continuous physical domain by a discrete one formed of non-overlapping elements that completely fill the physical domain. The grid support must provide two types of information: the geometric information and the topology information. The former concerns the area of elements, the length of edges, the coordinates of element centroids, and the components of the normal vectors of the edges. Whereas the topological information defines how mesh components are related and located one with respect to the other.

The problems related to the definition and to the storage of the topological information were not introduced before since in the one dimension the elements connectivity is implicitly defined.

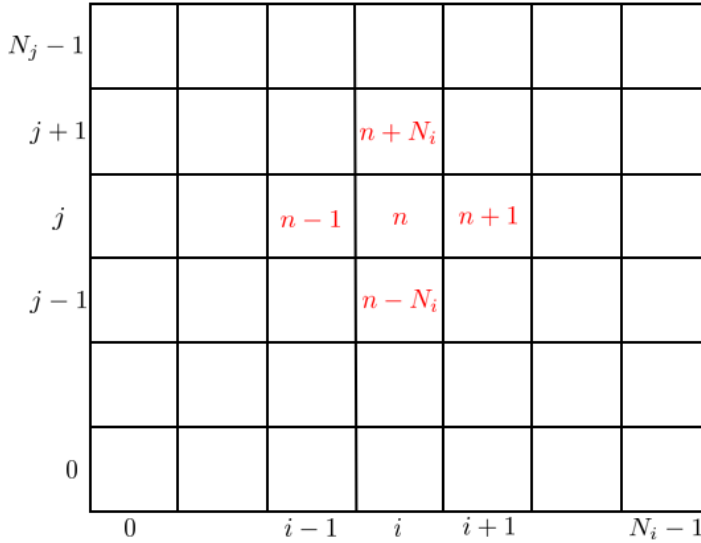


Figure 4.1: Example of structured grid. In black are reported local indices, while in red the global indices. The relation between local and global indices is $n = i + j N_i$.

Whereas, when working in the bi-dimensional domain, as well as in the tri-dimensional domain, the definition and the storage of the topological information is a key aspect. It is worth to note also in multi-dimensional domain the adoption of so-called structured or Cartesian grid relieve to need to explicitly define the grid topology. In fact, the connectedness of the elements derives directly from the indexing system. This structure reflects also in building the system of discretized equations. In fact, a key aspect when working with structured grid is the possibility to establish a direct correspondence between local indices, used to define the local stencil for an element, and the global indices, used to assembly the global matrix as shown in Fig. (4.1).

However, the use of structured grids presents two main limits. The first one is related to the limited geometric flexibility offered

by structured grids which hampers the quality of results by impeding reasonable parameterizations of spatial locations. This is a key aspect when applying a PDE solver to a real case study. The second one is related to development of reusable software in numerical computation. Specifically, when working with structured grid data is often melted into the grid data structure (Bader and Berti, 1998): as seen in the previous paragraph, grid indices can be used to traverse the grid, and at the same time to access data. This is computationally efficient but without any flexibility.

Therefore, in order to improve reusability WHETGEO-2D has been implemented by handling the computational grid as an unstructured grid. This requires to explicitly define the topological information. In fact, in unstructured grid there is no correspondence between local indices and global indices therefore it is necessary to resort to number grid elements and to define their reciprocal relationship through connectivity tables. It is worth to make clear that this approach on one side is more complex and less efficient compared to the one relying on a structured grid, but it allows to split the grid information into its topology information, and its geometric information (Bader and Berti, 1998; Berti, 2000). The adoption of unstructured grid permits to deal with complex geometries and to have better description of the heterogeneities of the domain. From an informatic point of view, this means keeping the algorithms separate from data. Put differently, the topology defines the connectedness and guides the iteration over the grid elements to access the geometric data and physical quantities involved in the PDE which are stored separately.

The first step to define the connectivity tables consist in numbering all the nodes of the grid as Fig. (4.2). Then we number all the edges of the grid and associate to each one the pairwise of nodes defining its extremes. This association is called Hasse diagram (Skiena, 1990). About the edges, it is worth to point out another

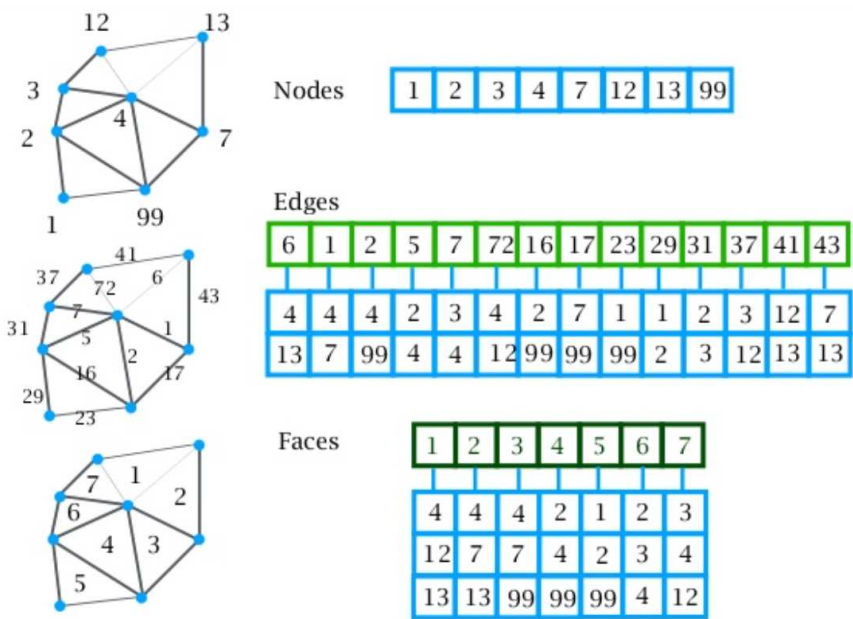


Figure 4.2: Hesse diagram to define grid topology. Nodes are univocally identified with a number. Each edge is numbered and defined by using the nodes defining its extremes. Similarly each face is defined by using their set of nodes.

difference to the structured grid. In a structured grid it is possible to know whether an edge is inside the domain or it is a border edge on which a boundary condition must be applied by using indices. This is not possible in an unstructured grid, therefore it is necessary to define the set of edges that constitute the border of the domain. In a similar way as for the edges it is possible to define faces by using their set of nodes. Furthermore we can associate to each face its set of edges. It is worth to note that this information is somehow redundant since can be retrieved for the knowledge of the set of nodes defining the face. However since the aim is to solve the PDE with a finite-volume method for which

it is necessary to compute for each element the fluxes through all its edges, it is convenient to explicit the set of edges for each element once for all.

Nevertheless, finite-volume methods are inherent conservative since for any edge common to two elements, the flux leaving the edge of one element is equal to the flux entering the neighbour element through the same edge. The magnitude of these fluxes is the same but they have opposite sign. From this property it is possible to speed-up the computation of fluxes by looping over edges. This is the so called face connectivity. For each edge it is necessary to explicit its neighbour elements consistently with the orientation of the edge. Therefore the algorithm for calculating fluxes is presented in Algorithm 1.

Algorithm 1 Compute fluxes by using a face connectivity.

```

for all edges  $f \in \text{Edges}$  do
2:   if  $f$  is on the boundary then
       compute boundary flux
4:   else
       compute  $\mathcal{F}$ 
6:   assign  $\mathcal{F}$  to the outward neighbour
       assign  $-\mathcal{F}$  to the inward neighbour
8:   end if
end for

```

Besides the connectivity information it is necessary to attribute to each entity of the grid its geometric information. For instance, for to each node it is necessary to associate its coordinate, to each edge its length and so on.

To associate to each entity of the grid its geometric information and the variables of the PDE we use the number of the entity. In light of this the grid data are stored in appropriate Java containers, `HashMap`, that allows to store *key* and *value* pair. The *key* is the

number of the grid entity, while the *value* can be a scalar or a vector and it can be the topological information, the value of the geometrical information, and the value of a physical variable of the problem.

4.2 ALGORITHMS

Differently from the one-dimensional case, the linear system derived from the discretization of the PDE, or its appropriate linearization, cannot be solved with a direct method such as the Thomas algorithm (Quarteroni et al., 2010) since the matrix is not tri-diagonal. Besides, the assembly of the matrix system is not trivial as in the one-dimensional case but requires a little more operations. We accomplish the latter task by using a ‘matop’ interface whose use we inherit from lectures by Prof. Vincezo Casulli and by Prof. Michael Dumbser that we acknowledge here.

4.2.1 Conjugate gradient method

To solve the linearized algebraic system obtained by using the NCZ algorithm we choose to adopt the conjugate gradient method (CG) (Shewchuk et al., 1994). The CG method, Algorithm 2, is proved to be globally convergent for all linear system whose coefficient matrix is symmetric and positive definite. These requirements on the coefficient matrix will pose some constrain on the discretization of advective fluxes. In fact the adoption of up-wind schemes requires an explicit time discretization with consequently limitation of the time step size (Casulli and Zanolli, 2005).

Moreover it is worth to point out that the CG method is an iterative solver whereas the Thomas algorithm is a direct method This significantly affect the computational time. To obtain a faster con-

Algorithm 2 Conjugate gradient method

```

1:  $\mathbf{r}_0 := \mathbf{b} - \mathbf{A}\mathbf{x}_0$ 
2: if  $\mathbf{r}_0 < \varepsilon$  then
3:   return  $\mathbf{x}_0$  and exit
4: end if
5:  $\mathbf{d}_0 := \mathbf{r}_0$ 
6:  $\mathbf{r}_0 := \mathbf{b} - \mathbf{A}\mathbf{x}_0$ 
7: for  $k = 0, \dots, N - 1$  do
8:    $\mathbf{v}_k = \mathbf{A}\mathbf{d}_k$ 
9:    $\alpha_k = \frac{\mathbf{r}_k^\top \mathbf{r}_k}{\mathbf{d}_k^\top \mathbf{v}_k}$ 
10:   $\mathbf{x}_{k+1} = \mathbf{x}_k + \alpha_k \mathbf{d}_k$ 
11:   $\mathbf{r}_{k+1} = \mathbf{r}_k - \alpha_k \mathbf{v}_k$ 
12:  if  $\mathbf{r}_{k+1} < \varepsilon$  then
13:    return  $\mathbf{x}_0$  and exit
14:  end if
15:   $\beta_{k+1} = \frac{\mathbf{r}_{k+1}^\top \mathbf{r}_{k+1}}{\mathbf{r}_k^\top \mathbf{r}_k}$ 
16:   $\mathbf{d}_{k+1} = \mathbf{r}_{k+1} + \beta_{k+1} \mathbf{d}_k$ 
17: end for

```

vergence rate in solving the linear system, we adopt a simple diagonal scaling preconditioner, Jacobi preconditioner (Quarteroni et al., 2010).

4.2.2 Matrix-free algorithm

A key operation used in iterative solver for solving most of PDE is sparse matrix-vector product (Berti, 2000). One of the problem it is necessary to cope with the solution of a PDE in a 2D domain is how to properly store the flux matrix \mathbf{T} , Eq. (18). In fact the flux matrix \mathbf{T} is a sparse matrix, i.e. it is mostly composed by zeros. Storing a sparse matrix impacts on both the memory usage and the algorithm efficiency. For this reason in literature several ways to efficiently handle sparse matrix are presented (Davis, 2006; Golub and Van Loan, 2013) as well as software libraries (Braun, 2015; Heimsund, 2011; Wendykier, 2010).

To avoid to use matrix algebra, which would require implementing or importing various libraries, I implemented the solver for the R^2 equation, WHETGEO-2D, in a matrix-free form. A matrix-free method does not require to explicitly store the coefficient of the flux matrix, but it directly evaluate the matrix-vector products. In fact a closer inspection of the NCZ algorithm and the CG algorithm reveals that in both algorithms a matrix-vector multiplication is required. This observation has lead to a specific design of the classes that deals with the solution of the nonlinear system.

4.3 CODE DESIGN

In developing the WHETGEO-2D component solving the R^2 equation I reused the classes developed for WHETGEO-1D implementing the SWRC,

ClosureEquation class, and the hydraulic conductivity models, ConductivityEquation class. As discussed in Section 2.3 and in Section 4.2 the algorithm required to solve a PDE in the bi-dimensional case are different from those used in the one-dimensional case. Of course one can argue that also for the one-dimensional case it is possible to adopt the same algorithms required for the bi-dimensional case, but this would have entailed an overburden both from the informatic and numerical point of view. About the former it is worth to clear that in the one-dimensional domain there is no need to explicitly define the topology, and the flux matrix can be easily stored in three vectors without and the need to resort to a matrix-free method.

4.3.1 The matrix-vector product, **Matop**

Since the matrix-vector product is an operation required both by the NCZ algorithm and by the CG method, it is convenient to implement it as a standalone class. The Matop is an abstract class, Fig. (4.3), defining an abstract method to compute the matrix-vector product without using a sparse matrix storages. The concrete implementation of Matop class is left to subclasses accordingly to the PDE under scrutiny.

4.3.2 The Conjugate gradient method, **ConjugateGradient**

The ConjugateGradient class implements the CG method. Looking at the Algorithm 2 to apply the CG method it is necessary to define the matrix-vector product. This is specific of each equation to be solved, thus the ConjugateGradient class contains a reference to the Matop object, Fig. (4.4). In this manner the ConjugateGradient class can be used for different PDE by simply creating the appropriate Matop object.

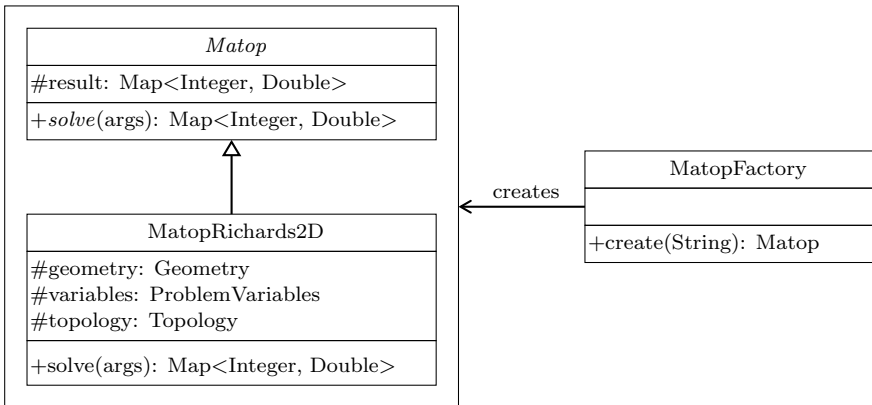


Figure 4.3: UML class diagram for the Simple Factory pattern applied for the choice of the required `Matop` object. `Matop` is the abstract class defining the interface that is implemented by the concrete class `MatopRichards2D`.

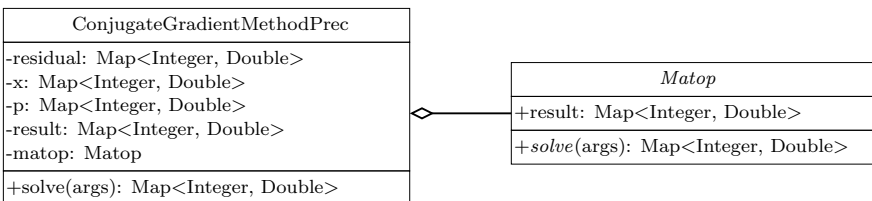


Figure 4.4: UML class diagram for the `ConjugateGradientPrec`. This class deals with the solution of a linear system whose coefficient matrix is symmetric and positive definite. The `ConjugateGradientPrec` class contains a reference to a `Matop` object implementing the matrix-vector product for the PDE under scrutiny.

4.3.3 The NCZ algorithm, `NestedNewtonCG`

As explained previously, for the bi-dimensional case the `NestedNewtonThomas` class, dealing with the NCZ algorithm, cannot be reused. Therefore a new implementation of the NCZ algorithm is required. Figure (4.5) provides the UML diagram of the `NestedNewtonCG` class. It contains a reference to the `ConjugateGradient` object, to the `Matop` object, to the `Variable` object, to the `Topology` object, and to a list of `EquationState` objects.

4.4 TEST CASES

In this Section I firstly test the WHETGEO-2D against the analytical solution presented by Srivastava and Yeh (1991) for the one-dimensional infiltration, and then I show the performance of WHETGEO-2D with some test problems presented in literature.

4.4.1 Analytical solution of Srivastava and Yeh (1991)

WHETGEO-2D has been tested against the numerical solution presented by Srivastava and Yeh (1991) for the one-dimensional transient infiltration in an homogeneous and layered soil. In this case the flux is provided on top of the domain uniformly along the x axis.

Homogeneous soil

We consider a one-dimension homogeneous soil layer of 1 m depth (TP1). The saturated hydraulic conductivity value is assumed to be $2.78 \times 10^{-6} \text{ ms}^{-1}$, with $\theta_s = 0.4 \text{ m}^3\text{m}^{-3}$, $\theta_r = 0.06 \text{ m}^3\text{m}^{-3}$, and $\alpha = 0.001 \text{ m}^{-1}$. The initial condition is determined by

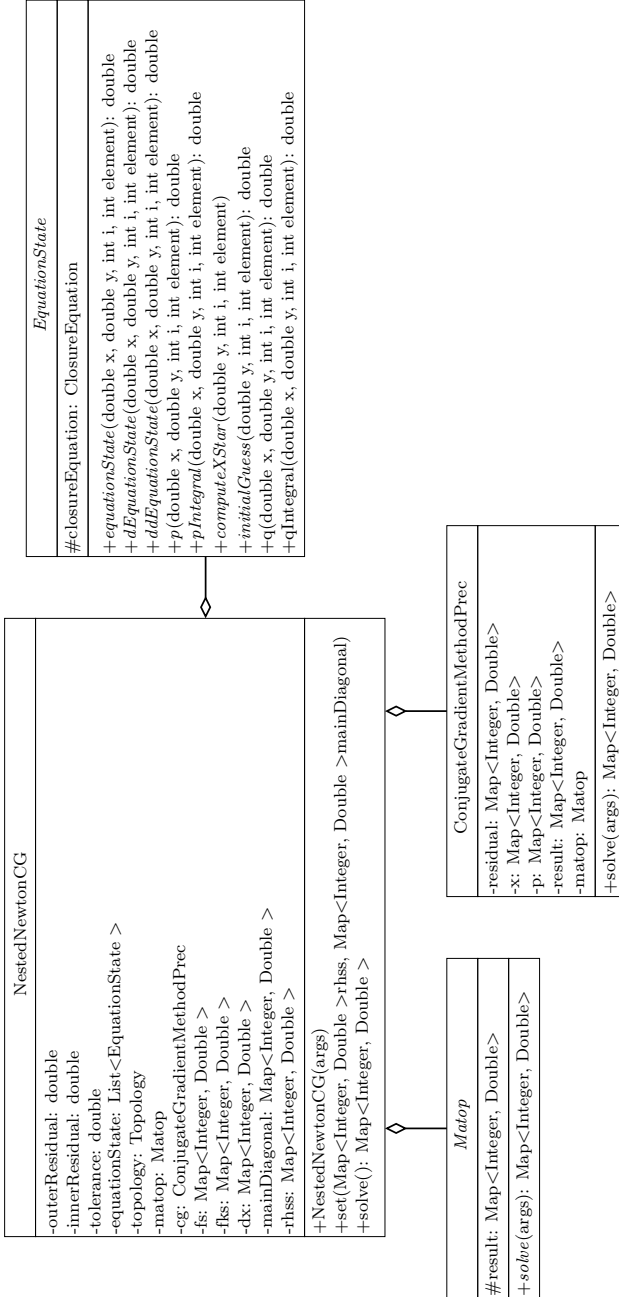


Figure 4.5: UML class diagram for the NestedNewtonCG. This class deals with the NCZ algorithm of a linear system whose coefficient matrix is symmetric and positive definite. The ConjugateGradientPrec class contains a reference to a Matop object implementing the matrix-vector product for the PDE under scrutiny.

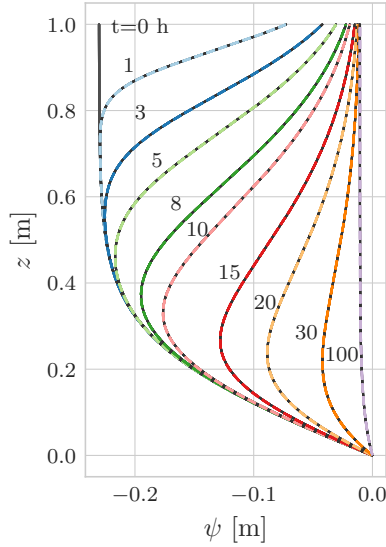


Figure 4.6: Comparison between the analytical and numerical solution for a wetting homogeneous soil.

imposing as lower boundary condition $\psi = 0$ m and a constant water flux at the soil surface $q_A = 2.78 \times 10^{-7} \text{ ms}^{-1}$. For times greater than 0 the water flux at the soil surface is $q_B = 2.5 \times 10^{-6} \text{ ms}^{-1}$. The domain is discretised with a uniform grid space $\Delta z = 0.001$ m and the time step is $\Delta t = 60$ s. Figure (4.6) shows a comparison between the numerical and the analytical solutions. Figure (4.7) shows the comparison between the analytical and numerical solution during a drainage scenario. The initial condition is determined by imposing as lower boundary condition $\psi = 0$ m and a constant water flux at the soil surface $q_A = 2.5 \times 10^{-6} \text{ ms}^{-1}$. For times greater than 0 the water flux at the soil surface is $q_B = 2.78 \times 10^{-7} \text{ ms}^{-1}$. The domain is discretised with a uniform grid space $\Delta z = 0.001$ m and the time step is $\Delta t = 60$ s.

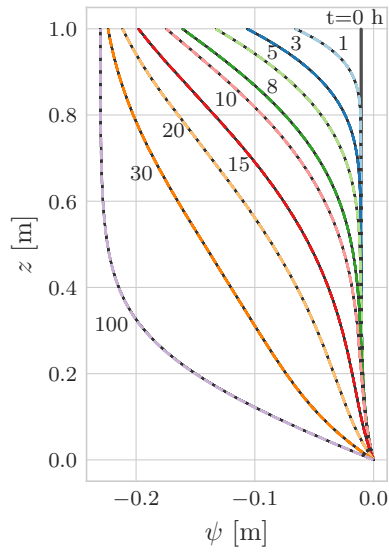


Figure 4.7: Comparison between the analytical and numerical solution for a wetting homogeneous soil.

Layered soil

We consider one-dimensional vertical infiltration toward the water table through a layered soil both for a wetting scenario and for a drainage scenario. The α of the two layers are set to be 0.001 m^{-1} , and the saturated hydraulic conductivities of the lower and upper layers are equal to $2.786 \times 10^{-6} \text{ ms}^{-1}$ and $2.786 \times 10^{-5} \text{ ms}^{-1}$, respectively. The thickness of each layer is 1 m. The saturated and residual water contents are taken as $0.40 \text{ m}^3\text{m}^{-3}$ and $0.06 \text{ m}^3\text{m}^{-3}$, respectively

For the wetting scenario, Fig. (4.8), the initial condition is determined by imposing as lower boundary condition $\psi = 0 \text{ m}$ and a constant water flux at the soil surface $q_A = 2.78 \times 10^{-7} \text{ ms}^{-1}$. For times greater than 0 the water flux at the soil surface is $q_B = 2.5 \times 10^{-6} \text{ ms}^{-1}$.

Whereas, for the drainage scenario, Fig. (4.9), the initial condition is determined by imposing as lower boundary condition $\psi = 0$ and a constant water flux at the soil surface $q_A = 2.5 \times 10^{-6} \text{ ms}^{-1}$. For times greater than 0 the water flux at the soil surface is $q_B = 2.78 \times 10^{-7} \text{ ms}^{-1}$.

In both the simulations the domain is discretized with a uniform grid space $\Delta z = 0.001 \text{ m}$ and the time step is $\Delta t = 60 \text{ s}$.

4.4.2 Test problem 1

In test problem (TP1) we consider a rectangular domain 5 m wide \times 3 m deep divided into alternating blocks of clay and sand (Kirkland et al., 1992; McBride et al., 2006). The Van Genuchten model is used to define the pressure-moisture relationship. The hydraulic properties of the sand and clay are reported in Tab. (4.1). A no-flow boundary condition is prescribed everywhere except for

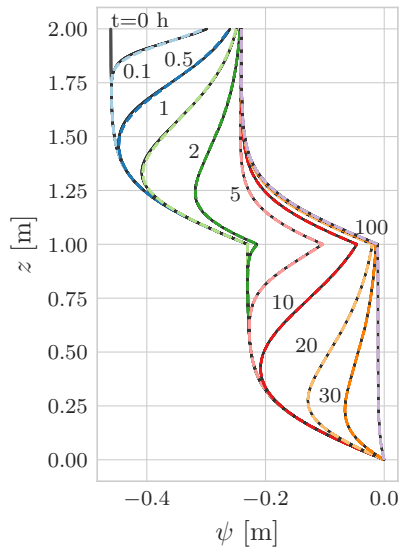


Figure 4.8: Comparison between the analytical and numerical solution for a layered soil in a wetting scenario.

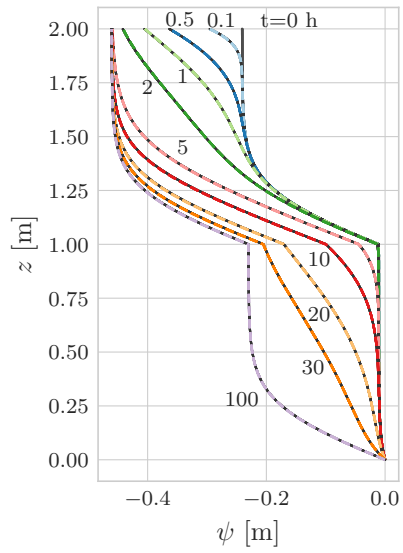
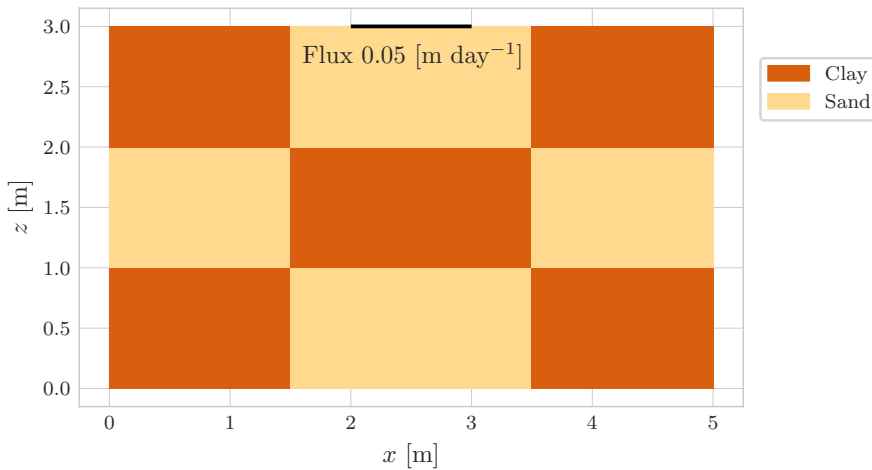


Figure 4.9: Comparison between the analytical and numerical solution for layered soil in a drainage scenario.

Table 4.1: Hydraulic properties of the soils for TP1.

	$\theta_s \text{ m}^3\text{m}^{-3}$	$\theta_r \text{ m}^3\text{m}^{-3}$	$\alpha \text{ m}^{-1}$	$n -$	$K_s \text{ m s}^{-1}$
Sand	0.3658	0.0286	2.8	2.239	6.262×10^{-5}
Clay	0.4686	0.1060	1.04	1.3954	1.516×10^{-6}

**Figure 4.10:** Scheme showing the setting of TP1. Zero flux boundary conditions except as noted, thick black line.

a constant water flux rate of 0.5 m per day applied to the top of the sand surface Fig. (4.10). The initial condition is a constant water suction of -500 m. The simulation was run using both a cartesian grid and an unstructured grid. The saturation degree is examined after 12.5 day of simulation, Fig. (4.11) and Fig. (4.12)

4.4.3 Test problem 2

This test problem (TP2) involves water flow into initially very dry layered soil of sand and clay with a developing water table (Casulli and Zanolli, 2010; Forsyth et al., 1995; Kirkland et al.,

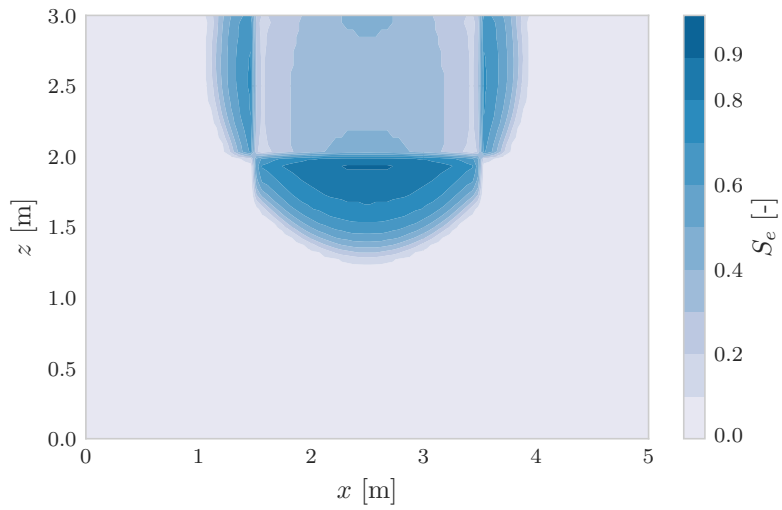


Figure 4.11: Solution for the saturation degree after 12.5 day of simulation. In this simulation a cartesian grid with a step size of 0.05 m was used.

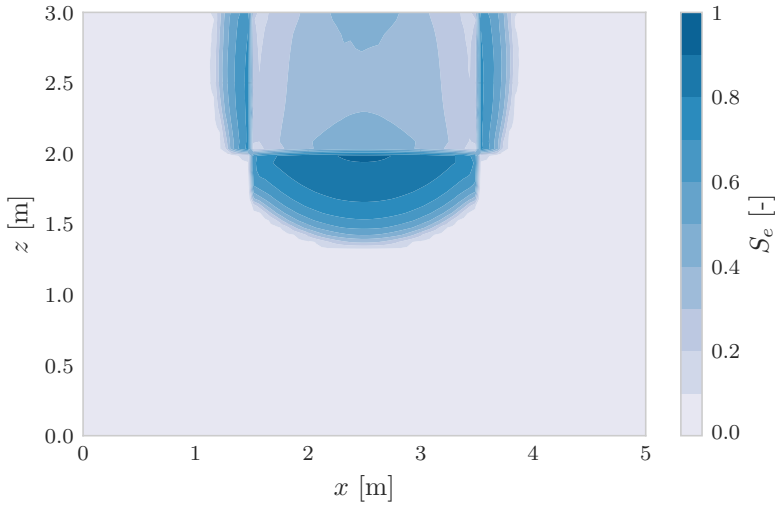
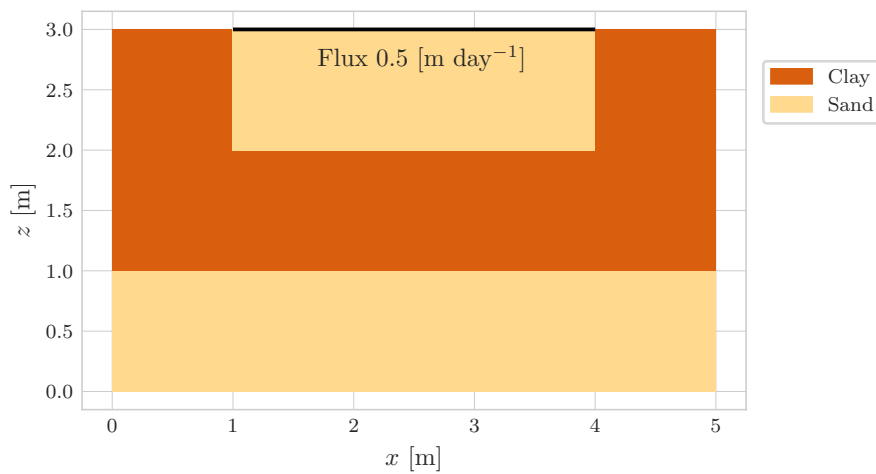


Figure 4.12: Solution for the saturation degree after 12.5 day of simulation. In this simulation an unstructured grid was used.

1992; McBride et al., 2006). The Van Genuchten model is used, and the hydraulic properties of the sand and clay are reported in Tab. (4.2). The domain is 5 m wide \times 3 m deep and to achieve a perched table, a 3 m \times 1 m region of sand was bounded by clay as shown in Fig. (4.13). A no-flow boundary condition is prescribed everywhere except for a constant water flux rate of 0.5 m per day applied to the top of the sand surface. The initial condition is a constant water suction of -500 m. The simulation was run using both a cartesian grid and an unstructured grid. The saturation degree is examined after 15 day of simulation, Fig. (4.14) and Fig. (4.15).

Table 4.2: Hydraulic properties of the soils for TP2.

	$\theta_s \text{ m}^3\text{m}^{-3}$	$\theta_r \text{ m}^3\text{m}^{-3}$	$\alpha \text{ m}^{-1}$	$n -$	$K_s \text{ m s}^{-1}$
Sand	0.3658	0.0286	2.8	2.239	6.262×10^{-5}
Clay	0.4686	0.1060	1.04	1.3954	1.516×10^{-6}

**Figure 4.13:** Scheme showing the setting of TP2. Zero flux boundary conditions except as noted, thick black line.

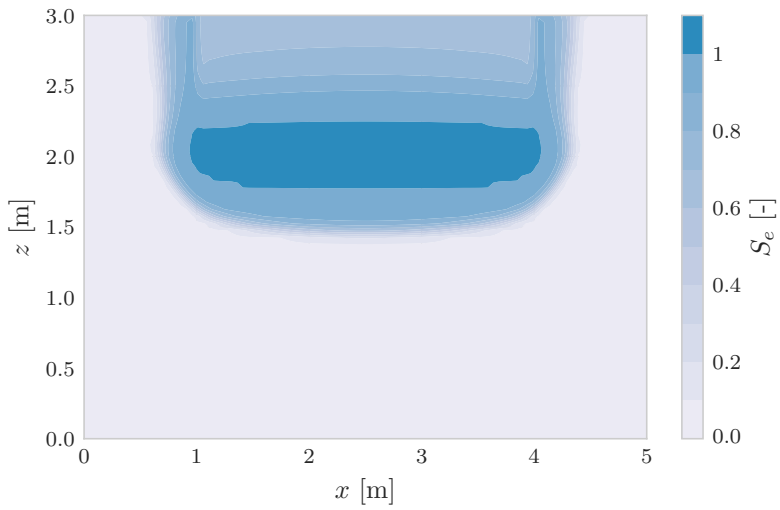


Figure 4.14: Solution for the saturation degree after 1 day of simulation. In this simulation a cartesian grid with a step size of 0.05 m was used.

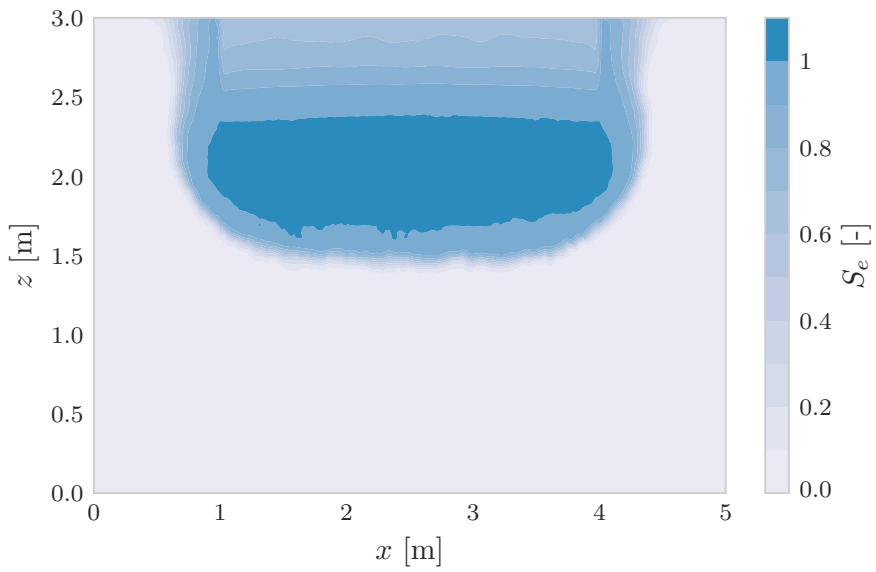


Figure 4.15: Solution for the saturation degree after 1 day of simulation. In this simulation an unstructured grid was used.

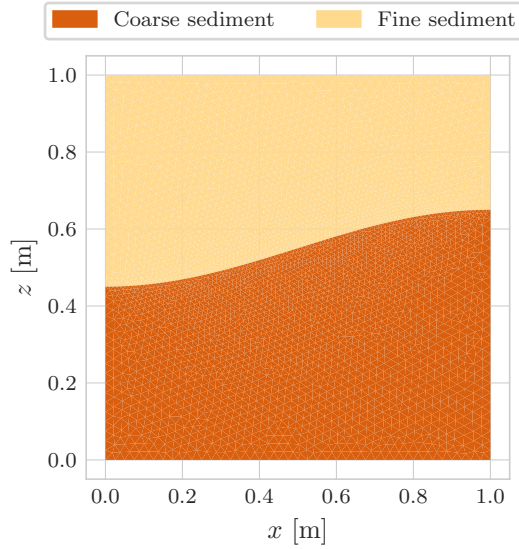


Figure 4.16: Scheme showing the setting of TP3.

4.4.4 Test problem 3

This test problem (TP3) has been presented by Manzini and Ferraris (2004) and involves the infiltration in a layered soil as presented in Fig. (4.16). The domain is a square of $L = 1$ m and the interface separating the two layers is

$$\zeta(x) = \left[0.1 \left(1 - \cos \left(\frac{\pi x}{L} \right) \right) + 0.45 \right] L \quad (68)$$

As regards the boundary conditions, at the top and bottom side an homogeneous Dirichlet boundary condition is prescribed, that is $\psi(x, z = 0) = \psi(z, z = L) = 0$ m, whereas on the two vertical sides a no flux boundary condition is prescribed. The initial condition is

$$\psi(x, z) = 0 - z \quad (69)$$

Table 4.3: Hydraulic properties of the soils for TP3.

	$\theta_s \text{ m}^3\text{m}^{-3}$	$\theta_r \text{ m}^3\text{m}^{-3}$	$\alpha \text{ m}^{-1}$	$n -$	$K_s \text{ m s}^{-1}$
Fine sediment	0.5	0.120	2.8	3	$5.56e - 06 \times 10^{-6}$
Coarse sediment	0.46	0.034	1.6	1.37	$6.945e - 07 \times 10^{-7}$

The van Genuchten model is used to prescribe the pressure-moisture relationship. The hydraulic properties are given in Tab. (4.3). The time step size is set to $\Delta t = 900 \text{ s}$. Figure (4.17) reports the time evolution of the water content. The result is in good agreement with that reported in (Manzini and Ferraris, 2004).

4.5 CONCLUSION REMARKS

This Chapter lays the groundwork for the development of WHETGEO-2D. The main effort has been the design and the implementation of the classes required to solve a PDE in a bi-dimensional domain. I presented the first deployment of the component solving the R^2 equation, and it has been succesfully tested against the analytical solution presented by Srivastava and Yeh (1991) and the benchmarks presented in (Kirkland et al., 1992; Manzini and Ferraris, 2004; McBride et al., 2006).

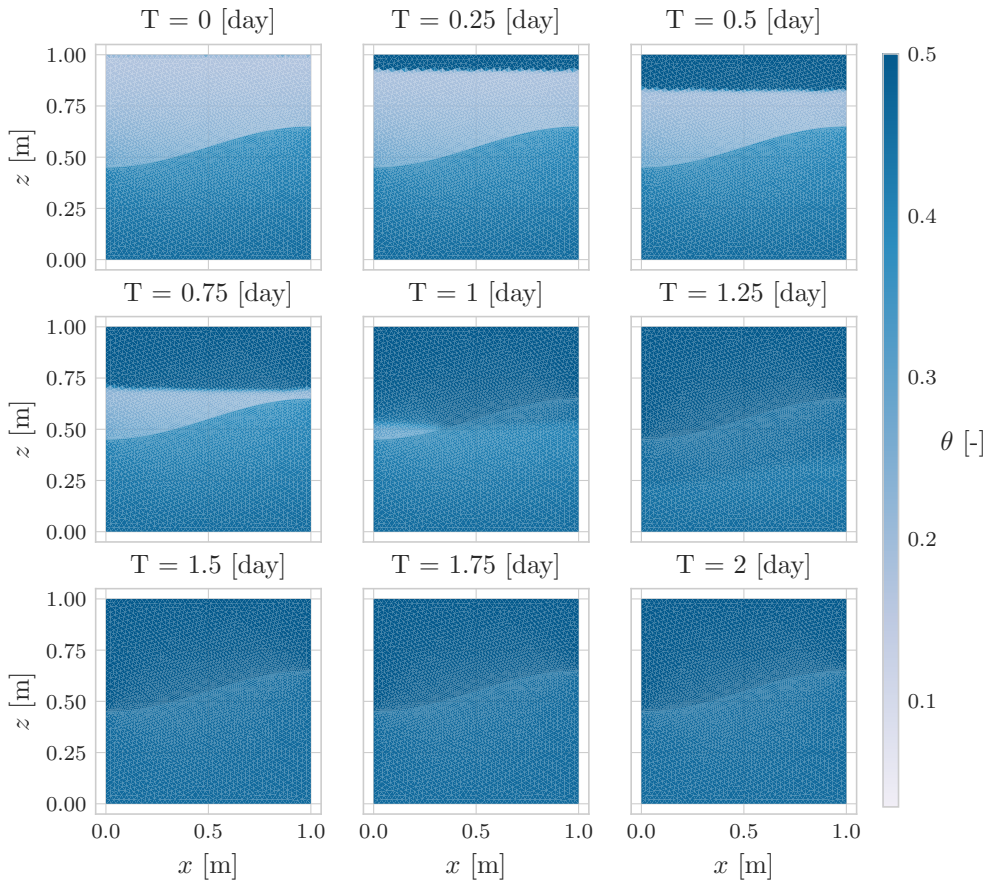


Figure 4.17: Test problem 3, time evolution of the water content.

5

SYNOPSIS

Contents

5.1	Concluding remarks	163
5.2	Contribution	165
5.3	Future research	166
5.3.1	Frozen ground	166
5.3.2	Lysimeter GEO	170
5.3.3	WHETGEO-2D	171

5.1 CONCLUDING REMARKS

This thesis presented the development of new tools to study the critical zone. In Chapter 2 it has been presented WHETGEO and its 1D deployment. WHETGEO-1D is a new, physically based model simulating the water and energy budgets in a soil column. This Chapter outlined the mathematical and numerical issues involved in solving the Richardson-Richards equation, conventionally known as Richards equation, and the heat equation in heterogeneous soils. In particular, for the Richardson-Richards equation (R2) we take advantage of the nested Newton-Casulli-Zanolli (NCZ) algorithm that ensures the convergence of the numerical solution in any condition. Starting from numerical and modelling needs, the Chapter presented the design of a software that is intended to be the first building block of a new, customisable, land-

surface model that is integrated with process-based hydrology. WHETGEO is developed as an open-source code, adopting the Object-Oriented paradigm and a generic programming approach in order to improve its usability and expandability. WHETGEO is fully integrated in the GEOframe/OMS₃ system allowing the use of the many ancillary tools it provides. Finally, the water budget was successfully tested against the analytical solutions presented in (Srivastava and Yeh, 1991) and in (Vanderborght et al., 2005). Then some behavioural tests on both the water budget and the heat budget are presented. A calibration exercise by joining WHETGEO-1D with the automatica calibrator LUCA has been presented too.

Chapter 3 presented the application of the NCZ algorithm in modeling the heat transfer in frozen soils, and an extensive review of commonly used simulation software in the Cryospheric field. The numerical model was implemented and verified against the Neumann and Lunardini analytical solutions. In both cases, the results were in good agreement even with an hourly integration time step. For the Neumann solution, we considered pure water instead of saturated soil since it is more numerically demanding, and no convergence problems were encountered despite choosing a narrow temperature range (0,0001 °C) over which phase change occurs. Numerical experiments demonstrated the robustness of the model by comparing results at differing temporal and spatial resolutions. Results obtained with time steps of 1 h, 1 day, and 10 days are consistent. The robustness of the numerics allows the user to choose both the space and time discretization without any restriction due to stability and convergence issues. As a consequence, this method is effective for simulating permafrost thaw, a phenomenon that occurs at depth, in response to seasonal and multi-annual cycles, and often over tens, hundreds or even thousands of years. Furthermore, phenomena like hysteresis or the

variation of solute concentration upon freezing (Clow, 2018) can be included in the numerical model if the enthalpy function (i.e. its parameters) does not change within the current time step of integration. Beyond applications to frozen soil, it can be used to study other geophysical phenomena that involve phase change of a substance simply by changing the definition of the enthalpy function and the thermal conductivity function. Examples include, glacier dynamics (Aschwanden et al., 2012), snow pack evolution (Brun et al., 1992; Lehning et al., 1999), and magma bodies (De Lorenzo et al., 2006). This may be even further expanded to industrial problems involving phase change materials used in energy recovery systems (Mongibello et al., 2018; Nazzi Ehms et al., 2019) or casting problems of pure metals and alloys (Lewis and Ravindran, 2000).

In Chapter 4 I outlined the ongoing development of WHET-GEO - 2D. The first part of the Chapter is dedicated to implementation of unstructured grids in order to have a reusable software. A particular focus has been paid to the importance in separating the topological information of the grid from the geometrical information. Then, the algorithms required to solve a PDE in a bi-dimensional domain were discussed as well as the design of the classes used to implement the numerical solver. Finally, the component solving the Richards' equation has been tested against the analytical solutions presented in (Srivastava and Yeh, 1991; Vanderborcht et al., 2005) and some benchmarks presented in (Kirkland et al., 1992; Manzini and Ferraris, 2004; McBride et al., 2006).

5.2 CONTRIBUTION

CHAPTER 2 has been accepted in peer review on the scientific journal *Geoscientific Model Development* with the title *Implement-*

ing the Water, HEat and Transport model in GEOframe WHETGEO-1D v.1.0: algorithms, informatics, design patterns, open science features, and 1D deployment. The paper has been coauthored by Prof. Riccardo Rigon. Author contributions: Conceptualization, R.R. and N.T.; Methodology: N.T. and R.R. Software engineering: N.T. and R.R.; Code writing N.T. Code Revision: RR and NT; Data curation and simulations, N.T.; Paper Writing, Review, Editing; N.T. and R.R.

CHAPTER 3 has been accepted to be published on the scientific journal *The Cryosphere* with the title *A method for solving heat transfer with phase change in ice or soil that allows for large time steps while guaranteeing energy conservation*. The paper has been coauthored by Prof. Stephan Gruber and Prof. Riccardo Rigon. Author contributions: NT, SG, and RR conceptualized the study; NT and RR developed the software; Data curation and simulations, N.T.; NT wrote the original draft; NT, SG, and RR reviewed and edited the manuscript. All the authors have read and agreed to the published version of the manuscript.

5.3 FUTURE RESEARCH

In this Section I will briefly outline possible future research directions of the tools developed during my Ph.D. studies.

5.3.1 Frozen ground

A first application of FreeThaw-1D has been presented in the master Thesis by Enrico Borinato that I co-supervised. Starting from the work by (Nicolisky and Romanovsky, 2018), that aimed to asses through numerical experiments the influence of unfrozen

liquid water on permafrost thawing and the redistribution of the incoming heat flux, Enrico Borinato applied FreeThaw-1D in order to understand which is the effect of the choice of the soil thermal conductivity model in simulating long-term permafrost degradation. In fact, the definition of the apparent thermal conductivity of the soil is always problematic since it depends on the fractions of soil components. One of the outcomes of this thesis is the choice of the soil thermal conductivity model affect the simulated soil thermal regime as far as the unfrozen liquid water content is higher.

In Chapter 3 it has been presented how to extend WHETGEO-1D to in order to model freezing-thawing processes as done in FreeThaw-1D model. Moreover, it has been shown a numerical experiment, although quite naive, in which WHETGEO-1D was used to simulate sub-lake talik evolution. The primary scope of this numerical experiment was to demonstrate that the software design allows the user to easily extend WHETGEO-1D in order to simulate new processes by simultaneously solving the heat conduction equation over two different domains. The possibility to deal with different equation state represent a novelty compared to FreeThaw-1D. Besides, while in Borinato's thesis FreeThaw-1D was use to test different soil thermal conductivity model in WHETGEO-1D it is possible to model each soil layer with a different soil freezing characteristic curve and soil thermal conductivity model. This adds more flexibility in the description of the soil properties since the spatial variability is can be controlled not only by specifying different set of parameters but also through the definition of parameterizations.

Although heat conduction-based models are widely used, their application is limited to setting with minimal groundwater flow (Wellman et al., 2013). Future developments should aim to consider the water flow and the associated heat advection and possibly an extension to a multi-domain. In fact the ongoing climate

change is reducing the the extent and the thickness of permafrost with a consequent deepening of the active layer and extent of discontinuous permafrost area (Kurylyk et al., 2016; Wellman et al., 2013). These changes in permafrost conditions in turn significantly affect the hydrological regime (Hinzman et al., 2005; Kurylyk et al., 2016; Michel and Van Everdingen, 1994). For instance, the distribution of permafrost modifies the groundwater flow regime (Carey and Woo, 2005; Metcalfe and Buttle, 1999; Quinton and Marsh, 1999), the thickness of the active layer exerts control on the timing and magnitude of subsurface runoff and streamflow (Cheng and Jin, 2013; Kane et al., 2013; Woo et al., 2008). Therefore in discontinuous permafrost are heat conduction-based models are not suitable to be applied since they overlook at the the heat advection transport that represents a significant contribution in the soil energy budget.

Many permafrost area are interested by ice-rich ground (Brown et al. 1997). Excess ice, defined as ice that exists in excess of the thawed consolidated pore space, is particularly important as its thawing can cause loss of soil strength, slope instability (Couture et al., 2003), differential subsidence and thermokarst (Kokelj and Jorgenson, 2013). Variation of the surface microtopography significantly affects the thermal and hydrologic condition of the soil Zona et al., 2011. Nonetheless subsidence constitutes a threat for infrastructure (Streletskiy et al., 2012). As pointed out by Shur et al. (2005) it is necessary to move from the simple conceptual model based on the existence of a seasonally frozen ground, active layer, overlying permafrost, to a the three layer model which foresees the existence of a transition layer between the active layer and permafrost. The transition zone is characterised by being ice-rich. Because of this high thermal inertia, the transition zone serves as a buffer between the active layer and the underlying permafrost promoting the thermal stability of the ground and limiting the

thaw penetration (Hinkel and Nelson, 2003; Nelson et al., 1998; Shur et al., 2005). As a matter of fact several model-based studies predict widespread permafrost degradation under the current climate warming, but field-based studies reveal that permafrost system may be more resilient than such scenarios imply (Couture and Pollard, 2017). It is evident that this apparent thermal stability will last until the transition zone will not be completely thawed (Shiklomanov et al., 2013). Besides the supplementary thermal inertia there is another aspect that is strictly related to the transition zone: heave and subsidence of the ground surface. A recent study in the Mackenzie Delta (O'Neill et al., 2019) demonstrates that overlooking the surface subsidence, due to excess ice thawing, leads to a misleading interpretation of ALT measurements. When excess ice and the associated ground subsidence is ignored in permafrost models, simulations tends to overestimate thaw penetration (O'Neill et al., 2019). Excess ice is therefore a key process in permafrost system that is often poorly described in many numerical models (Ekici et al., 2019; Lee et al., 2014).

Finally, it is worth to point out that there is the urgency to adopt an integrated approach in studying permafrost time evolution (Vincent et al., 2017). Though climate is the main factor in determining the presence of permafrost, also ecological processes concur in controlling permafrost formation and degradation (Shur and Jorgenson, 2007). This require to move from a perspective describing permafrost as a two-layer system, where the active layer overlies the frozen permafrost, to a perspective in which we include a third layer that lies between the active layer and the Atmosphere above (Vincent et al., 2017). The third layer includes both ecological processes and human activities and its importance lies in controlling the surface heat balance (Shur and Jorgenson, 2007; Vincent et al., 2017). In accordance with what Freeze and Harlan

(1969) said more than 50 years ago it is necessary to consider *interfaces as zones rather than sharp discontinuities* (Vincent et al., 2017).

5.3.2 Lysimeter GEO

A possible application of WHETGEO-1D is Lysimeter GEO (LysGEO), a numerical ecohydrological model of the soil-vegetation-atmosphere (SVA) continuum system. LysGEO is currently developed by Concetta D'Amato, a Ph.D. student of Prof. Riccardo Rigon. In the SVA system, measuring and modelling water and solute fluxes, is a challenge because of the several non-linear and dynamic interacting processes controlling the water flux (Romano et al., 2011). LysGEO modelling idea is coupling infiltration and evapotranspiration processes by using a numerical model which considers the root water uptake and the water stress factor to compute the actual evapotranspiration. Root water uptake affect and is affected by soil moisture and at the same time drives the dynamics of soil CO₂ (Teodosio et al., 2017), affecting in a significant way the modulation of actual transpiration (Caldwell et al., 1998; Da Rocha et al., 2004; Howard et al., 2009). Root water uptake has a key role in the soil water balance and its effect is determined by root water compensation and hydraulic redistribution. These two important mechanisms regulate root water uptake, but also enhancing nutrient uptake and in very dry condition the evaporation flux from the soil surface through hydraulic descent in extremely dry conditions (Teodosio et al., 2017). Considering the one-dimensional problem, LysGEO links infiltration and evapotranspiration processes by using appropriate stress factors (Ball et al., 1987; Jarvis, 1976), with which actual evapotranspiration is computed and the corresponding amount of water removed from Richards' equation balance (Casulli and Zanolli, 2010) by using the sink term. As regards the IT implementation, LysGEO is a system of components

built upon the OMS₃. The infiltration component of this virtual lysimeter is WHETGEO 1D - Water, Heat and Transport in GEOframe, which is a new, physically based model estimating the water and energy budgets in a soil column. Evapotranspiration flow (ET) is estimated using the GEOframe-ETP component (Bottazzi et al., 2021; Formetta et al., 2014a). This component includes three evapotranspiration models: Priestley-Taylor depending on radiation and weakly from temperature (Formetta et al., 2014a; Priestley and Taylor, 1972), Penman-Monteith (FAO), where evapotranspiration is affected by temperature, radiation, air humidity and wind speed (Allen et al., 1998) and Prospero (Bottazzi et al., 2021), which is based on computing the ET using a multi-layer canopy model, solving the energy balance both for the sunlight and shadow vegetation, extending the recently developed Schymanski and Or method from a leaf to the canopy level. In LysGEO the coupling between infiltration and evapotranspiration is made possible by BrokerGEO component, which computes the water stress factor for vegetation by using Jarvis model (Jarvis, 1976) or the Ball-Berry one (Ball et al., 1987), taking information about the water content by WHETGEO-1D model. BrokerGEO uses root density from which it is computed how much water is removed from the column of soil, according to the root distribution. The code of LysGEO and BrokerGEO are open-source and available on GitHub GEOframe web page: https://github.com/GEOframeOMSProjects/OMS_Project_LysimeterGEO; <https://github.com/geoframecomponents/BrokerGEO>.

5.3.3 WHETGEO-2D

Currently WHETGEO-2D solves only the R^2 equation. As first development it is necessary to implement the coupling with the shallow water equation as presented in (Gugole, 2016; Gugole

et al., 2018) in order to correctly define the surface boundary condition for the Richards' equation, as deeply discussed in the Introduction. A possible application of WHETGEO-2D regards the analysis of slope cross-section stability. In such application, WHETGEO-2D is used to simulate the surface-subsurface flow, and specifically to compute the spatial distribution of the soil water pressure, and it is coupled with the hillslope-stability described in (Formetta et al., 2014a; Formetta et al., 2016c; Formetta et al., 2016d) model to compute the safety factor. The point of strength of WHETGEO-2D is represented by its robust numerics combined with the adoption of unstructured grids that allow to properly discretize complex geometries and soil stratigraphy. As pointed out by Tufano et al. (2021) thickness and stratigraphic settings are often overlooked in the slope stability analysis whereas they exert a strong control on both the spatial distribution of soil water pressure and the depth of failure surface. Although WHETGEO-2D permit to properly consider the soil setting, only with its extension in the tri-dimensional domain will be possible to taking into account of the effect of hillslope morphology on soil water pressure distribution (Formetta et al., 2016d).

A

OBJECT MODELLING SYSTEM V. 3

The Object Modeling System v.3 (OMS₃) is a component-based environmental modelling framework that provides a consistent and efficient way to: 1) create science simulation components; 2) develop, parameterise, and evaluate environmental models, and modify and adjust them as science advances; and 3) re-purpose environmental models for emerging customer requirements (David et al., 2013).

In OMS₃ the term component refers to self-contained, separate software units that implement independent functions in a context-independent manner (David et al., 2013). This means that developers and researchers can build their model as composition of stand-alone components, moving away from the monolithic approach. The entire GEOframe system is built upon the OMS₃ framework.

Compared to other Environmental Modelling Frameworks (EMF), OMS₃ is characterised by being a non-invasive and lightweight framework (Lloyd et al., 2011). That is to say, the model code is not tightly coupled with the underlying framework - OMS₃ -, i.e. the environmental modeller does not need a deep knowledge of the API, and the modelling components can still function and continue to evolve outside the framework (David et al., 2013). In fact, OMS₃ relies on specific annotations to provide meta data for Java code. These annotations describe elements such as classes, fields, and methods, and are used by the framework to interpret the component as a building block of the modelling solution (MS), hence controlling its connectivity and data flow (David et al., 2013). It is worth noting that, being meta data, these annotations do not

directly affect the execution of the source code outside the OMS3 - non-invasive and lightweight framework.

Besides the technical aspects, the adoption of a software framework has a positive effect on "non-functional" quality attributes, such as maintainability, portability, reusability and understandability (David et al., 2013). The component-based approach allows the developer to break down the problem into smaller parts, each one tackled by a specific component. Hence, the components are joined together to build the desired modelling solution (point B). This facilitates the construction of new MSs, thanks to the plug-in system of model components (David et al., 2013; Peckham et al., 2013; Serafin, 2019). Thanks to the modularity, the updating of a component with the most recent scientific advances is facilitated and has no side effects on the other components. The other advantage regards the long term development of the code. From past experiences, one of the main limits to model development and maintenance was related to the lack of a proper software architectural design (Bancheri, 2017; David et al., 2013; Formetta et al., 2014a; Rizzoli et al., 2006; Serafin, 2019). Moreover, it is interesting to note that the component-based approach encourages collective model development (Serafin, 2019) and also eases the attribution of authorship since any component is a stand-alone chunk of code and can be authored separately.

Besides, the adoption of an environmental modelling framework promotes the concept of reproducible research, easing third parties inspection and providing consistent and verifiable model results (Bancheri, 2017; Formetta et al., 2013; Serafin, 2019).

Another advantage of using OMS3 is represented by the opportunity to keep the code development transparent to the user.

B | GEOFRAME

WHETGEO-1D was implemented as a Java component within the GEOframe, an open-source, component-based hydrological modelling system. Within GEOframe, each part of the hydrological cycle is implemented in a self-contained building block, an OMS3 component (David et al., 2013). Components can be joined together to obtain multiple modelling solutions that can accomplish from simple to very complicated tasks. GEOframe has proved great flexibility and robustness in several applications (Abera et al., 2017a; Abera et al., 2017b; Bancheri et al., 2020). There are more than 50 components available that can be grouped into the following categories:

- Geomorphic and DEM analyses;
- Spatial extrapolation/interpolation of meteorological variables;
- Estimation of the radiation budget;
- Estimation of evapotranspiration;
- Estimation of runoff production with integral distributed models;
- Channel routing;
- Travel time analysis;
- Calibration algorithms.

Using the components for geomorphic and DEM analyses Rigon et al., 2006b, the basin can be discretised into Hydrological Response Units (HRUs), i.e., hydrologically similar parts, such as a catchment or a hillslope or one of its parts. The meteorological forcing data can be spatially interpolated using a geostatistical approach, such as the Kriging technique (Bancheri et al., 2018). Both shortwave and longwave radiation components are available for the estimation of the radiation budget (Formetta et al., 2013; Formetta et al., 2016a). Evapotranspiration can be estimated using three different formulations: the FAO Evapotranspiration model (Allen et al., 1998), the Priestley-Taylor model (Priestley and Taylor, 1972), and the Prospero model, (Bottazzi, 2020; Bottazzi et al., 2021). Snow melting and the snow water equivalent can also be simulated with three models, as described in (Formetta et al., 2014b). Runoff production is performed by using the Embedded Reservoir Model (ERM) or a combination of its reservoirs (Bancheri et al., 2020). The discharge generated at each hillslope is routed to the outlet using the Muskingum-Cunge method (Bancheri et al., 2020). Travel time analysis of a generic pollutant within the catchment can be done using the approach proposed in (Rigon et al., 2016a; Rigon et al., 2016b). Model parameters can be calibrated using two algorithms, and several objective functions: Let Us CALibrate (LUCA) (Hay et al., 2006) and Particle Swarm Optimization (PSO) (Kennedy and Eberhart, 1995). A graph-based structure, called NET₃ (Serafin, 2019), is employed for the management of process simulations. NET₃ is designed using a river network/graph structure analogy, where each HRU is a node of the graph, and the channel links are the connections between the nodes. In any NET₃ node, a different modelling solution can be implemented and nodes (HRUs or channels) can be connected or disconnected at run-time through scripting. GEOframe is open source and helps the reproducibility and replica-

bility of research (Bancheri, 2017). Developers and users can easily collaborate, share documentation, and archive examples and data within the GEOframe community.

C | ENTHALPY AND INTERNAL ENERGY

Following the work by Dall'Amico (2010), the internal energy in its canonical form, U_c , can be written as

$$U_c = U_c(S, V, M) \quad (70)$$

where S is the entropy, V is the volume, and M the mass of the constituents. These are the independent variables and are called extensive variables since they depend linearly on the mass of the substance. The first differential of Eq. (70) is

$$dU_c = \left(\frac{\partial U_c}{\partial S} \right) dS + \left(\frac{\partial U_c}{\partial V} \right) dV + \left(\frac{\partial U_c}{\partial M} \right) dM \quad (71)$$

According to Callen (1985) it is possible to define

$$\left(\frac{\partial U_c}{\partial S} \right) \equiv T, \text{ the temperature} \quad (72)$$

$$- \left(\frac{\partial U_c}{\partial V} \right) \equiv p, \text{ the pressure} \quad (73)$$

$$\left(\frac{\partial U_c}{\partial M} \right) \equiv \mu, \text{ the chemical potential} \quad (74)$$

With this notation, Eq. (71) becomes

$$dU_c = TdS - pdV + \mu dM \quad (75)$$

By making use of the Legendre transformation it is possible to define the enthalpy potential H_c as

$$H_c(S, p, M) = U_c(S, V, M) + pV(S, p, M) \quad (76)$$

The differential of the enthalpy is

$$dH_c = d[U_c + pV] = TdS - pdV + \mu dM + Vdp + pdV = TdS + \mu dM + Vdp \quad (77)$$

If we assume that the transformation occurs at constant pressure and volume then Eq. (75) becomes

$$dU_c = TdS + \mu dM \quad (78)$$

and Eq. (77)

$$dH_c = TdS + \mu dM \quad (79)$$

Hence, from Eq. (78) and Eq. (79) the differential of the internal energy and the differential of enthalpy are equal. Therefore the governing equation, Eq. (52), can be equivalently written in term of either the specific enthalpy or the specific internal energy.

D | NEUMANN ANALYTICAL SOLUTION

In this section we report the derivation of the Neumann analytical. The enthalpy is defined as

$$h(T) = \begin{cases} \rho_w c_w (T - T_{ref}) + \rho_w l_f & \text{if } T \geq T_m \\ \rho_i c_i (T - T_{ref}) & \text{if } T < T_m - \epsilon \\ \rho_i c_i (T - \epsilon - T_{ref}) + h'(T - (T_m - \epsilon)) & \text{otherwise} \end{cases} \quad (80)$$

where the singularity of the enthalpy function at $T = T_m$ has been linearized with

$$h' = \frac{\rho_w c_w (T_m - T_{ref}) + \rho_w l_f - \rho_i c_i (T_m - \epsilon - T_{ref})}{\epsilon} \quad (81)$$

and ϵ is a parameter defining the temperature range over which the phase change of water occurs, Fig. (D.1). In the following tests ϵ is set to be equal to 0.0001 °C. The introduction of this linearization is necessary since the enthalpy function needs to be continuously differentiable according to assumption A1 in Section 2.3.1. It is worth to underline that the temperature range ϵ can be chosen sufficiently small in order to make this approximation negligible when compared to the physical behaviour of water, considering that: (a) The melting of water in temperate ice is known to actually occur progressively below 0 °C along grain boundaries (Langham, 1974; Nye and Frank, 1973). (b) Freezing often occurs below the melting point when nucleation is relevant. (c) In porous media such as soil, ice melts across a range of temperatures due to the Gibbs-Thompson effect in pores and surface affects at the

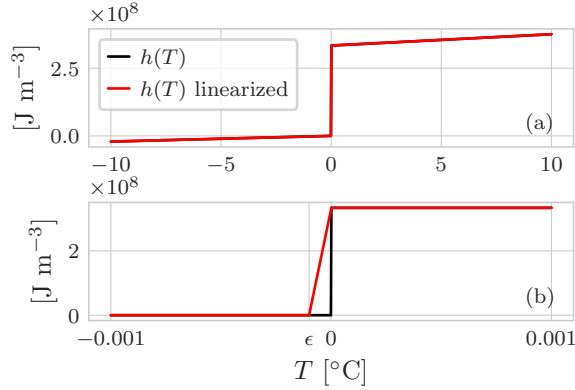


Figure D.1: (a) Comparison between the enthalpy function of pure water and the enthalpy function used in the numerical model. (b) Note that the energy jump due to the latent heat at $T_m = 0$ $^{\circ}\text{C}$ has been linearized and the steepness is controlled by the parameter ϵ .

interfaces between ice and particles (Rempel et al., 2004; Watanabe and Mizoguchi, 2002).

Even though the internal energy function is very steep, the code used does not suffer of convergence problem with a time step of 3600 s. The thermal conductivity is defined as:

$$\lambda(T) = \begin{cases} \lambda_w & \text{if } T \geq T_m \\ \lambda_i & \text{if } T < T_m \end{cases} \quad (82)$$

Defining the following constant:

$$\alpha_w = \frac{\lambda_w}{\rho_w c_w} \quad \alpha_i = \frac{\lambda_i}{\rho_i c_i} \quad (83)$$

$$A = \frac{T_m - T_s}{\text{erf}(\gamma)} \quad B = \frac{T_m - T_0}{\text{erf}\left(\gamma \sqrt{\frac{\alpha_i}{\alpha_w}}\right)} \quad (84)$$

the moving boundary function is

$$\zeta(t) = 2\gamma\sqrt{\alpha_i t} \quad \text{for } t > 0 \quad (85)$$

where the coefficient γ can be found solving the following equation

$$\gamma\sqrt{\alpha_i} l_f \rho - \frac{\lambda_i}{\sqrt{\pi\alpha_i}} A e^{-\gamma^2} - \frac{\alpha_w}{\sqrt{\pi\alpha_w}} B e^{\gamma^2 \frac{\alpha_i}{\alpha_w}} = 0 \quad (86)$$

Finally the analytical solution for problem with Dirichlet boundary condition for the thawed and frozen zones are:

$$\begin{cases} T(z, t) = T_s + \frac{T_m - T_s}{\text{erf}(\gamma)} \text{erf}\left(\frac{z}{2\sqrt{\alpha_i t}}\right) & 0 < z < \zeta(t) \\ T(z, t) = T_0 + \frac{T_m - T_0}{\text{erfc}\left(\gamma\sqrt{\frac{\alpha_i}{\alpha_w}}\right)} \text{erfc}\left(\frac{z}{2\sqrt{\alpha_w t}}\right) & z > \zeta(t) \end{cases} \quad (87)$$

Table D.1: Input parameters for the comparison between Neumann analytical solution and the numerical solution with the NCZ algorithm.

Symbol	Parameter	Value	Unit
Δt	time step	60, 300, 3600	s
Δz	control volume size	0.001, 0.005, 0.01	m
l_f	latent heat of fusion	333700	J kg ⁻¹
c_w	specific heat capacity of water	4187	J m ⁻³ °C ⁻¹
c_i	specific heat capacity of ice	2108	J m ⁻³ °C ⁻¹
ρ_w	water density	1000	kg m ⁻³
ρ_i	ice density	970	kg m ⁻³
λ_w	thermal conductivity of water	0.6	W m ⁻¹ °C ⁻¹
λ_i	thermal conductivity of ice	2.09	W m ⁻¹ °C ⁻¹
ϵ	melting temperature range	0.0001	°C
T_0	initial temperature	+5	°C
T_s	surface temperature	-5	°C

E

LUNARDINI ANALYTICAL SOLUTION

equations and table of parameters The solution fo the Lunardini problem (i.e. the Lunardini solution) as described by McKenzie (McKenzie et al., 2007) is given by the following set of equations:

$$T_1 = (T_m - T_s) \frac{\operatorname{erf}\left(\frac{x}{2\sqrt{\alpha_1 t}}\right)}{\operatorname{erf}(\psi)} + T_s \quad (88)$$

$$T_2 = (T_m - T_f) \frac{\operatorname{erf}\left(\frac{x}{2\sqrt{\alpha_4 t}}\right) - \operatorname{erf}(\gamma)}{\operatorname{erf}(\gamma) - \operatorname{erf}\left(\psi \sqrt{\frac{\alpha_1}{\alpha_4}}\right)} + T_f \quad (89)$$

$$T_3 = (T_0 - T_f) \frac{-\operatorname{erfc}\left(\frac{x}{2\sqrt{\alpha_3 t}}\right)}{\operatorname{erfc}\left(\psi \sqrt{\frac{\alpha_4}{\alpha_3}}\right)} + T_0 \quad (90)$$

where T_1 , T_2 , and T_3 are the temperatures at distance, x , from the temperature boundary for the frozen, partially frozen, and unfrozen zone respectively; erf and $erfc$ are the error function, and the complementary error function respectively; T_0 , T_m , T_f , and T_s are the temperatures of the initial condition; the solidus, the liquidus, and the boundary temperature, respectively; α_1 and α_3 are the thermal diffusivities for the frozen, and unfrozen zone respectively, defined as λ_1/C_1 and λ_3/C_3 where C_1 and C_3 are the volumetric bulk-heat capacities of the frozen and unfrozen zones.

The thermal diffusivity of the partially frozen zone is assumed to be constant across the transition region, and the thermal diffusivity with latent heat term included, α_4 , is defined as:

$$\alpha_4 = \frac{\lambda_2}{C_2 + \frac{\gamma_d l_f \Delta \xi}{(T_f - T_m)}} \quad (91)$$

where γ_d is the dry unit of soil solids, and $\Delta \xi = \xi_0 - \xi_f$ where ξ_0 and ξ_f are the ratio of unfrozen water to soil solids for the fully thawed and frozen conditions respectively. For a time, t , in the region $0 \leq x \leq X_1(t)$ the temperature is T_1 and $X_1(t)$ is given by

$$X_1(t) = 2\psi\sqrt{\alpha_1 t} \quad (92)$$

and from $X_1(t) \leq x \leq X(t)$ the temperature is T_2 , where $X(t)$ is given by

$$X(t) = 2\gamma\sqrt{\alpha_4 t} \quad (93)$$

and for $x \geq X(t)$ the temperature is T_3 . The unknowns, ψ and γ , are solving the set of these two equations:

$$\frac{T_m - T_s}{T_m - T_f} \exp^{-\psi^2(1-\alpha_1/\alpha_4)} = \frac{\frac{\lambda_2}{\lambda_1} \sqrt{\frac{\alpha_1}{\alpha_4}} \operatorname{erf}(\psi)}{\operatorname{erf}(\gamma) - \operatorname{erf}\left(\psi \sqrt{\frac{\alpha_1}{\alpha_4}}\right)} \quad (94)$$

$$\frac{(T_m - T_f) \frac{\lambda_2}{\lambda_3} \frac{\alpha_3}{\alpha_4} \exp^{-\gamma^2(1-\alpha_4/\alpha_3)}}{T_m - T_f} = \frac{\operatorname{erf}(\gamma) - \operatorname{erf}\left(\sqrt{\frac{\alpha_1}{\alpha_4}} \psi\right)}{\operatorname{erf}\left(\gamma \sqrt{\frac{\alpha_4}{\alpha_3}}\right)} \quad (95)$$

Table E.1: Input parameters for the comparison between Lunardini analytical solution and the numerical solution with the NCZ algorithm.

Symbol	Parameter	Value	Unit
Δt	time step	300, 900, 3600	s
Δx	control volume size	0.01	m
L_f	latent heat of fusion	334560	J kg ⁻¹
C_1	volumetric heat capacity, forzen	690030	J m ⁻³ °C ⁻¹
C_2	volumetric heat capacity, partially forzen	690030	J m ⁻³ °C ⁻¹
C_3	volumetric heat capacity, unfrozen	690030	J m ⁻³ °C ⁻¹
γ_d	dry unit density of soil solids	1680	kg m ⁻³
ξ_0	ratio of liq. water to soil solids, unfrozen	0.2	-
ξ_f	ratio of liq. water to soil solids, frozen	0.0782	-
λ_1	thermal conductivity, frozen	3.462696	W m ⁻¹ °C ⁻¹
λ_2	thermal conductivity, partially frozen	2.939946	W m ⁻¹ °C ⁻¹
λ_3	thermal conductivity, unfrozen	2.417196	W m ⁻¹ °C ⁻¹
γ	solution parameter for Eq. (94) and Eq. (95)	5.616, 2.060, 1.397 ^a	-
ψ	solution parameter for Eq. (94) and Eq. (95)	0.158, 0.137, 0.061 ^a	-
T_0	initial temperature	+4	°C
T_s	boundary temperature	-6	°C
T_f	liquidus temperature	0	°C
T_f	solidus temperature	-0.1, -1, -4	°C

^a The first value refers to $T_m = -0.1$ °C the second value to $T_m = -1$ °C, and the third value to $T_m = -4$ °C.

BIBLIOGRAPHY

- Abera, W., Formetta, G., Borga, M., & Rigon, R. (2017a). Estimating the water budget components and their variability in a pre-alpine basin with JGrass-NewAge. *Advances in Water Resources*, 104, 37–54.
- Abera, W., Formetta, G., Brocca, L., & Rigon, R. (2017b). Modeling the water budget of the Upper Blue Nile basin using the JGrass-NewAge model system and satellite data. *Hydrology and Earth System Sciences*, 21(6), 3145–3165.
- Allen, R. G., Pereira, L. S., Raes, D., Smith, M., et al. (1998). Crop evapotranspiration-Guidelines for computing crop water requirements-FAO Irrigation and drainage paper 56. *Fao, Rome*, 300(9), D05109.
- Anderson, D. M., & Tice, A. R. (1972). Predicting unfrozen water contents in frozen soils from surface area measurements. *Highway research record*, 393, 12–18.
- Arp, C. D., Jones, B. M., Grosse, G., Bondurant, A. C., Romanovsky, V. E., Hinkel, K. M., & Parsekian, A. D. (2016). Threshold sensitivity of shallow Arctic lakes and sublake permafrost to changing winter climate. *Geophysical Research Letters*, 43(12), 6358–6365.
- Aschwanden, A., & Blatter, H. (2009). Mathematical modeling and numerical simulation of polythermal glaciers. *Journal of Geophysical Research: Earth Surface*, 114(F1).
- Aschwanden, A., & Blatter, H. (2005). Meltwater production due to strain heating in Storglaciären, Sweden. *Journal of Geophysical Research: Earth Surface*, 110(F4).

- Aschwanden, A., Bueller, E., Khroulev, C., & Blatter, H. (2012). An enthalpy formulation for glaciers and ice sheets. *Journal of Glaciology*, 58(209), 441–457.
- Ashby, S. F., & Falgout, R. D. (1996). A parallel multigrid preconditioned conjugate gradient algorithm for groundwater flow simulations. *Nuclear science and engineering*, 124(1), 145–159.
- Bachmann, J., Horton, R., Grant, S. A., & Van der Ploeg, R. (2002). Temperature dependence of water retention curves for wettable and water-repellent soils. *Soil Science Society of America Journal*, 66(1), 44.
- Bader, G., & Berti, G. (1998). Design principles of reusable software components for the numerical solution of PDE problems. *Concepts of Numerical Software*. Vieweg Verlag, To appear. *Proceedings of the 14th GAMM Seminar, Kiel*.
- Ball, J. T., Woodrow, I. E., & Berry, J. A. (1987). A model predicting stomatal conductance and its contribution to the control of photosynthesis under different environmental conditions. *Progress in photosynthesis research* (pp. 221–224). Springer.
- Bancheri, M. (2017). *A flexible approach to the estimation of water budgets and its connection to the travel time theory* (Doctoral dissertation). University of Trento.
- Bancheri, M., Rigon, R., & Manfreda, S. (2020). The GEOframe-NewAge modelling system applied in a data scarce environment. *Water*, 12(1), 86.
- Bancheri, M., Serafin, F., Bottazzi, M., Abera, W., Formetta, G., & Rigon, R. (2018). The design, deployment, and testing of kriging models in GEOframe with SIK-0.9. 8. *Geoscientific Model Development*, 11(6), 2189–2207.
- Bao, H., Koike, T., Yang, K., Wang, L., Shrestha, M., & Lawford, P. (2016). Development of an enthalpy-based frozen soil model and its validation in a cold region in China. *Journal of Geophysical Research: Atmospheres*, 121(10), 5259–5280.

- Bartelt, P., & Lehning, M. (2002). A physical SNOWPACK model for the swiss avalanche warning: Part i: Numerical model. *Cold Regions Science and Technology*, 35(3), 123–145.
- Benard, P., Zarebanadkouki, M., & Carminati, A. (2019). Physics and hydraulics of the rhizosphere network. *Journal of Plant Nutrition and Soil Science*, 182(1), 5–8.
- Berti, G. (2000). *Generic software components for scientific computing*. Citeseer.
- Bisht, G., & Riley, W. J. (2019). Development and verification of a numerical library for solving global terrestrial multiphysics problems. *Journal of Advances in Modeling Earth Systems*, 11(6), 1516–1542.
- Bloch, J. (2001). *Effective Java: Programming Language Guide*. Addison-Wesley Professional.
- Bonan, G. (2019). *Climate change and terrestrial ecosystem modeling*. Cambridge University Press.
- Boone, A., & Etchevers, P. (2001). An intercomparison of three snow schemes of varying complexity coupled to the same land surface model: Local-scale evaluation at an Alpine site. *Journal of Hydrometeorology*, 2(4), 374–394.
- Borinato, E. (2021). *Advances in permafrost modelling: Application of the nested Newton algorithm for solving the heat equation*. (Master's thesis). University of Trento.
- Bottazzi, M. (2020). *Transpiration theory and the Prospero component of GEOframe* (Doctoral dissertation). University of Trento.
- Bottazzi, M., Bancheri, M., Mobilia, M., Bertoldi, G., Longobardi, A., & Rigon, R. (2021). Comparing evapotranspiration estimates from the GEOframe-Prospero model and three empirical models under different climate conditions. *Water*, 19(9), 1221.

- Bouyoucos, G. (1920). Degree of temperature to which soils can be cooled without freezing. *Monthly Weather Review*, 48(12), 718–718.
- Bouyoucos, G. J. (1923). Movement of soil moisture from small capillaries to the large capillaries of the soil upon freezing. *Journal of Agricultural Research*, 24(5), 427–432.
- Bouyoucos, G. J. (1913). An investigation of soil temperature and some of the most important factors influencing it. *Technical Bulletin of Michigan Agriculture Experimental Station*, 17, 1–196.
- Bouyoucos, G., & McCool, M. (1915). The freezing point method as a new means of measuring the concentration of the soil solution directly in the soil. • mich. *Michigan State University. Agricultural Experiment Station*, 24.
- Braun, M. L. (2015). <http://jblas.org/>
- Brooks, R., & Corey, T. (1964). Hydraulic properties of porous media. *Hydrology Papers, Colorado State University*, 24, 37.
- Brugnano, L., & Casulli, V. (2008). Iterative solution of piecewise linear systems. *SIAM Journal on Scientific Computing*, 30(1), 463–472.
- Brugnano, L., & Casulli, V. (2009). Iterative solution of piecewise linear systems and applications to flows in porous media. *SIAM Journal on Scientific Computing*, 31(3), 1858–1873.
- Brun, E., David, P., Sudul, M., & Brunot, G. (1992). A numerical model to simulate snow-cover stratigraphy for operational avalanche forecasting. *Journal of Glaciology*, 38(128), 13–22.
- Brun, E., Martin, E., Simon, V., Gendre, C., & Coleou, C. (1989). An energy and mass model of snow cover suitable for operational avalanche forecasting. *Journal of Glaciology*, 35(121), 333–342.

- Caldwell, M. M., Dawson, T. E., & Richards, J. H. (1998). Hydraulic lift: Consequences of water efflux from the roots of plants. *Oecologia*, 113(2), 151–161.
- Callen, H. B. (1985). *Thermodynamics and an introduction to thermostatistics*. John Wiley; Sons, Inc.
- Campbell, G. S., Jungbauer Jr, J., Bristow, K. L., & Hungerford, R. D. (1995). Soil temperature and water content beneath a surface fire. *Soil Science*, 159(6), 363–374.
- Carey, S. K., & Woo, M.-k. (2005). Freezing of subarctic hillslopes, Wolf Creek Basin, Yukon, Canada. *Arctic, Antarctic, and Alpine Research*, 37(1), 1–10.
- Casulli, V. (2017a). Lectures notes on advanced numerical methods for free-surface hydrodynamics.
- Casulli, V. (2009). A high-resolution wetting and drying algorithm for free-surface hydrodynamics. *International Journal for Numerical Methods in Fluids*, 60(4), 391–408.
- Casulli, V. (2017b). A coupled surface-subsurface model for hydrostatic flows under saturated and variably saturated conditions. *International Journal for Numerical Methods in Fluids*, 85(8), 449–464.
- Casulli, V., & Walters, R. A. (2000). An unstructured grid, three-dimensional model based on the shallow water equations. *International Journal for Numerical Methods in Fluids*, 32(3), 331–348.
- Casulli, V., & Zanolli, P. (2005). High resolution methods for multidimensional advection–diffusion problems in free-surface hydrodynamics. *Ocean Modelling*, 10(1-2), 137–151.
- Casulli, V., & Zanolli, P. (2010). A nested Newton-type algorithm for finite volume methods solving Richards' equation in mixed form. *SIAM Journal on Scientific Computing*, 32(4), 2255–2273.

- Casulli, V., & Zanolli, P. (2012). Iterative solutions of mildly non-linear systems. *Journal of Computational and Applied Mathematics*, 236(16), 3937–3947.
- Celia, M. A., Bouloutas, E. T., & Zarba, R. L. (1990). A general mass-conservative numerical solution for the unsaturated flow equation. *Water Resources Research*, 26(7), 1483–1496.
- Cheng, G., & Jin, H. (2013). Permafrost and groundwater on the Qinghai-Tibet Plateau and in northeast China. *Hydrogeology Journal*, 21(1), 5–23.
- Chistyakov, V. (1997). On mappings of bounded variation. *Journal of Dynamical and Control Systems*, 3(2), 261.
- Clark, M. P., Fan, Y., Lawrence, D. M., Adam, J. C., Bolster, D., Gochis, D. J., Hooper, R. P., Kumar, M., Leung, L. R., Mackay, D. S., et al. (2015a). Improving the representation of hydrologic processes in Earth System Models. *Water Resources Research*, 51(8), 5929–5956.
- Clark, M. P., Nijssen, B., Lundquist, J. D., Kavetski, D., Rupp, D. E., Woods, R. A., Freer, J. E., Gutmann, E. D., Wood, A. W., Brekke, L. D., et al. (2015b). A unified approach for process-based hydrologic modeling: 1. modeling concept. *Water Resources Research*, 51(4), 2498–2514.
- Clark, M. P., Zolfaghari, R., Green, K. R., Trim, S., Knoben, W. J. M., Bennet, A., & Nijssen, B. (2021). The numerical implementation of land models: Problem formulation and laugh tests. *Journal of Hydrometeorology*, 22(6), 2498–2514.
- Clow, G. D. (2018). CVPM 1.1: A flexible heat-transfer modeling system for permafrost. *Geoscientific Model Development*, 11(12), 4889–4908.
- Constantz, J. (1982). Temperature dependence of unsaturated hydraulic conductivity of two soils. *Soil Science Society of America Journal*, 46(3), 466–470.

- Constantz, J., & Murphy, F. (1991). The temperature dependence of ponded infiltration under isothermal conditions. *Journal of Hydrology*, 122(1-4), 119–128.
- Couture, N. J., & Pollard, W. H. (2017). A model for quantifying ground-ice volume, Yukon Coast, Western Arctic Canada. *Permafrost and Periglacial Processes*, 28(3), 534–542.
- Couture, R., Smith, S., Robinson, S., Burgess, M., & Solomon, S. (2003). On the hazards to infrastructure in the Canadian north associated with thawing of permafrost. *Proceedings of Geohazards*.
- Da Rocha, H. R., Goulden, M. L., Miller, S. D., Menton, M. C., Pinto, L. D., de Freitas, H. C., & e Silva Figueira, A. M. (2004). Seasonality of water and heat fluxes over a tropical forest in eastern Amazonia. *Ecological applications*, 14(sp4), 22–32.
- Dai, Y., Wei, N., Yuan, H., Zhang, S., Shangguan, W., Liu, S., Lu, X., & Xin, Y. (2019). Evaluation of soil thermal conductivity schemes for use in land surface modeling. *Journal of Advances in Modeling Earth Systems*, 11(11), 3454–3473.
- Dai, Y., Zeng, X., Dickinson, R. E., Baker, I., Bonan, G. B., Bosilovich, M. G., Denning, A. S., Dirmeyer, P. A., Houser, P. R., Niu, G., et al. (2003). The common land model. *Bulletin of the American Meteorological Society*, 84(8), 1013–1024.
- Dall'Amico, M., Endrizzi, S., Gruber, S., & Rigon, R. (2011). A robust and energy-conserving model of freezing variably-saturated soil. *The Cryosphere*, 5(2), 469–484.
- Dall'Amico, M. (2010). *Coupled water and heat transfer in permafrost modeling* (Doctoral dissertation). University of Trento.
- D'Amato, C. (n.d.).
- D'Amato, C., Tubini, N., & Rigon, R. (2022). Lysimeter geo a 1d land surface model for the virtual investigation of the interaction of critical zone, vegetation and atmosphere. *in*

- preparation for Geophysical Research Geoscientific Model Development Letters.*
- D'Amboise, C. J., Müller, K., Oxarango, L., Morin, S., & Schuler, T. (2017). Implementation of a physically based water percolation routine in the crocus/surfex (v7. 3) snowpack model. *Geophysical Research Geoscientific Model Development Letters*, 10(9), 3547–3566.
- David, O. (n.d.).
- David, O., Ascough II, J. C., Lloyd, W., Green, T. R., Rojas, K., Leavesley, G. H., & Ahuja, L. R. (2013). A software engineering perspective on environmental modeling framework design: The Object Modeling System. *Environmental Modelling & Software*, 39, 201–213.
- David Olaf. (n.d.). <https://alm.engr.colostate.edu/cb/wiki/17118>
- Davis, T. A. (2006). *Direct methods for sparse linear systems*. Society for Industrial; Applied Mathematics.
- De Lorenzo, S., Di Renzo, V., Civetta, L., D'antonio, M., & Gasparini, P. (2006). Thermal model of the Vesuvius magma chamber. *Geophysical Research Letters*, 33(17).
- Di Nucci, C. (2014). Theoretical derivation of the conservation equations for single phase flow in porous media: A continuum approach. *Meccanica*, 49(12), 2829–2838.
- Dong, Y., McCartney, J. S., & Lu, N. (2015). Critical review of thermal conductivity models for unsaturated soils. *Geotechnical and Geological Engineering*, 33(2), 207–221.
- Dunne, T., & Black, R. D. (1970). An experimental investigation of runoff production in permeable soils. *Water Resources Research*, 6(2), 478–490.
- Eckel, B. (2003). *Thinking in JAVA*. Prentice Hall Professional.
- Eisenberg, D., Kauzmann, W., & Kauzmann, W. (2005). *The structure and properties of water*. Oxford University Press on Demand.

- Ekici, A., Beer, C., Hagemann, S., Boike, J., Langer, M., & Hauck, C. (2014). Simulating high-latitude permafrost regions by the JSBACH terrestrial ecosystem model. *Geophysical Research Geoscientific Model Development Letters*, 7(2), 631–647.
- Ekici, S. A., Lee, H., Lawrence, D. M., Swenson, S. C., & Prigent, C. (2019). Ground subsidence effects on simulating dynamic high-latitude surface inundation under permafrost thaw using CLM5. *Geophysical Research Geoscientific Model Development Letters (GMD)*, 12(12), 5291–5300.
- Endrizzi, S., Gruber, S., Dall'Amico, M., & Rigon, R. (2014). Geotop 2.0: Simulating the combined energy and water balance at and below the land surface accounting for soil freezing, snow cover and terrain effects. *Geophysical Research Geoscientific Model Development Letters*, 7(6), 2831–2857.
- Engeler, I., Franssen, H. H., Müller, R., & Stauffer, F. (2011). The importance of coupled modelling of variably saturated ground-water flow-heat transport for assessing river-aquifer interactions. *Journal of Hydrology*, 397(3-4), 295–305.
- Farthing, M. W., & Ogden, F. L. (2017). Numerical solution of Richards' equation: A review of advances and challenges. *Soil Science Society of America Journal*, 81(6), 1257–1269.
- Feddes, R. A., Hoff, H., Bruen, M., Dawson, T., De Rosnay, P., Dirmeyer, P., Jackson, R. B., Kabat, P., Kleidon, A., Lilly, A., et al. (2001). Modeling root water uptake in hydrological and climate models. *Bulletin of the American Meteorological Society*, 82(12), 2797–2810.
- Foley, J. A., Prentice, I. C., Ramankutty, N., Levis, S., Pollard, D., Sitch, S., & Haxeltine, A. (1996). An integrated biosphere model of land surface processes, terrestrial carbon balance, and vegetation dynamics. *Global Biogeochemical Cycles*, 10(4), 603–628.

- Formetta, G., Rigon, R., Chávez, J., & David, O. (2013). Modeling shortwave solar radiation using the jgrass-newage system. *Geophysical Research Geoscientific Model Development Letters*, 6(4), 915–928.
- Formetta, G. (2013). *Hydrological modelling with components: The OMS₃ NewAge-JGrass system* (Doctoral dissertation). University of Trento.
- Formetta, G., Antonello, A., Franceschi, S., David, O., & Rigon, R. (2014a). Hydrological modelling with components: A GIS-based open-source framework. *Environmental Modelling & Software*, 55, 190–200.
- Formetta, G., Bancheri, M., David, O., & Rigon, R. (2016a). Performance of site-specific parameterizations of longwave radiation. *Hydrology and Earth System Sciences*, 20(11), 4641–4654.
- Formetta, G., Capparelli, G., David, O., Green, T. R., & Rigon, R. (2016b). Integration of a three-dimensional process-based hydrological model into the object modeling system. *Water*, 8(1), 12.
- Formetta, G., Capparelli, G., & Versace, P. (2016c). Evaluating performance of simplified physically based models for shallow landslide susceptibility. *Hydrology and Earth System Sciences*, 20(11), 4585–4603.
- Formetta, G., Kampf, S. K., David, O., & Rigon, R. (2014b). Snow water equivalent modeling components in NewAge-JGrass. *Geophysical Research Geoscientific Model Development Letters*, 7(3), 725–736.
- Formetta, G., Simoni, S., Godt, J. W., Lu, N., & Rigon, R. (2016d). Geomorphological control on variably saturated hillslope hydrology and slope instability. *Water Resources Research*, 52(6), 4590–4607.
- Forsyth, P. A., Wu, Y., & Pruess, K. (1995). Robust numerical methods for saturated-unsaturated flow with dry initial condi-

- tions in heterogeneous media. *Advances in Water Resources*, 18(1), 25–38.
- Forums, P. P. D. (n.d.). <https://www.pc-progress.com/forum/vi-ewtopic.php?f=3&t=3632>
- Frampton, A., Painter, S. L., & Destouni, G. (2013). Permafrost degradation and subsurface-flow changes caused by surface warming trends. *Hydrogeology Journal*, 21(1), 271–280.
- Freeman, E., Robson, E., Bates, B., & Sierra, K. (2008). *Head first design patterns*. O'Reilly Media, Inc."
- Freeze, R. A., & Harlan, R. (1969). Blueprint for a physically-based, digitally-simulated hydrologic response model. *Journal of Hydrology*, 9(3), 237–258.
- Furman, A. (2008). Modeling coupled surface–subsurface flow processes: A review. *Vadose Zone Journal*, 7(2), 741–756.
- Gamma, E., Helm, R., Johnson, R., Vlissides, J., & Patterns, D. (1995). Elements of reusable object-oriented software. *Design Patterns*. massachusetts: Addison-Wesley Publishing Company.
- Germann, P., & Beven, K. (1981). Water flow in soil macropores I. an experimental approach. *Journal of Soil Science*, 32(1), 1–13.
- Golub, G. H., & Van Loan, C. F. (2013). *Matrix computations* (Vol. 3). Johns Hopkins University Press.
- Goodrich, L. (1978). Some results of a numerical study of ground thermal regimes. *Proceedings of the Third International Conference on Permafrost*.
- Goodrich, L. (1982). The influence of snow cover on the ground thermal regime. *Canadian Geotechnical Journal*, 19(4), 421–432.
- Greenspan, D., & Casulli, V. (1988). *Numerical analysis for applied mathematics, science, and engineering*. Addison Wesley.

- Greve, R. (1997a). Application of a polythermal three-dimensional ice sheet model to the greenland ice sheet: Response to steady-state and transient climate scenarios. *Journal of Climate*, 10(5), 901–918.
- Greve, R. (1997b). A continuum–mechanical formulation for shallow polythermal ice sheets. *Philosophical Transactions of the Royal Society of London. Series A: Mathematical, Physical and Engineering Sciences*, 355(1726), 921–974.
- Greve, R., & Blatter, H. (2016). Comparison of thermodynamics solvers in the polythermal ice sheet model SICOPOLIS. *Polar Science*, 10(1), 11–23.
- Gubler, S., Endrizzi, S., Gruber, S., & Purves, R. S. (2013). Sensitivities and uncertainties of modeled ground temperatures in mountain environments. *Geophysical Research Geoscientific Model Development Letters*, 6(4), 1319–1336.
- Gugole, F. (2016). *A fast semi-implicit 3D algorithm for the solution of coupled free-surface and variably saturated sub-surface flows*. (Master's thesis). University of Trento.
- Gugole, F., Dumbser, M., & Stelling, G. (2018). An efficient three-dimensional semi-implicit finite volume scheme for the solution of coupled free-surface and variably saturated sub-surface flow. *EGU General Assembly Conference Abstracts*, 600.
- Hansson, K., Šimůnek, J., Mizoguchi, M., Lundin, L.-C., & Van Genuchten, M. T. (2004). Water flow and heat transport in frozen soil. *Vadose Zone Journal*, 3(2), 693–704.
- Harris, C., Arenson, L. U., Christiansen, H. H., Eitzelmüller, B., Frauenfelder, R., Gruber, S., Haeberli, W., Hauck, C., Hoelzle, M., Humlum, O., et al. (2009). Permafrost and climate in Europe: Monitoring and modelling thermal, geomorphological and geotechnical responses. *Earth-Science Reviews*, 92(3-4), 117–171.

- Hay, L. E., Leavesley, G. H., Clark, M. P., Markstrom, S. L., Viger, R. J., & Umemoto, M. (2006). Step wise, multiple objective calibration of a hydrologic model for a snowmelt dominated basin 1. *Journal of the American Water Resources Association*, 42(4), 877–890.
- Heimsund, B.-O. (2011). <https://github.com/fommil/matrix-toolkits-java>
- Hewitt, I., & Schoof, C. (2016). A model for polythermal ice incorporating gravity-driven moisture transport. *Journal of Fluid Mechanics*, 797(June).
- Hinkel, K., & Nelson, F. (2003). Spatial and temporal patterns of active layer thickness at Circumpolar Active Layer Monitoring (CALM) sites in northern Alaska, 1995–2000. *Journal of Geophysical Research: Atmospheres*, 108(D2).
- Hinzman, L. D., Bettez, N. D., Bolton, W. R., Chapin, F. S., Dyurgerov, M. B., Fastie, C. L., Griffith, B., Hollister, R. D., Hope, A., Huntington, H. P., et al. (2005). Evidence and implications of recent climate change in northern Alaska and other arctic regions. *Climatic change*, 72(3), 251–298.
- Hollesen, J., Elberling, B., & Jansson, P.-E. (2011). Future active layer dynamics and carbon dioxide production from thawing permafrost layers in northeast Greenland. *Global Change Biology*, 17(2), 911–926.
- Horton, R. E. (1933). The role of infiltration in the hydrologic cycle. *Transactions American Geophysical Union*, 14(1), 446–460.
- Howard, A. R., Van Iersel, M. W., Richards, J. H., & Donovan, L. A. (2009). Night-time transpiration can decrease hydraulic redistribution. *Plant, Cell & Environment*, 32(8), 1060–1070.
- Hrachowitz, M., Benettin, P., Van Breukelen, B. M., Fovet, O., Howden, N. J., Ruiz, L., Van Der Velde, Y., & Wade, A. J. (2016). Transit times—the link between hydrology and water qual-

- ity at the catchment scale. *Wiley Interdisciplinary Reviews: Water*, 3(5), 629–657.
- Hu, H., & Argyropoulos, S. A. (1996). Mathematical modelling of solidification and melting: A review. *Modelling and Simulation in Materials Science and Engineering*, 4(4), 371.
- InterFrost Project. (n.d.). https://wiki.lsce.ipsl.fr/interfrost/doku.php?id=test_cases:one
- Jansson, P., & Karlberg, L. (2011). Coupled heat and mass transfer model for soil-plant-atmosphere systems.
- Jarvis, P. (1976). The interpretation of the variations in leaf water potential and stomatal conductance found in canopies in the field. *Philosophical Transactions of the Royal Society of London. Biological Sciences*, 273(927), 593–610.
- Johansen, O. (1977). *Thermal conductivity of soils* (tech. rep.). Cold Regions Research and E.
- Jones, J. E., & Woodward, C. S. (2001). Newton–Krylov-multigrid solvers for large-scale, highly heterogeneous, variably saturated flow problems. *Advances in Water Resources*, 24(7), 763–774.
- Kane, D. L., Yoshikawa, K., & McNamara, J. P. (2013). Regional groundwater flow in an area mapped as continuous permafrost, NE Alaska (USA). *Hydrogeology Journal*, 21(1), 41–52.
- Kelley, C. T. (2003). *Solving nonlinear equations with Newton's method*. Society for Industrial; Applied Mathematics.
- Kennedy, J., & Eberhart, R. (1995). Particle swarm optimization. *Proceedings of ICNN'95-international conference on neural networks*, 4, 1942–1948.
- Kirkland, M. R., Hills, R., & Wierenga, P. (1992). Algorithms for solving Richards' equation for variably saturated soils. *Water Resources Research*, 28(8), 2049–2058.

- Kokelj, S. V., & Jorgenson, M. (2013). Advances in thermokarst research. *Permafrost and Periglacial Processes*, 24(2), 108–119.
- Kollet, S. J., & Maxwell, R. M. (2006). Integrated surface–groundwater flow modeling: A free-surface overland flow boundary condition in a parallel groundwater flow model. *Advances in Water Resources*, 29(7), 945–958.
- Kosugi, K. (1999). General model for unsaturated hydraulic conductivity for soils with lognormal pore-size distribution. *Soil Science Society of America Journal*, 63(2), 270–277.
- Krinner, G., Viovy, N., de Noblet-Ducoudré, N., Ogée, J., Polcher, J., Friedlingstein, P., Ciais, P., Sitch, S., & Prentice, I. C. (2005). A dynamic global vegetation model for studies of the coupled atmosphere-biosphere system. *Global Biogeochemical Cycles*, 19(1).
- Kurylyk, B. L., Hayashi, M., Quinton, W. L., McKenzie, J. M., & Voss, C. I. (2016). Influence of vertical and lateral heat transfer on permafrost thaw, peatland landscape transition, and groundwater flow. *Water Resources Research*, 52(2), 1286–1305.
- Kurylyk, B. L., MacQuarrie, K. T., & McKenzie, J. M. (2014a). Climate change impacts on groundwater and soil temperatures in cold and temperate regions: Implications, mathematical theory, and emerging simulation tools. *Earth-Science Reviews*, 138, 313–334.
- Kurylyk, B. L., McKenzie, J. M., MacQuarrie, K. T., & Voss, C. I. (2014b). Analytical solutions for benchmarking cold regions subsurface water flow and energy transport models: One-dimensional soil thaw with conduction and advection. *Advances in Water Resources*, 70, 172–184.
- Kurylyk, B. L., & Watanabe, K. (2013). The mathematical representation of freezing and thawing processes in variably-saturated, non-deformable soils. *Advances in Water Resources*, 60, 160–177.

- Lafaysse, M., Cluzet, B., Dumont, M., Lejeune, Y., Vionnet, V., & Morin, S. (2017). A multiphysical ensemble system of numerical snow modelling. *The Cryosphere*, 11(3), 1173.
- Langer, M., Westermann, S., Boike, J., Kirillin, G., Grosse, G., Peng, S., & Krinner, G. (2016). Rapid degradation of permafrost underneath waterbodies in tundra landscapes—toward a representation of thermokarst in land surface models. *Journal of Geophysical Research: Earth Surface*, 121(12), 2446–2470.
- Langham, E. (1974). Phase equilibria of veins in polycrystalline ice. *Canadian Journal of Earth Sciences*, 11(9), 1280–1287.
- Larwa, B. (2019). Heat transfer model to predict temperature distribution in the ground. *Energies*, 12(1), 25.
- Lawrence, D., Fisher, R., Koven, C., Oleson, K., Swenson, S., & Vertenstein, M. (2019). *CLM5 documentation* (tech. rep.). Technical report, Boulder, CO: National Center for Atmospheric Research.
- Lee, H., Swenson, S. C., Slater, A. G., & Lawrence, D. M. (2014). Effects of excess ground ice on projections of permafrost in a warming climate. *Environmental Research Letters*, 9(12), 124006.
- Lehning, M., Bartelt, P., Brown, B., Russi, T., Stöckli, U., & Zimmerli, M. (1999). SNOWPACK model calculations for avalanche warning based upon a new network of weather and snow stations. *Cold Regions Science and Technology*, 30(1-3), 145–157.
- Lewis, R., & Ravindran, K. (2000). Finite element simulation of metal casting. *International Journal for Numerical Methods in Engineering*, 47(1-3), 29–59.
- Ling, F., & Zhang, T. (2003). Numerical simulation of permafrost thermal regime and talik development under shallow thaw lakes on the Alaskan Arctic Coastal Plain. *Journal of Geophysical Research: Atmospheres*, 108(D16).

- Liu, S., Lu, L., Mao, D., & Jia, L. (2007). Evaluating parameterizations of aerodynamic resistance to heat transfer using field measurements. *Hydrology and Earth System Sciences*, 11(2), 769–783.
- Lliboutry, L., & Duval, P. (1985). Various isotropic and anisotropic ices found in glaciers and polar ice caps and their corresponding rheologies. *Annales Geophysicae*, 3(2), 207–224.
- Lloyd, W., David, O., Ascough II, J. C., Rojas, K. W., Carlson, J. R., Leavesley, G. H., Krause, P., Green, T. R., & Ahuja, L. R. (2011). Environmental modeling framework invasiveness: Analysis and implications. *Environmental Modelling & Software*, 26(10), 1240–1250.
- Lu, N. (2016). Generalized soil water retention equation for adsorption and capillarity. *Journal of Geotechnical and Environmental Engineering*, 142(10), 04016051.
- Lu, N., & Godt, J. W. (2013). *Hillslope hydrology and stability*. Cambridge University Press.
- Lunardini, V. J. (1988). *Freezing of soil with an unfrozen water content and variable thermal properties* (tech. rep. No. 88-2). US Army Corps of Engineers, Cold Regions Research & Engineering Laboratory.
- Manzini, G., & Ferraris, S. (2004). Mass-conservative finite volume methods on 2-D unstructured grids for the Richards' equation. *Advances in Water Resources*, 27(12), 1199–1215.
- Marchenko, S., Romanovsky, V., & Tipenko, G. (2008). Numerical modeling of spatial permafrost dynamics in Alaska. *Proceedings of the 9th International Conference on Permafrost*, 29, 1125–1130.
- Martin, R. C. (2009). *Clean code: A handbook of agile software craftsmanship*. Pearson Education.
- McBride, D., Cross, M., Croft, N., Bennett, C., & Gebhardt, J. (2006). Computational modelling of variably saturated flow in porous

- media with complex three-dimensional geometries. *International Journal for Numerical Methods in Fluids*, 50(9), 1085–1117.
- McDonough, J. M. (2004). *Introductory lectures on turbulence physics, mathematics and modeling* (tech. rep.). University of Kentucky.
- McKenzie, J. M., & Voss, C. I. (2013). Permafrost thaw in a nested groundwater-flow system. *Hydrogeology Journal*, 21(1), 299–316.
- McKenzie, J. M., Voss, C. I., & Siegel, D. I. (2007). Groundwater flow with energy transport and water-ice phase change: Numerical simulations, benchmarks, and application to freezing in peat bogs. *Advances in Water Resources*, 30(4), 966–983.
- Menard, C. B., Essery, R., Krinner, G., Arduini, G., Bartlett, P., Boone, A., Brutel-Vuilmet, C., Burke, E., Cuntz, M., Dai, Y., et al. (2020). Scientific and human errors in a snow model intercomparison. *Bulletin of the American Meteorological Society*, 1–46.
- Metcalf, R., & Buttle, J. (1999). Semi-distributed water balance dynamics in a small boreal forest basin. *Journal of Hydrology*, 226(1-2), 66–87.
- Michel, F. A., & Van Everdingen, R. O. (1994). Changes in hydrogeologic regimes in permafrost regions due to climatic change. *Permafrost and Periglacial Processes*, 5(3), 191–195.
- Mongibello, L., Bianco, N., Caliano, M., & Graditi, G. (2018). Numerical simulation of an aluminum container including a phase change material for cooling energy storage. *Applied System Innovation*, 1(3), 34.
- Morin, S., Lejeune, Y., Lesaffre, B., Panel, J.-M., Poncet, D., David, P., & Sudul, M. (2012). An 18-yr long (1993–2011) snow and meteorological dataset from a mid-altitude mountain site (Col de Porte, France, 1325 m alt.) for driving and evaluating snowpack models. *Earth System Science Data*, 4(1), 13.

- Mualem, Y. (1976). A new model for predicting the hydraulic conductivity of unsaturated porous media. *Water Resources Research*, 12(3), 513–522.
- Muskat, M., & Meres, M. W. (1936). The flow of heterogeneous fluids through porous media. *Physics*, 7(9), 346–363.
- National Research Council. (2001). Basic research opportunities in earth science.
- Nazzi Ehms, J. H., De Césaró Oliveski, R., Oliveira Rocha, L. A., Biserni, C., & Garai, M. (2019). Fixed grid numerical models for solidification and melting of phase change materials (PCMs). *Applied Sciences*, 9(20), 4334.
- Nedjar, B. (2002). An enthalpy-based finite element method for nonlinear heat problems involving phase change. *Computers & Structures*, 80(1), 9–21.
- Nelson, F., Outcalt, S., Brown, J., Shiklomanov, N., & Hinkel, K. (1998). Spatial and temporal attributes of the active layer thickness record, Barrow, Alaska, USA. *Proceedings of the Seventh International Conference on Permafrost, Yellowknife, NWT, 23-27 June 1998*, (57), 797–802.
- Nicolosky, D., Romanovsky, V., & Tipenko, G. (2007a). Using in-situ temperature measurements to estimate saturated soil thermal properties by solving a sequence of optimization problems. *The Cryosphere*, 1(1), 41–58.
- Nicolosky, D., Romanovsky, V., Alexeev, V., & Lawrence, D. (2007b). Improved modeling of permafrost dynamics in a gcm land-surface scheme. *Geophysical Research Letters*, 34(8).
- Nicolosky, D., & Romanovsky, V. E. (2018). Modeling long-term permafrost degradation. *Journal of Geophysical Research: Earth Surface*, 123(8), 1756–1771.
- Nobel, P. (1999). *Physicochemical & environmental plant physiology*. Academic Press.

- Nye, J., & Frank, F. (1973). Hydrology of the intergranular veins in a temperate glacier. *Symposium on the Hydrology of Glaciers*, 95, 157–161.
- Ochsner, T. E., Horton, R., & Ren, T. (2001). A new perspective on soil thermal properties. *Soil Science Society of America Journal*, 65(6), 1641–1647.
- Oleson, K., Dai, Y., Bonan, B., Bosilovich, M., Dickinson, R., Dirmeyer, P., Hoffman, F., Houser, P., Levis, S., Niu, G.-Y., et al. (2004). *Technical description of the Community Land Model (CLM)* (tech. rep.). NCAR.
- O'Neill, H. B., Smith, S., & Duchesne, C. (2019). Long-term permafrost degradation and thermokarst subsidence in the Mackenzie Delta area indicated by thaw tube measurements. *Cold Regions Engineering 2019* (pp. 643–651). American Society of Civil Engineers Reston, VA.
- Painter, S. L. (2011). Three-phase numerical model of water migration in partially frozen geological media: Model formulation, validation, and applications. *Computational Geosciences*, 15(1), 69–85.
- Paniconi, C., & Putti, M. (1994). A comparison of Picard and Newton iteration in the numerical solution of multidimensional variably saturated flow problems. *Water Resources Research*, 30(12), 3357–3374.
- Paniconi, C., & Putti, M. (2015). Physically based modeling in catchment hydrology at 50: Survey and outlook. *Water Resources Research*, 51(9), 7090–7129.
- Paniconi, C., & Wood, E. F. (1993). A detailed model for simulation of catchment scale subsurface hydrologic processes. *Water Resources Research*, 29(6), 1601–1620.
- Peckham, S. D., Hutton, E. W., & Norris, B. (2013). A component-based approach to integrated modeling in the geosciences: The design of CSDMS. *Computers & Geosciences*, 53, 3–12.

- Penna, D., Hopp, L., Scandellari, F., Allen, S. T., Benettin, P., Beyer, M., Geris, J., Klaus, J., Marshall, J. D., Schwendenmann, L., et al. (2018). Ideas and perspectives: Tracing terrestrial ecosystem water fluxes using hydrogen and oxygen stable isotopes—challenges and opportunities from an interdisciplinary perspective. *Biogeosciences*, 15(21), 6399–6415.
- Pienitz, R., Doran, P. T., & Lamoureux, S. F. (2008). Origin and geomorphology of lakes in the polar regions. *Polar lakes and rivers: limnology of Arctic and Antarctic aquatic ecosystems*, 25–41.
- Prentice, I. C., Liang, X., Medlyn, B. E., & Wang, Y.-P. (2015). Reliable, robust and realistic: The three R's of next-generation land-surface modelling. *Atmospheric Chemistry and Physics*, 15(10), 5987–6005.
- Priestley, C. H. B., & Taylor, R. J. (1972). On the assessment of surface heat flux and evaporation using large-scale parameters. *Monthly Weather Review*, 100(2), 81–92.
- Quarteroni, A., Sacco, R., & Saleri, F. (2010). *Numerical mathematics* (Vol. 37). Springer Science & Business Media.
- Quinton, W., & Marsh, P. (1999). A conceptual framework for runoff generation in a permafrost environment. *Hydrological Processes*, 13(16), 2563–2581.
- Raupach, M., & Thom, A. S. (1981). Turbulence in and above plant canopies. *Annual Review of Fluid Mechanics*, 13(1), 97–129.
- Rempel, A. W., Wettlaufer, J., & Worster, M. G. (2004). Premelting dynamics in a continuum model of frost heave. *Journal of Fluid Mechanics*, 498, 227.
- Richards, L. A. (1931). Capillary conduction of liquids through porous mediums. *Physics*, 1(5), 318–333.
- Richardson, L. F. (1922). *Weather prediction by numerical process*. Cambridge University Press.

- Rigon, R., Bancheri, M., Formetta, G., & de Lavenne, A. (2016a). The geomorphological unit hydrograph from a historical-critical perspective. *Earth Surface Processes and Landforms*, 41(1), 27–37.
- Rigon, R., Bancheri, M., & Green, T. R. (2016b). Age-ranked hydrological budgets and a travel time description of catchment hydrology. *Hydrology and Earth System Sciences*, 20(12), 4929–4947.
- Rigon, R., Bertoldi, G., & Over, T. M. (2006a). GEOtop: A distributed hydrological model with coupled water and energy budgets. *Journal of Hydrometeorology*, 7(3), 371–388.
- Rigon, R., Ghesla, E., Tiso, C., & Cozzini, A. (2006b). *The HORTON machine: A system for dem analysis the reference manual*. (tech. rep.). University of Trento.
- Riseborough, D., Shiklomanov, N., Etzelmüller, B., Gruber, S., & Marchenko, S. (2008). Recent advances in permafrost modelling. *Permafrost and Periglacial Processes*, 19(2), 137–156.
- Rizzoli, A., Svensson, M., Rowe, E., Donatelli, M., Muetzelfeldt, R., van der Wal, T., van Evert, F., & Villa, F. (2006). *Modelling framework (SeamFrame) requirements* (tech. rep.). SEAMLESS.
- Roe, P. L. (1981). Approximate Riemann solvers, parameter vectors, and difference schemes. *Journal of Computational Physics*, 43(2), 357–372.
- Romano, N., Palladino, M., & Chirico, G. (2011). Parameterization of a bucket model for soil-vegetation-atmosphere modeling under seasonal climatic regimes. *Hydrology and Earth System Sciences*, 15(12), 3877–3893.
- Romano, N., Brunone, B., & Santini, A. (1998). Numerical analysis of one-dimensional unsaturated flow in layered soils. *Advances in Water Resources*, 21(4), 315–324.
- Ronan, A. D., Prudic, D. E., Thodal, C. E., & Constantz, J. (1998). Field study and simulation of diurnal temperature effects

- on infiltration and variably saturated flow beneath an ephemeral stream. *Water Resources Research*, 34(9), 2137–2153.
- Ruhaak, W., Anbergen, H., Grenier, C., McKenzie, J., Kurylyk, B., Molson, J., Roux, N., & Sass, I. (2015). Benchmarking numerical freeze/thaw models. *Energy Procedia*.
- Saito, H., Šimůnek, J., & Mohanty, B. P. (2006). Numerical analysis of coupled water, vapor, and heat transport in the vadose zone. *Vadose Zone Journal*, 5(2), 784–800.
- Schuur, E. A., McGuire, A. D., Schädel, C., Grosse, G., Harden, J., Hayes, D. J., Hugelius, G., Koven, C. D., Kuhry, P., Lawrence, D. M., et al. (2015). Climate change and the permafrost carbon feedback. *Nature*, 520(7546), 171–179.
- Serafin, F. (2019). *Enabling modeling framework with surrogate modeling capabilities and complex networks* (Doctoral dissertation). University of Trento.
- Sergueev, D., Tzipenko, G., Romanovsky, V., & Romanovskii, N. (2003). Mountain permafrost thickness evolution under influence of long-term climate fluctuations (results of numerical simulation). *Proceedings of the VII International Permafrost Conference, Switzerland*, 21–25.
- Shewchuk, J. R. et al. (1994). An introduction to the conjugate gradient method without the agonizing pain.
- Shiklomanov, N. I., Streletskiy, D. A., Little, J. D., & Nelson, F. E. (2013). Isotropic thaw subsidence in undisturbed permafrost landscapes. *Geophysical Research Letters*, 40(24), 6356–6361.
- Shiklomanov, N. I., Streletskiy, D. A., Nelson, F. E., Hollister, R. D., Romanovsky, V. E., Tweedie, C. E., Bockheim, J. G., & Brown, J. (2010). Decadal variations of active-layer thickness in moisture-controlled landscapes, Barrow, Alaska. *Journal of Geophysical Research: Biogeosciences*, 115(G4).

- Shur, Y. L., & Jorgenson, M. (2007). Patterns of permafrost formation and degradation in relation to climate and ecosystems. *Permafrost and Periglacial Processes*, 18(1), 7–19.
- Shur, Y., Hinkel, K. M., & Nelson, F. E. (2005). The transient layer: Implications for geocryology and climate-change science. *Permafrost and Periglacial Processes*, 16(1), 5–17.
- Šimůnek, J., Van Genuchten, M. T., & Sejna, M. (2012). The HYDRUS software package for simulating the two-and three-dimensional movement of water, heat, and multiple solutes in variably-saturated porous media. *Technical manual*.
- Šimůnek, J., Van Genuchten, M. T., & Sejna, M. (2005). The HYDRUS-1D software package for simulating the one-dimensional movement of water, heat, and multiple solutes in variably-saturated media. *University of California-Riverside Research Reports*, 3, 1–240.
- Skiena, S. (1990). Graph isomorphism. *Implementing Discrete Mathematics: Combinatorics and Graph Theory with Mathematica*, 181–187.
- Sophocleous, M. (1979). Analysis of water and heat flow in unsaturated-saturated porous media. *Water Resources Research*, 15(5), 1195–1206.
- Srivastava, R., & Yeh, T.-C. J. (1991). Analytical solutions for one-dimensional, transient infiltration toward the water table in homogeneous and layered soils. *Water Resources Research*, 27(5), 753–762.
- Streletskiy, D. A., Shiklomanov, N. I., & Nelson, F. E. (2012). Permafrost, infrastructure, and climate change: A GIS-based landscape approach to geotechnical modeling. *Arctic, Antarctic, and Alpine Research*, 44(3), 368–380.
- Streletskiy, D. A., Suter, L. J., Shiklomanov, N. I., Porfiriev, B. N., & Eliseev, D. O. (2019). Assessment of climate change impacts on buildings, structures and infrastructure in the russian

- regions on permafrost. *Environmental Research Letters*, 14(2), 025003.
- Tan, X., Chen, W., Tian, H., & Cao, J. (2011). Water flow and heat transport including ice/water phase change in porous media: Numerical simulation and application. *Cold Regions Science and Technology*, 68(1-2), 74–84.
- Teodosio, B., Pauwels, V. R., Loheide, S. P., & Daly, E. (2017). Relationship between root water uptake and soil respiration: A modeling perspective. *Journal of Geophysical Research: Biogeosciences*, 122(8), 1954–1968.
- Tomin, P., & Lunati, I. (2016). Investigating Darcy-scale assumptions by means of a multiphysics algorithm. *Advances in Water Resources*, 95, 80–91.
- Tubini, N., & R, R. (2021). *Geoframepy* [Last accessed: 25 August 2021]. <https://pypi.org/project/geoframepy/>
- Tubini, N. (2020a). <https://zenodo.org/record/4017668#.X4l3f-1S82w>
- Tubini, N. (2020b). *FreeThaw-1D OMS project* [Last accessed: 16 October 2020]. https://github.com/GEOframeOMSProjects/OMS_FreeThaw1D
- Tubini, N. (2020c). *FreeThaw-1D source code* [Last accessed: 16 October 2020]. <https://github.com/geoframecomponents/FreeThaw1D>
- Tubini, N., Gruber, S., & Rigon, R. (2020). A method for solving heat transfer with phase change in ice or soil that allows for large time steps while guaranteeing energy conservation. *The Cryosphere*, 1–41.
- Tufano, R., Formetta, G., Calcaterra, D., & De Vita, P. (2021). Hydrological control of soil thickness spatial variability on the initiation of rainfall-induced shallow landslides using a three-dimensional model. *Landslides*, 1–14.

- Unidata. (n.d.-a). *Chunking Data with NetCDF-4* [Last accessed: 1 April 2021].
- Unidata. (n.d.-b). *Formats and performance* [Last accessed: 1 April 2021].
- Unidata. (2021). *NetCDF version 4.3.22*. Boulder, CO: UCAR/Unidata Program Center. <https://doi.org/https://doi.org/10.5065/D6H70CW6>
- Van Genuchten, M. T. (1980). A closed-form equation for predicting the hydraulic conductivity of unsaturated soils. *Soil Science Society of America Journal*, 44(5), 892–898.
- Vanderborght, J., Kasteel, R., Herbst, M., Javaux, M., Thiéry, D., Vanclooster, M., Mouvet, C., & Vereecken, H. (2005). A set of analytical benchmarks to test numerical models of flow and transport in soils. *Vadose Zone Journal*, 4(1), 206–221.
- Verseghy, D. L. (1991). CLASS—A canadian land surface scheme for GCMs. I. Soil model. *International Journal of Climatology*, 11(2), 111–133.
- Vincent, W. F., Lemay, M., & Allard, M. (2017). Arctic permafrost landscapes in transition: Towards an integrated earth system approach. *Arctic Science*, 3(2), 39–64.
- Vionnet, V., Brun, E., Morin, S., Boone, A., Faroux, S., Moigne, P. L., Martin, E., & Willemet, J.-M. (2012). The detailed snowpack scheme crocus and its implementation in SURFEX v7. 2. *Geophysical Research Geoscientific Model Development Letters*, 5(3), 773–791.
- Voller, V. R., Swaminathan, C. R., & Thomas, B. G. (1990). Fixed grid techniques for phase change problems: A review. *International Journal for Numerical Methods in Engineering*, 30(4), 875–898.
- Voller, V., & Cross, M. (1981). Accurate solutions of moving boundary problems using the enthalpy method. *International Journal of Heat and Mass Transfer*, 24(3), 545–556.

- Voller, V. R. (1990). Fast implicit finite-difference method for the analysis of phase change problems. *Numerical Heat Transfer*, 17(2), 155–169.
- Voss, C. I., & Provost, A. (2002). *SUTRA: A model for 2D or 3D saturated-unsaturated, variable-density ground-water flow with solute or energy transport* (tech. rep.). U.S. Geological Survey Water-Resources Investigations Report.
- Vuik, C. (1993). Some historical notes about the stefan problem.
- Walvoord, M. A., & Kurylyk, B. L. (2016). Hydrologic impacts of thawing permafrost—A review. *Vadose Zone Journal*, 15(6).
- Walvoord, M. A., Voss, C. I., & Wellman, T. P. (2012). Influence of permafrost distribution on groundwater flow in the context of climate-driven permafrost thaw: Example from Yukon Flats Basin, Alaska, United States. *Water Resources Research*, 48(7).
- Wang, T., Ottlé, C., Boone, A., Ciais, P., Brun, E., Morin, S., Krinner, G., Piao, S., & Peng, S. (2013). Evaluation of an improved intermediate complexity snow scheme in the ORCHIDEE land surface model. *Journal of Geophysical Research: Atmospheres*, 118(12), 6064–6079.
- Watanabe, K., & Mizoguchi, M. (2002). Amount of unfrozen water in frozen porous media saturated with solution. *Cold Regions Science and Technology*, 34(2), 103–110.
- Wellman, T. P., Voss, C. I., & Walvoord, M. A. (2013). Impacts of climate, lake size, and supra-and sub-permafrost groundwater flow on lake-talik evolution, Yukon Flats, Alaska (USA). *Hydrogeology Journal*, 21(1), 281–298.
- Wendykier, P. (2010). <https://sites.google.com/site/piotrwendykier/software/parallelcolt>
- Westermann, S., Langer, M., Boike, J., Heikenfeld, M., Peter, M., Etzelmüller, B., & Krinner, G. (2016). Simulating the thermal regime and thaw processes of ice-rich permafrost ground

- with the land-surface model cryogrid 3. *Geophysical Research Geoscientific Model Development Letters*, 9(2), 523–546.
- Westermann, S., Schuler, T., Gisnås, K., & Etzelmüller, B. (2013). Transient thermal modeling of permafrost conditions in Southern Norway. *The Cryosphere*, 7(2), 719–739.
- Wever, N., Fierz, C., Mitterer, C., Hirashima, H., & Lehning, M. (2014). Solving Richards equation for snow improves snowpack meltwater runoff estimations in detailed multi-layer snowpack model. *The Cryosphere*, 8(1), 257.
- Whitaker, S. (1986). Flow in porous media I: A theoretical derivation of Darcy's law. *Transport in porous media*, 1(1), 3–25.
- Wierenga, P., Hagan, R. M., & Nielsen, D. (1970). Soil temperature profiles during infiltration and redistribution of cool and warm irrigation water. *Water Resources Research*, 6(1), 230–238.
- Woo, M.-K., Kane, D. L., Carey, S. K., & Yang, D. (2008). Progress in permafrost hydrology in the new millennium. *Permafrost and Periglacial Processes*, 19(2), 237–254.
- Yang, Y., Wu, J., Zhao, S., Han, Q., Pan, X., He, F., & Chen, C. (2018). Assessment of the responses of soil pore properties to combined soil structure amendments using X-ray computed tomography. *Scientific reports*, 8(1), 1–10.
- Zha, Y., Yang, J., Zeng, J., Tso, C.-H. M., Zeng, W., & Shi, L. (2019). Review of numerical solution of Richardson–Richards equation for variably saturated flow in soils. *Wiley Interdisciplinary Reviews: Water*, 6(5), e1364.
- Zhang, S., Meurey, C., & Calvet, J.-C. (2019). Identification of soil-cooling rains in southern France from soil temperature and soil moisture observations. *Atmospheric Chemistry and Physics*, 19(7), 5005–5020.
- Zhang, Y., Carey, S. K., & Quinton, W. L. (2008). Evaluation of the algorithms and parameterizations for ground thawing

- and freezing simulation in permafrost regions. *Journal of Geophysical Research: Atmospheres*, 113(D17).
- Zhang, Y., Chen, W., & Cihlar, J. (2003). A process-based model for quantifying the impact of climate change on permafrost thermal regimes. *Journal of Geophysical Research: Atmospheres*, 108(D22).
- Zona, D., Lipson, D., Zulueta, R., Oberbauer, S., & Oechel, W. (2011). Microtopographic controls on ecosystem functioning in the Arctic Coastal Plain. *Journal of Geophysical Research: Biogeosciences*, 116(G4).

